

Limiting factors for planar solid oxide fuel cells under different trace compound concentrations

Original

Limiting factors for planar solid oxide fuel cells under different trace compound concentrations / Papurello, Davide; Lanzini, Andrea; Drago, Davide; Leone, Pierluigi; Santarelli, Massimo. - In: ENERGY. - ISSN 0360-5442. - 95:(2016), pp. 67-78. [10.1016/j.energy.2015.11.070]

Availability:

This version is available at: 11583/2648242 since: 2016-09-12T15:54:58Z

Publisher:

Elsevier Ltd

Published

DOI:10.1016/j.energy.2015.11.070

Terms of use:

This article is made available under terms and conditions as specified in the corresponding bibliographic description in the repository

Publisher copyright

Elsevier postprint/Author's Accepted Manuscript

© 2016. This manuscript version is made available under the CC-BY-NC-ND 4.0 license
<http://creativecommons.org/licenses/by-nc-nd/4.0/>. The final authenticated version is available online at:
<http://dx.doi.org/10.1016/j.energy.2015.11.070>

(Article begins on next page)

Limiting factors for planar solid oxide fuel cells under different trace compound concentrations

1 *Davide Papurello*^{*}, *Andrea Lanzini*, *Davide Drago*, *Pierluigi Leone*, *Massimo Santarelli*

2 *Department of Energy (DENERG), Politecnico di Torino, Corso Duca degli Abruzzi, 24, 10129, Turin, Italy.*

3 [*Corresponding author. Tel.:+393402351692. Email address: davide.papurello@polito.it](mailto:davide.papurello@polito.it)

4 **Abstract**

5 The present work investigates the performance of anode supported solid oxide fuel cells under the
6 influence of different trace compounds. Electrochemical impedance spectroscopy (EIS) has been
7 used to deconvolute the impedance spectra of an SOFC in order to identify the main losses. The
8 impact of single and double contaminants on the SOFC performance has also been investigated.
9 Typical biogas trace contaminants, obtained after a clean-up stage, such as sulfur, chlorine,
10 aromatic compounds and siloxanes, have been taken into consideration. The results show how the
11 ohmic contribution is almost independent of the H₂S concentration. H₂S acts mainly on the
12 polarization losses and especially on the mass transport resistance. The impact of HCl on the SOFC
13 performance is mainly connected to the charge transfer process. D4, as the model compound for
14 siloxanes, already acts on SOFC performance at ppb(v) levels. The polarization losses have been
15 influenced the most, and the largest increase has been recorded for the low frequency term, R_{low},
16 related to the mass transport resistance for naphthalene and toluene. H₂S, introduced with other
17 contaminants, causes the instantaneous deterioration of the SOFC performance and the more the
18 types of contaminants co-fed to the SOFC, the larger the initial anode degradation.

19 **Keywords**

20 Trace compounds, Biogas, SOFC, anode based fuel cell, Electrochemical Impedance Spectroscopy
21 (EIS), Nyquist diagram.

22 **Nomenclature**

23 ASC, Anode Supported Cell;

24 ASR, Area Specific Resistance;

25 CPE, Constant Phase Element;

26 DIR, Direct Internal Reforming;

27 EIS, Electrochemical Impedance Spectroscopy;

28 FU, Fuel Utilization;

- 29 OCV, Open Circuit Voltage;
- 30 OFMSW, Organic Fraction of Municipal Solid Waste;
- 31 POx, Partial Oxidation;
- 32 ppb(v), parts per billion by volume;
- 33 ppm(v), parts per million by volume;
- 34 Re, ohmic resistance;
- 35 Rp, polarization resistance;
- 36 S/C, Steam to Carbon ratio;
- 37 SOFC, Solid Oxide Fuel Cell;
- 38 TCE, Tetrachloroethylene;
- 39 TOFC, TOPsoe Fuel Cell;
- 40 TPB, Three Phase Boundary;
- 41 VOCs, Volatile Organic Compounds;
- 42 WGS, Water Gas Shift;
- 43 WWTPs, Waste Water Treatment Plants.

44

45 **Introduction**

46 Among all the different fuel cells that are available, Solid Oxide Fuel Cells (SOFCs) can be
47 considered as the most flexible energy generators in relation to fuel selections [1][2][3]. SOFC
48 systems offer electrical efficiencies of more than 50%, even for small-case units with low calorific
49 fuels [1][4]. Various types of fuels can be adopted, from fossil fuels to biogenous fuels
50 [5][3][1][6][7]. The possible fossil fuels for SOFCs include kerosene, gasoline, natural gas, coal gas
51 and liquid petroleum gas. Fuels from renewable matrices, mostly biogas, are appropriate for high
52 temperature fuel cell energy production. Biogenous fuels, with respect to fossil fuels, allow the
53 global warming potential impact to be reduced in order to meet EU 20-20-20 requirements. The

54 European climate and energy change protocol, EU 20-20-20, incorporates these points in order to
55 reduce the energy demand from fossil fuels that are not renewable, and to increase the exploitation
56 of resources that are already distributed locally [5][8]. However, these practical fuels contain minor
57 constituents as impurities. These impurities are mainly volatile organic compounds (VOCs), which
58 are contained in a biogas mixture that originates from the dry anaerobic digestion of the organic
59 fraction of municipal solid waste (OFMSW) [9]. As reported by Papurello et al., (2014, 2015,
60 2015(1)), a gas cleaning section is mandatory to feed a SOFC generator due to the stringent VOC
61 requirements currently in force, which are especially rigorous as far as sulfur, chlorine and siloxane
62 compounds are concerned [1,10,11]. Sigot et al., (2015) have provided another example of sulfur
63 and siloxane removal for biogas conversion in a solid oxide fuel cell [12] in which the SOFC
64 tolerance limits for trace contaminants have been matched with already available gas cleaning
65 technologies. Sasaki et al., (2011) investigated the chemical degradation of SOFCs with trace
66 compounds through long-term poisoning tests of up to 3000 h, in which microstructural
67 observations were considered [5]. H₂S, PH₃, Cl₂ and D₅ were among the trace compounds that
68 Sasaki et al., (2011) investigated, together with their effect on an NiScSz anode based fuel cell. The
69 compounds with the most detrimental effects on SOFC performance are H₂S, HCl and siloxanes
70 [5,13–18]. As reported by Haga et al. (2008), D₅ was selected as the model compound for
71 siloxanes, and 10 ppm(v) was demonstrated to be fatal for SOFCs [19]. No studies have been
72 conducted on siloxanes at ultra-low concentrations, even though they seem to have an important
73 influence on cell performances at the ppm(v) level [20]. In order to conduct a detailed investigation
74 into the effect of VOCs on the performance of SOFCs, proper testing and modeling tools have to be
75 identified, especially considering the remarkable growth in SOFC pilot plant applications [1].

76 These following methods have been used to detect the performance limiting factors of an in-
77 operating fuel cell. A powerful method adopted to analyze fuel cell operation and diagnostics is
78 electrochemical impedance spectroscopy (EIS) [21–27]. The use of EIS analysis as a diagnosis tool

79 is well known at a laboratory level. EIS analysis could be adopted for the on-line diagnostics of
80 operating fuel cell stacks in order to follow and to investigate the SOFC performance of real
81 machines. The other possible methods that could be used as alternatives to investigate cell
82 performance losses could be detrimental for cell operation. For instance, if I-V curve analysis is
83 adopted for the evaluation of the area specific resistance (ASR) for each test condition, detrimental
84 problems could arise related to the current density variation and these could compromise the
85 integrity of the entire test. Leone et al., (2013) conducted an interesting study on the limiting factors
86 for a planar SOFC under different flow and temperature conditions with EIS analysis [27]. The EIS
87 analysis of a fuel cell is carried out under transient and almost equilibrium conditions in order to
88 avoid causing rapid changes in the current [23,26–31] . Two possible conditions can be selected: an
89 open circuit voltage (OCV) or a current density value. In the latter case, polarization of the cell
90 becomes an independent variable. The potential difference between the thermodynamic open circuit
91 potential and the operational potential is the polarization or the overpotential of a fuel cell [32]. This
92 voltage loss is a function of the current density, and it mainly depends on the processes that occur
93 during fuel cell operation. It is generally difficult to interpret the obtained impedance diagrams. For
94 this reason, a specific method is adopted for the EIS spectra deconvolution to separate the ASR
95 value into the different contributions that describe the cell losses related to the cell functional layers
96 [23,28–31]. Three main potential losses [33] can be recognized and connected to: (i) the ohmic
97 resistances of the materials and interfaces due to the transport of ions and electrons through the
98 materials; (ii) concentration polarizations that are caused by the resistance to fuel and oxidant mass
99 transport through the electrodes; (iii) activation polarizations related to the electrochemical
100 reactions of the electrolyte/electrodes. With these techniques, impedance diagrams can at least
101 provide a breakdown of the total loss (ASR). The ASR value can be divided into ohmic resistance,
102 R_e , measured at high frequency, and polarization resistance, R_p , measured at medium and low
103 frequencies, reflecting losses due to chemical, electrochemical, and transport processes.

104 The goal of this work was to investigate cell performance losses related to the different trace
105 compound concentrations contained in a biogenous fuel adopting an EIS analysis.

106 **Materials and methods**

107 A simulated gas mixture representing different fuel conditions has been considered with different
108 trace compounds. Experiments were performed with nickel-based anode supported solid oxide fuel
109 cells (ASC). Three circular planar type seal-less anode supported cells were used. The tested cells
110 have a diameter of 80 mm and a screen printed cathode of 78 mm:

- 111 1. the ASC700 cell ([SOFCpower, Italy](#)) consists of a 240-260 μm porous Ni/8YSZ anode support,
112 a 8-10 μm dense electrolyte YSZ and a 50-60 μm porous GDC/LSCF cathode bilayer;
- 113 2. the ASC4 cell ([H.C. Starck, Germany](#)) consists of a 465-555 μm porous NiO/YSZ anode
114 support with a 5-10 μm NiO/YSZ porous active layer, a 4-6 μm dense electrolyte YSZ and a
115 2.4 μm YDC blocking layer plus a 30-60 μm porous LSCF cathode layer;
- 116 3. the TOFC cell ([Topsoe fuel cell, Denmark](#)) consists of a porous Ni/8YSZ anode support, a
117 dense electrolyte YSZ and a porous CGO/LSCF cathode bilayer.

118 The design of SOFC supported anodes has been extensively investigated over the last few years
119 because of their relatively easy of manufacturing and potentially high power density. Moreover, the
120 cathode material of LSCFs has been investigated for intermediate temperature SOFC applications
121 [23,28–33] and a polarization resistance of 0.018 Ωcm^2 has been shown at 750 °C as well as
122 relative stability (400% of increased polarization resistance in 700 h) [34].

123 Planar SOFCs have been used for the experimental test session. They were fed with synthetic
124 biogas and syngas obtained by mixing pure gas feeds from CH₄, CO₂, CO, N₂ and H₂ cylinders
125 (Siad, Italy). A variable concentration of trace compounds was added to the fuel stream. If it is not
126 explicitly reported the trace compound was added to the fuel mixture and the EIS analysis was
127 conducted after a stabilization time within 2 h. An extensive experimental campaign was scheduled

128 and the details are reported in Table 1. The experiments were performed by varying the fuel
 129 composition and the trace compound concentrations in order to investigate SOFC losses.

Pollutant test	Conc. Range (ppm(v))	Cell adopted	H ₂ (ml min ⁻¹)	CO (ml min ⁻¹)	CO ₂ (ml min ⁻¹)	CH ₄ (ml min ⁻¹)	N ₂ (ml min ⁻¹)	H ₂ O (ml min ⁻¹)	H ₂ O (g h ⁻¹)	T (°C)	FU	Fuel condition
H ₂ S high conc.	0.84-6.4	ASC700	151.5	136.4	68.2	15.2	386.4	60.2	2.9	750	30.0	Syngas
H ₂ S high conc.	0.8-6.7	ASC4	250	0	41.7	62.5	0	124.5	6	750	20.9	DIR 50% biogas
H ₂ S low conc.	0.078-0.174	ASC4	250	0	41.7	62.5	0	124.5	6	750	20.9	DIR 50% biogas
HCl	1-1000	ASC700	348	133.7	62.1	5		136.5	6.58	750	29.9	biogas reformate
D4	0.11-1.92	TOFC	348	133.7	62.1	5		136.5	6.58	750	20.8	biogas reformate
C ₇ H ₈	3.8-24.2	ASC700	151.5	136.4	68.2	15.2	386.4	269.8	13	750	30.0	Syngas
C ₁₀ H ₈	0-9.3	ASC700	151.5	136.4	68.2	15.2	386.4	269.8	13	750	30.0	Syngas
C ₂ H ₂	371.2	ASC700	250	0	42	63	0	0.0	0	750	20.8	POx 50% biogas
H ₂ S	1.34	ASC700	250	0	42	63	0	0.0	0	750	20.8	POx 50% biogas
H ₂ S+C ₂ Cl ₄	0-4/1.7-0	ASC700	151.5	136.4	68.2	15.2	386.4	269.8	13	750	30.0	Syngas
H ₂ S+C ₂ H ₂	1.34/371.2	ASC700	250	0	42	63	0	0.0	0	750	20.8	POx 50% biogas
H ₂ S + C ₇ H ₈	4/3.7	ASC700	151.5	136.4	68.2	15.2	386.4	269.8	13	750	30.0	Syngas

130 **Table 1 – Test conditions.**

131 The oxidant flow (air) at the cathode side was 0.5 Nl min⁻¹ during the start-up and shut-down
 132 procedures, otherwise it was fixed at 1.2 Nl min⁻¹ for all the performed experiments. The fuel gas
 133 mixtures, contained in certified gas bottles ([Siad spa, Italy](#)), were fed to the anode and regulated by
 134 means of mass flow controllers ([Bronkhorst, The Netherlands](#)). All the cells were first activated
 135 with hydrogen. The fuel mixture was restored to clean conditions after each poisoning phase with
 136 the trace compound of interest. Four gas mixtures were adopted for the experimental tests:

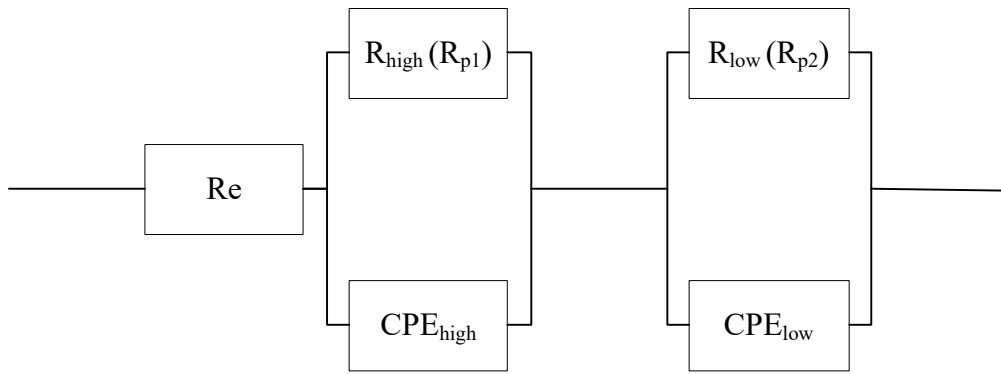
- 137 1. A syngas mixture, used to represent a wood gasification plant.
- 138 2. A direct internal reforming case (DIR 50%), used to represent a mixture of biogas reformed
 139 internally with steam (50% vol.-electrochemical), while the remaining part was reformed
 140 externally.
- 141 3. A partial oxidation case (POx 50%), used to represent a biogas mixture reformed internally with
 142 air (50% vol.-electrochemical), while the remaining part was reformed externally.

143 4. A biogas reformat case, used to represent a biogas mixture completely reformed externally in a
144 steam reformer with a steam-to-carbon (S/C) ratio equal to 2.

145 The electrochemical characterization of the fuel cell was carried out with an electronic load
146 (Kikusui Electronics Corp., Japan) in conjunction with an additional power supply in current-
147 following mode (Delta Elektronica, The Netherlands). Electrochemical impedance spectroscopy
148 analyses were performed using a GAMRY FC350 in the 10 Hz to 300 kHz range. The oven
149 temperature was kept constant at 750 °C. Temperature control was provided by a thermocouple
150 placed in the center of the anodic ceramic housing, 1 mm from the anode surface. The seal-less cell
151 arrangement was adopted to allow the excess fuel and oxidant in the outer border of the cell to
152 combust. Nickel and platinum double meshes were used for current collection at the anode and
153 cathode electrodes, respectively.

154 **Results**

155 The electrochemical impedance analysis results are reported in this section. The analysis focused on
156 a more detailed investigation of cell performance, which was affected by the trace compounds
157 through the deconvolution of the impedance spectrum. The Nyquist diagrams that were obtained for
158 the different measurement conditions are also reported. The behavior of the cell was simulated by
159 means of the equivalent electrical circuit shown in figure 1, and the impedance data were analyzed
160 at different trace compound concentrations. The equivalent circuit is constituted by the ohmic
161 resistance, R_e and two parallel combinations of a resistance and a constant phase element, CPE
162 [25]. The polarization resistance, R_p , is obtained by summing the R_{high} and R_{low} resistances. The
163 first term is related to the electrochemical processes that take place at the electrodes, whereas the
164 second contribution accounts for the mass transport phenomena [35].



165

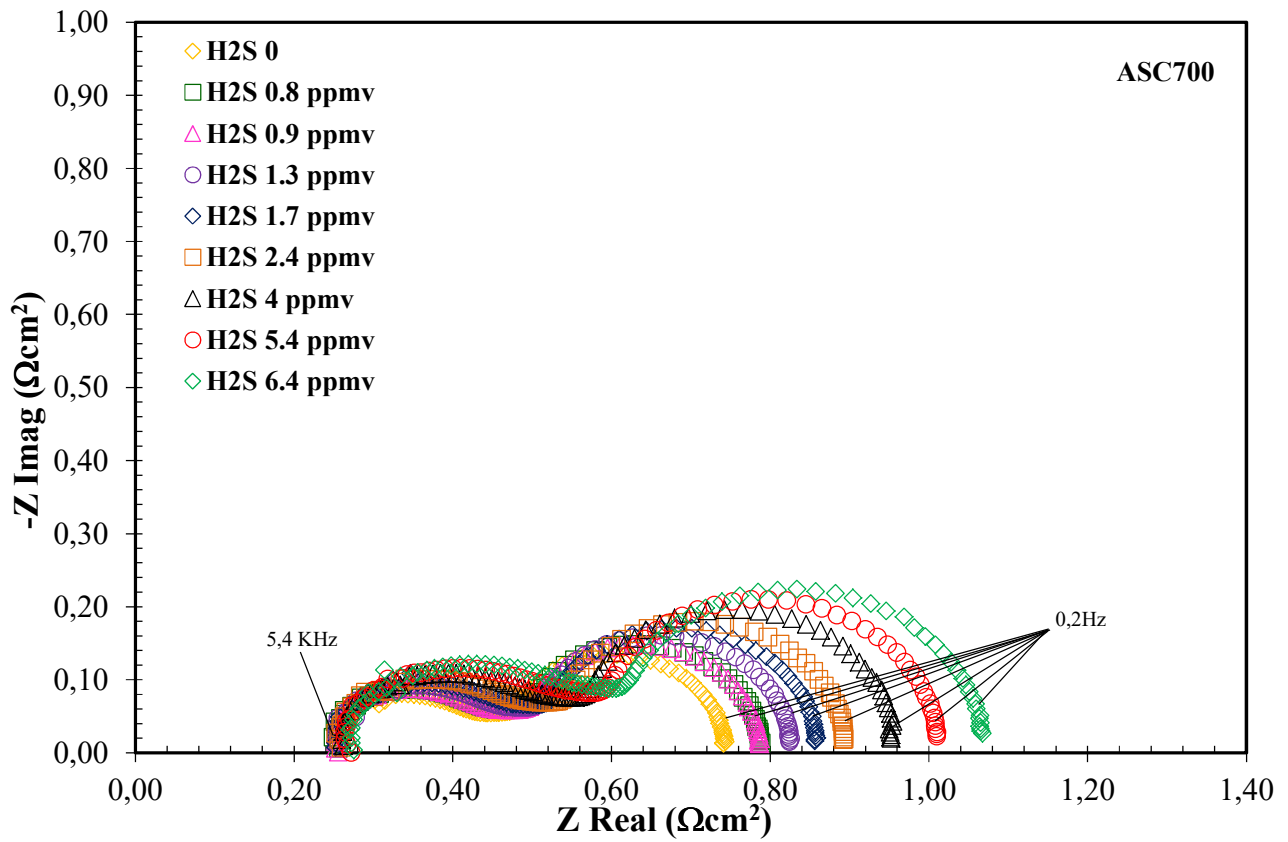
166 **Figure 1 – Equivalent fuel cell circuit: R_e , R_{high} and CPE_{high} are associated with the high frequency semi-circle,**
 167 **R_{low} and CPE_{low} with the low frequency semi-circle.**

168 The influence of Hydrogen sulfide on SOFC performance

169 The main pollutant compound for SOFC operation is widely recognized to be H_2S [3,13–15,36–38].
 170 As reported elsewhere, the H_2S concentration is one of the main trace compounds contained in a
 171 biogas mixture [9]. Four separate tests were carried out with three different commercial cells:
 172 ASC4, ASC700 and TOFC. The operating temperature was fixed at 750 °C, while the current
 173 density was fixed at 0.32 A cm⁻². The first test was carried out in order to investigate the impact of
 174 H_2S on cell performance, considering a concentration ranging from 0.8 to 6.4 ppm(v), with a
 175 mixture that simulates a syngas produced from a wood gasifier. This concentration range has here
 176 been named “high concentration”, as it is high compared to the limit H_2S concentration value
 177 currently fixed for SOFCs, which is around 1 ppm(v) [5,6,39–41]. The second test considered the
 178 same H_2S concentration range in order to simulate the partial direct internal reforming (DIR 50%)
 179 of a biogas mixture derived from, for example, an anaerobic digestion process. In the next step, the
 180 H_2S test was conducted with the goal of testing the H_2S concentration limit and studying its impact
 181 on SOFCs in a POx biogas mixture. Finally, a low H_2S range, from 78 to 174 ppb(v), was tested to
 182 identify any changes in SOFC performance.

183 High H_2S concentration test

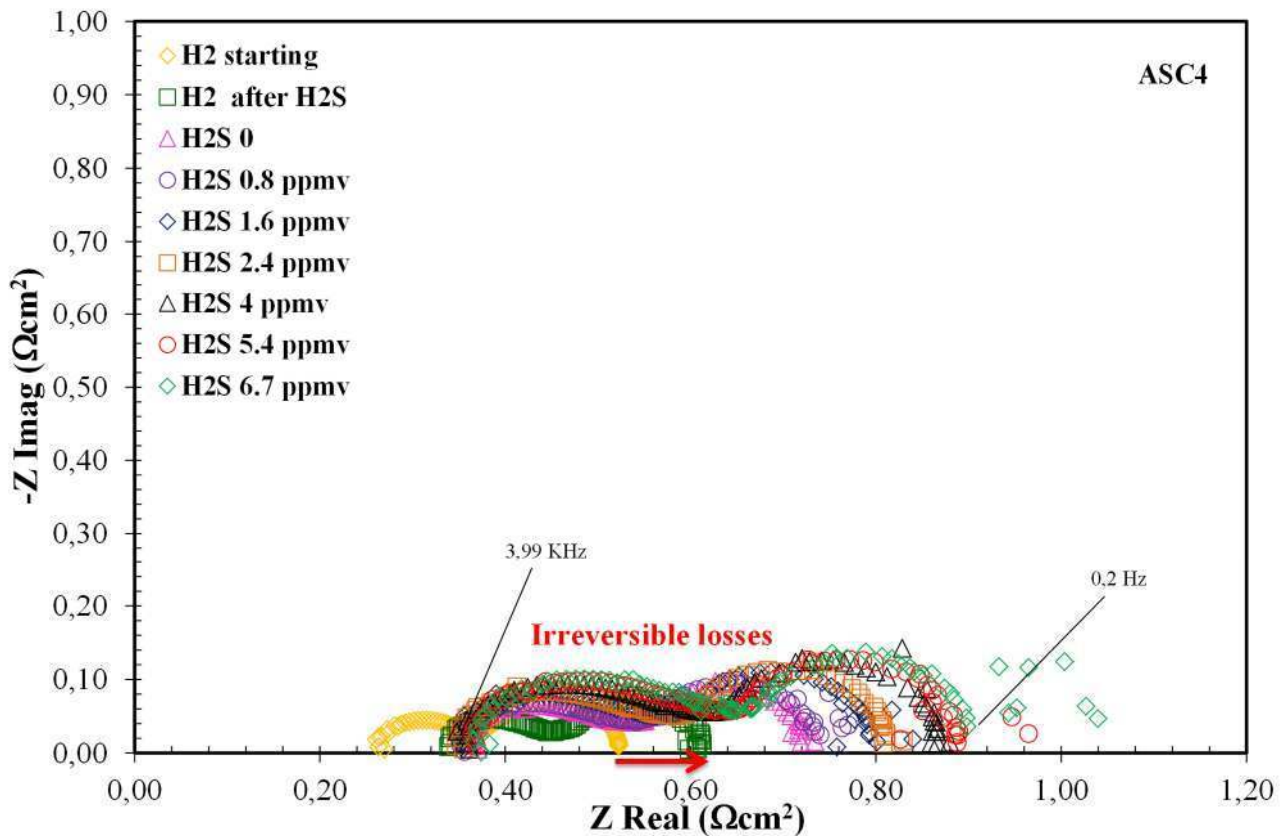
184 Figure 2 depicts the Nyquist diagram for the ASC700 cell with a variable H₂S concentration, while
185 figure 3 shows the Nyquist diagram for the ASC4 cell.



186

187

Figure 2 – Nyquist diagram for variations of the H₂S concentration – ASC700.



188

189

Figure 3 – Nyquist diagram for variations of the H₂S concentration – ASC4.

190

191

192

193

194

195

196

197

198

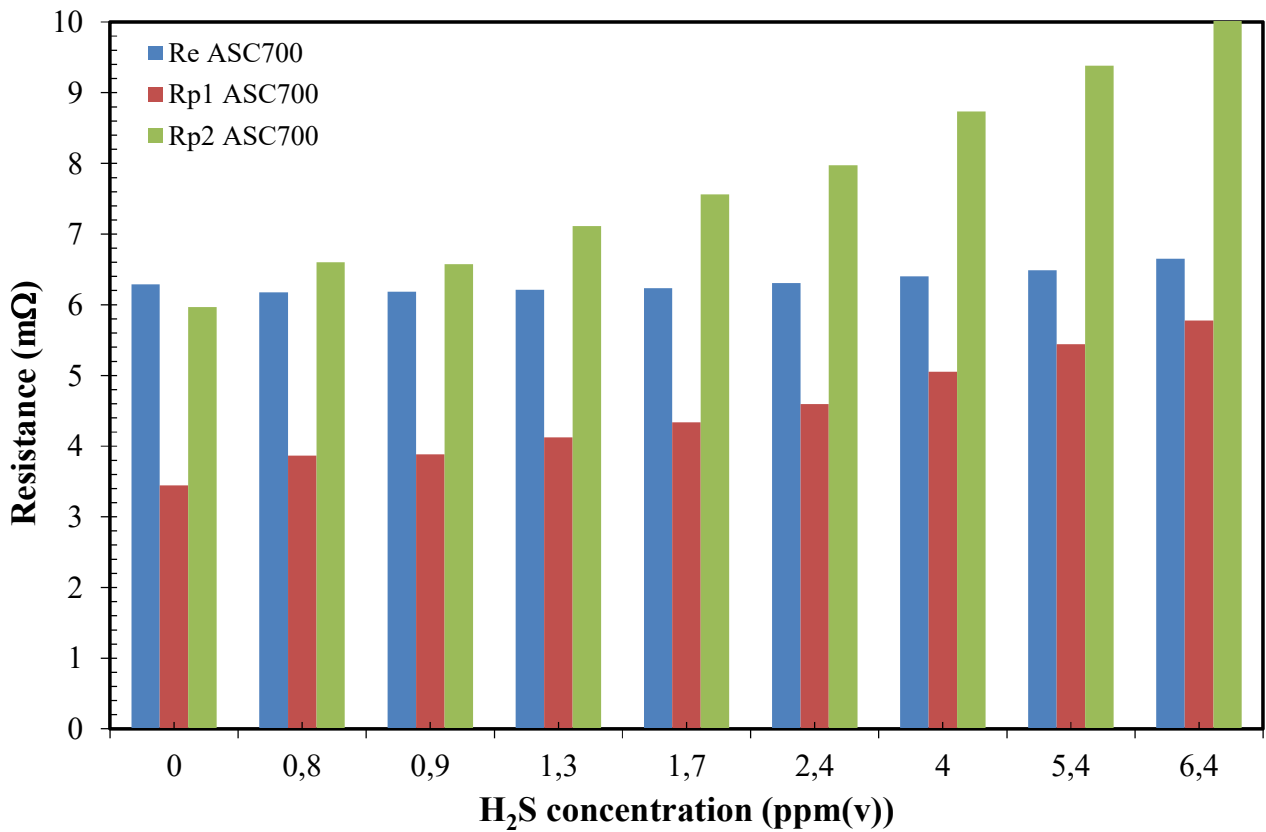
199

200

201

The ohmic contribution to the ASR value represents the materials and interface resistances due to the transport of ions and electrons through the materials. This value is almost independent of the fuel composition and it is only minimally affected by the H₂S concentration value, as shown in figures 2-3 and 4-5. Comparing the ohmic value of ASC700 and ASC4, it is evident that the latter shows a higher value. This is due to the lower fuel flow compared to the ASC700 case (N₂ content), which causes air backflow. The reason for this air backflow is that the seal-less design could lead to nickel oxidation. The nitrogen content, which on one hand allows nickel oxidation to be avoided, on the other hand, causes a dilution effect of the gas mixture, thereby increasing the total ASR value (see the ASC700 cell results). The H₂S concentration, as reported in figures 2-3 and 4-5, does not cause an important variation of the ohmic resistance value, but instead acts on the R_{high} and R_{low} values. By increasing the H₂S concentration, an increase in the low frequency circle amplitude is obtained, compared to the high frequency circle (see figures 2-3). This result can also be confirmed

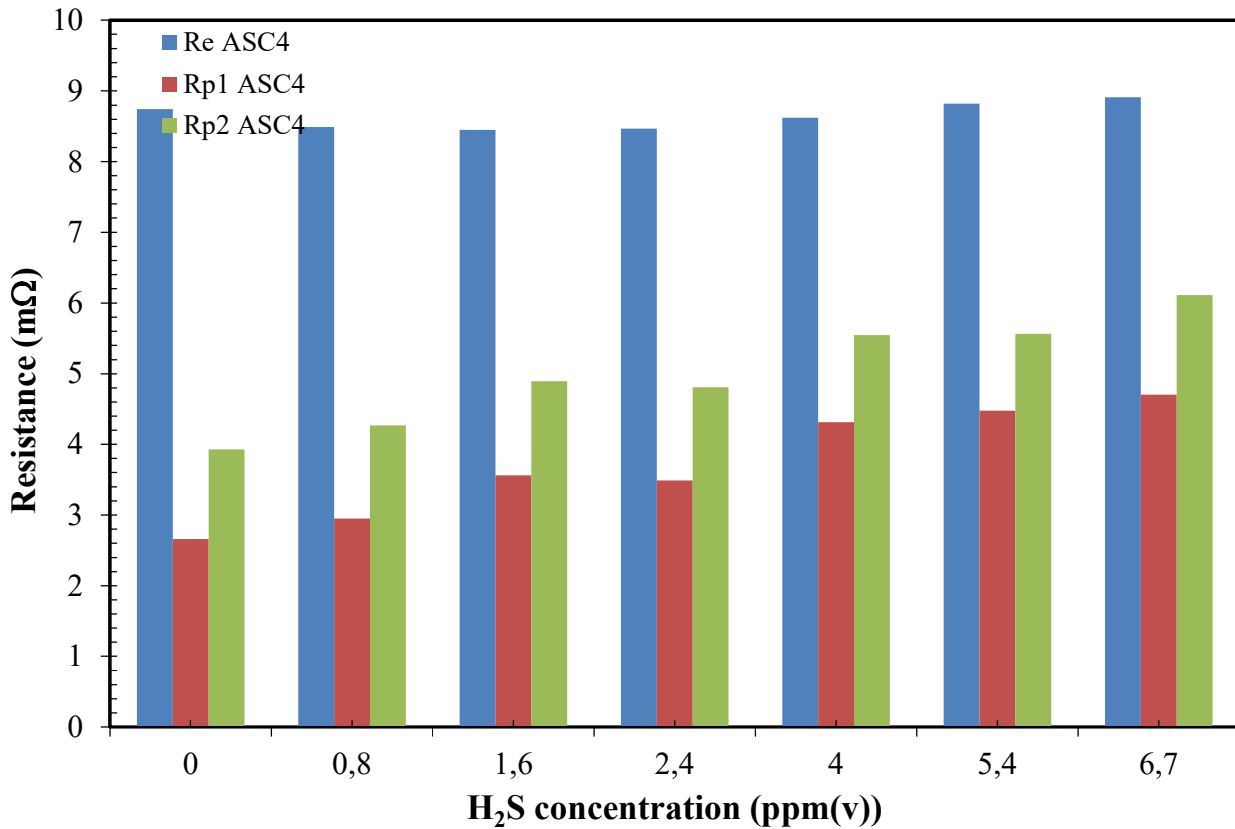
202 by observing figures 4-5, where the R_{p2} (R_{low}) trend rises when the H_2S concentration increases.
203 This is due to the mass transport resistance through the electrodes caused by the sulfur blocking
204 sites. An increase in the R_{high} value is also registered when the H_2S concentration rises. This is due
205 to the three phase boundary (TPB) reduction from the nickel active sites which is blocked by the
206 sulfur compound.



207

208

Figure 4 – Re and Rp values for variations of the H_2S concentration – ASC700.



209

210

Figure 5 – Re and Rp values for variations of the H₂S concentration – ASC4.

211

Figure 3 shows that, after the H₂S “high concentration” test, the cell performance is irreversibly affected, as shown by the Nyquist profile for H₂ before and after the H₂S. As reported above, pollutants affect the performance of a SOFC and the voltage potential of a single cell, in terms of electrical power, which is reduced according to the following equation:

215

$$\Delta P = \Delta R \cdot I^2 \text{ (eq.1)}$$

216

Where ΔP is the power loss due to the variation of the overall resistance of the cell (ΔR), which is obtained from the sum of the ohmic and polarization contributions.

218

Considering an H₂S concentration in the 0.8 to 6.4 ppm(v) range, the power loss increases by up to

219

10.7%, compared to the nominal power value. This means that if the exposure time to the pollutants

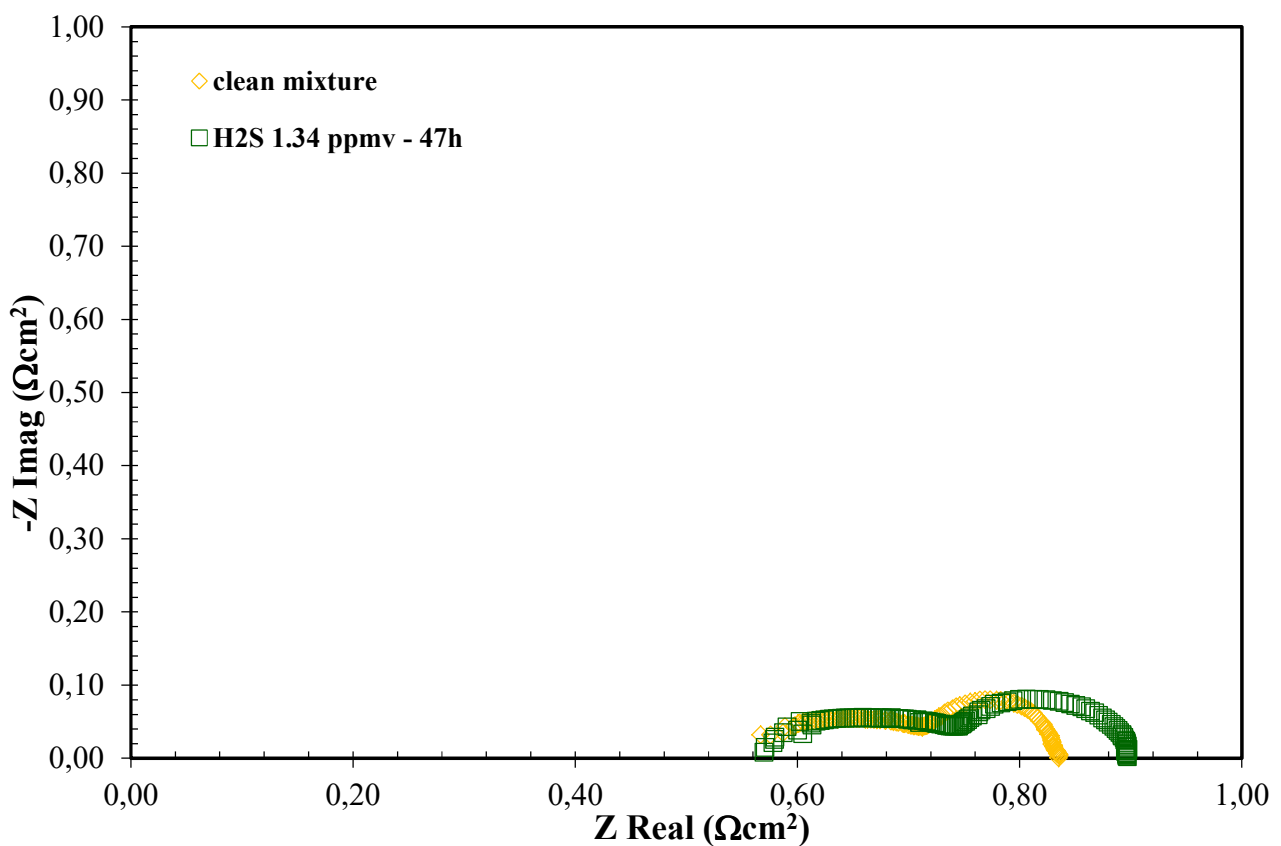
220

is increased, the electrical power loss will also increase, due to an overall higher ASR value.

221

H₂S threshold value test

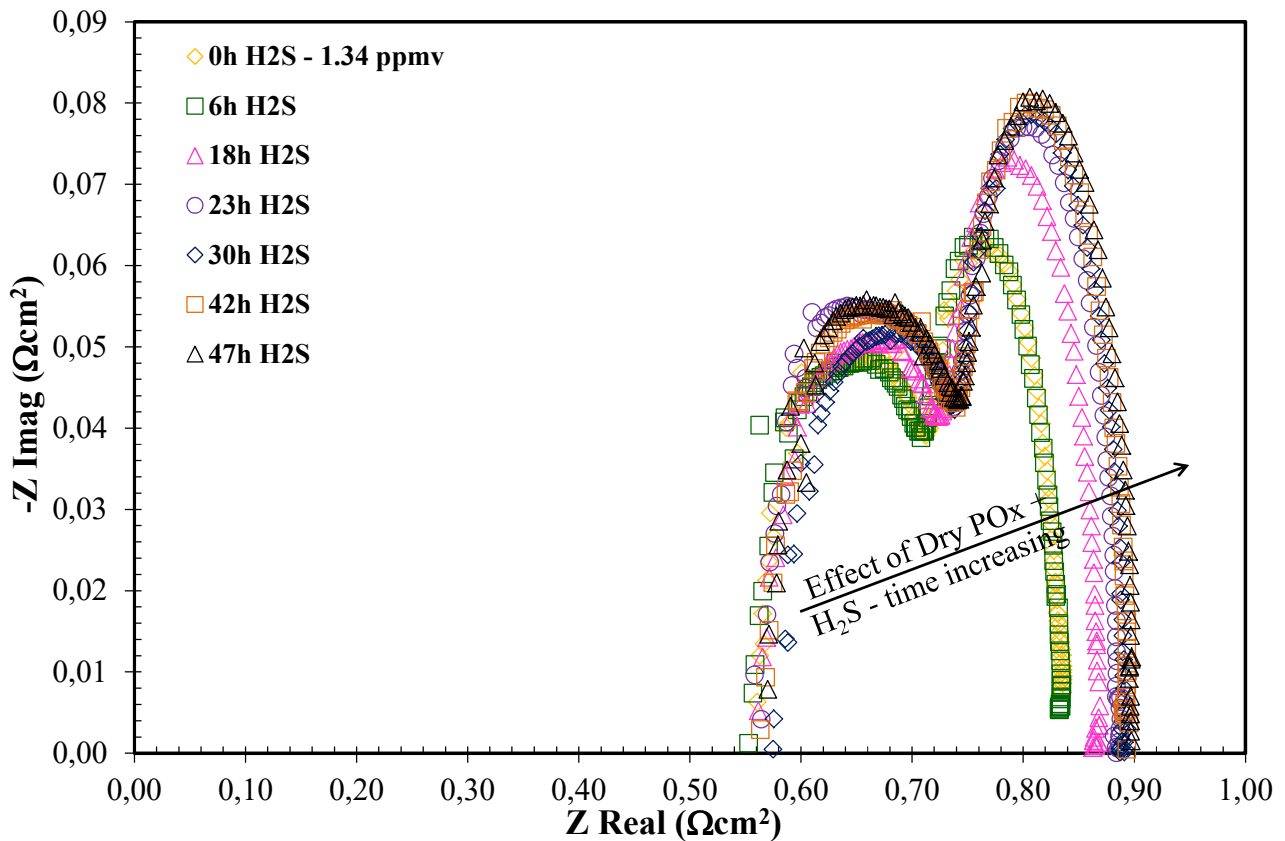
222 Figure 6 depicts the Nyquist diagram for the POx test, with the threshold concentration value of
223 H₂S fixed at 1 ppm(v) on the basis of results from literature studies. The gas mixture has an
224 important effect on the ohmic value, and a high increase is recorded, compared to the ASC4 case
225 with “high sulfur concentration values”. This is due to the amount of air that is added to the reactive
226 fuel sent to the anode side, which may cause combustion and Ni oxidation phenomena. Even at this
227 concentration value, the H₂S concentration influences the polarization losses and, more precisely,
228 the mass transport (R_{low}), and, to a lesser extent, the electrochemical contribution (R_{high}).



229

230 **Figure 6 – Nyquist diagram for the H₂S threshold concentration value – ASC700.**

231 It has been found that increasing the exposure time to the H₂S concentration raises the total ASR
232 value. This is mainly due to the mass transport limitation, caused by Sulfur adsorption on active
233 sites, as can be seen by observing the amplitude of the low frequency circle, which increases more
234 than the high frequency circle (see figure 7).



235

236

Figure 7 – Nyquist diagram for the H₂S threshold concentration value – time variation – ASC700.

237

Low H₂S concentration test

238

Figure 8 shows the Nyquist diagram for an SOFC cell fed with a gas mixture in which increasing

239

concentrations of H₂S, that is, from 78 ppb(v) to 174 ppb(v), have been added. These H₂S

240

concentration values are below the tolerable threshold value of 1 ppm(v). In fact, Figure 9 shows an

241

almost constant trend for the three different contributions to the ASR value. It appears evident that

242

these H₂S concentrations are well tolerated by the SOFC cell. The ohmic resistance is the main

243

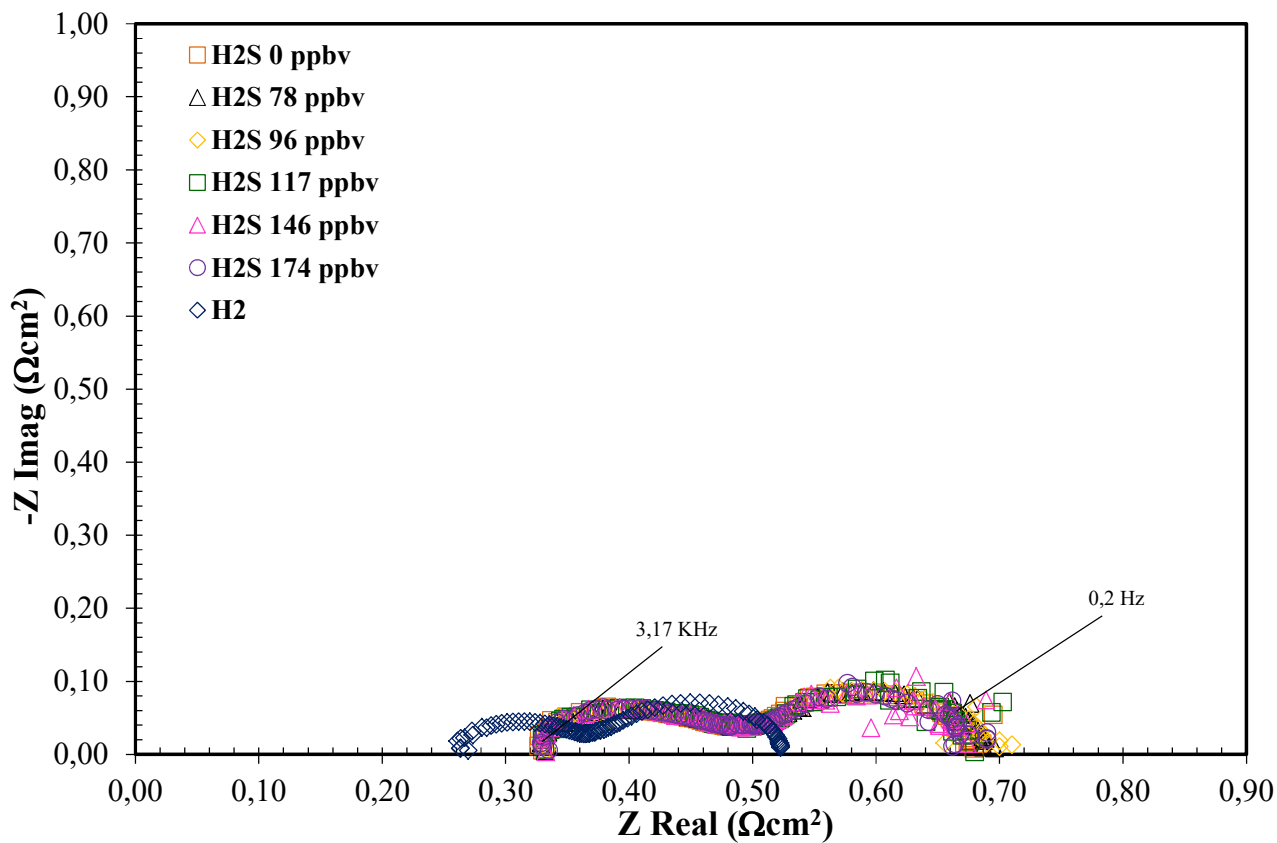
contribution. The ohmic losses account for more than 50% of the total cell resistance, and an

244

enhancement of the performance could be achieved by developing thin layer electrolytes and

245

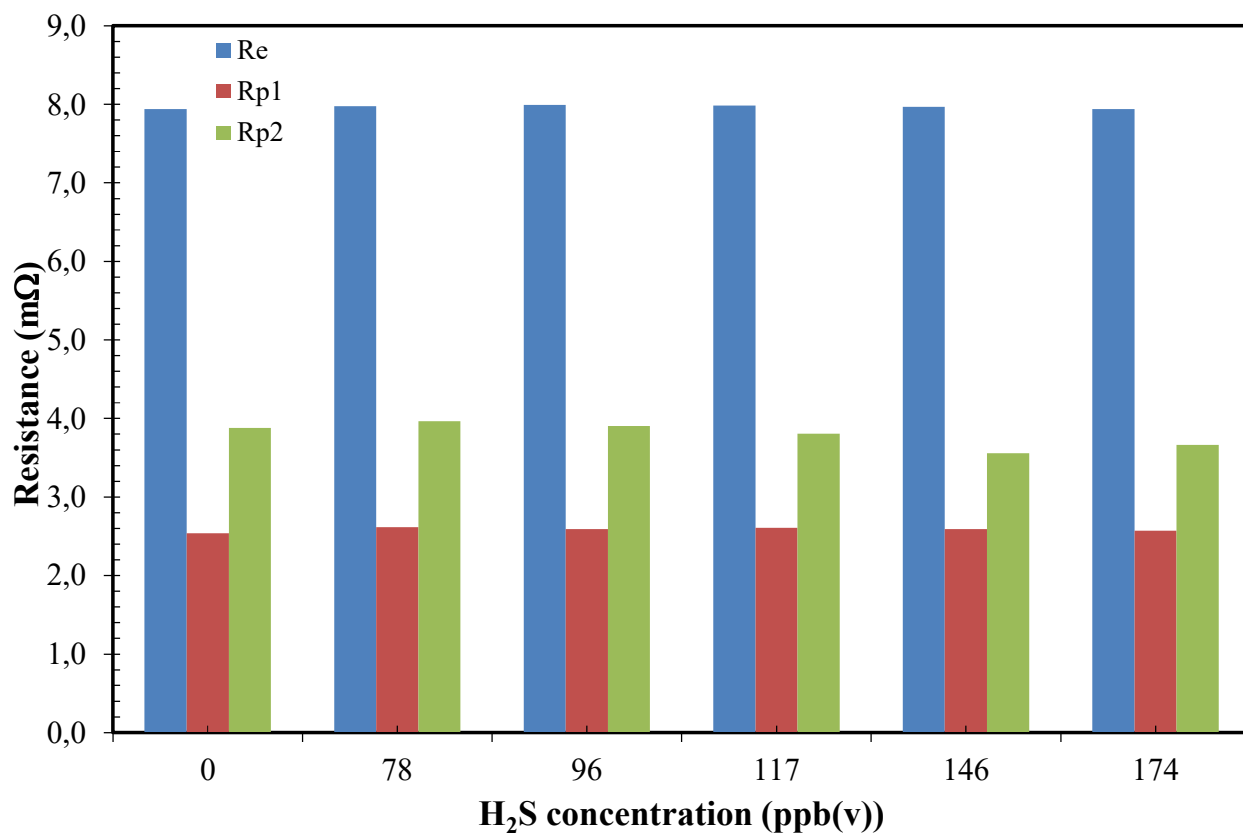
improved interfaces.



246

247

Figure 8 – Nyquist diagram for variations of the H₂S “low concentration level” – ASC4.



248

249 **Figure 9 – Re and Rp values for variations of the H₂S “low concentration level” – ASC4.**

250 Figure 8 shows how the ohmic contribution is low in the H₂ case, compared to the mixture adopted
251 with the pollutants. This is due to the different electrochemical molar flows that are available.

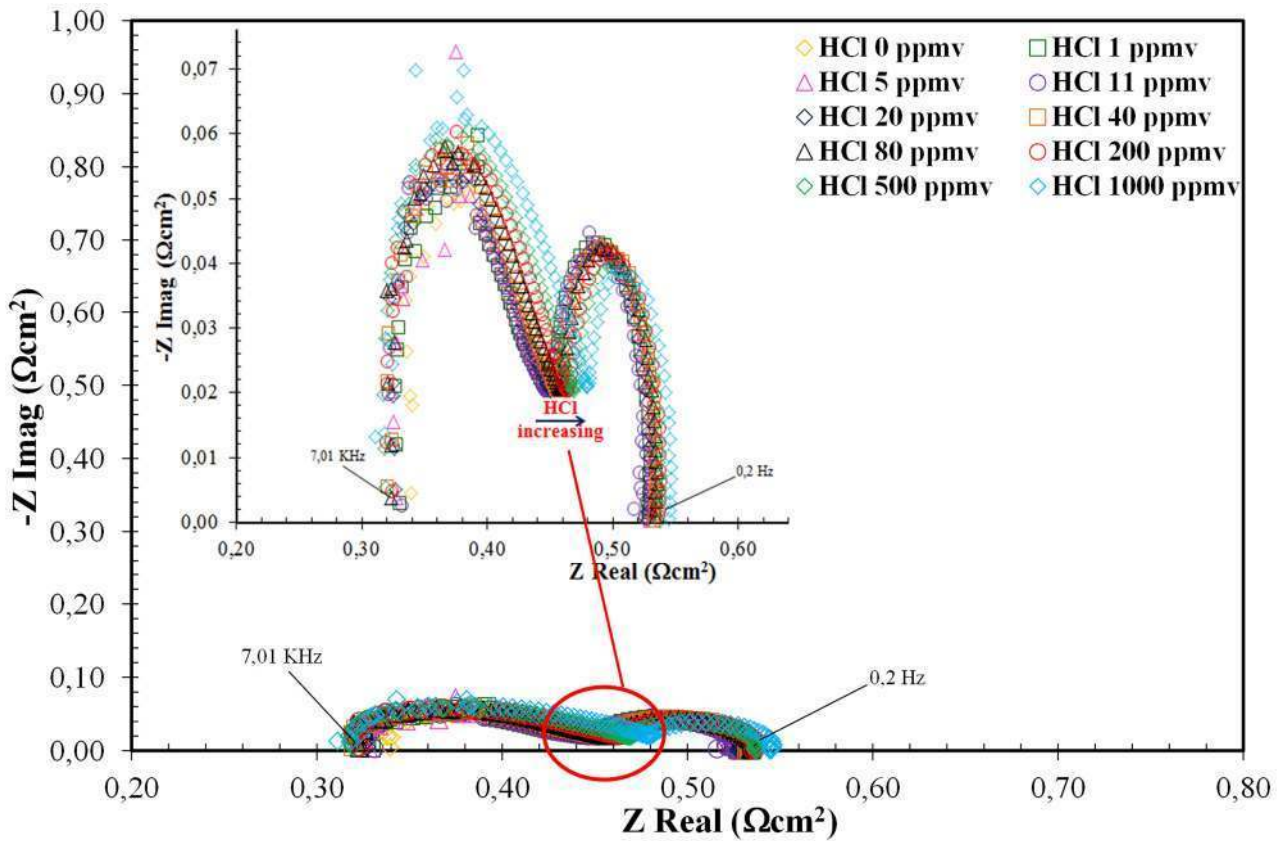
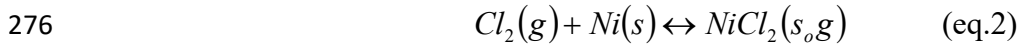
252 If H₂S concentrations ranging from 78 to 174 ppb(v) are considered, the power loss remains quite
253 stable and ranges from 0.13 – 0.4% of the nominal power value at zero time. This means that if the
254 exposure time to the pollutants is increased, the electrical power loss will remain unchanged.

255 The influence of Hydrogen chloride on SOFC performance

256 The dependence of hydrogen chloride on the limiting factors of an anode supported fuel cell has
257 been investigated, considering the addition of a variable concentration of HCl, ranging from 1
258 ppm(v) to 1000 ppm(v), to the gas reformat mixture. Figure 10 shows the Nyquist diagram with
259 variations in the HCl concentration content in the gas mixture. Increasing the HCl content to 100,
260 500 or even 1000 ppm(v), does not result in a notable increase in ASR. Figure 11 clearly highlights
261 how, below 20 ppm(v), the HCl concentration does not affect the SOFC performance. The three
262 contributions to the EIS analysis are almost constant. If the HCl concentration is increased from 40
263 to 1000 ppm(v), the most influential contribution is from R_{high}. The first circle, related to the high
264 frequency, rises and the trace compound concentration therefore increases. This circle is related to
265 the electrochemical processes that occur at the electrodes. In accordance with these results, it has
266 been shown how the Ni catalyst mainly acts by adsorbing HCl. HCl behaves in a similar way to
267 H₂S, but less aggressively; in fact, the tolerable limit appears to be around 20 ppm(v) or more.

268 These results are in agreement with those of Cayan et al., (2008), where HCl was added to an anode
269 supported fuel cell (NiYSZ/YSZ/LSM) and unstable performance occurred at 40 and 160 ppm(v)
270 [42]. Another study by Aravind et al., (2008) has shown how the impact of 9 ppm(v) of HCl on an
271 NiGDC anode supported fuel cell produced no significant losses [43]. Another study on an NiYSZ
272 cell with HCl + NH₃ (1 ppm(v) + 5000 ppm(v)) has shown no significant performance degradation

273 [44]. Ammonia, which is often present in coal syngas, does not represent a pollutant for SOFCs, as
 274 reported by Cayan et al., (2008) [42]. According to Haga et al., (2008), chlorine compounds react
 275 with Ni particles [19]. The formation of NiCl₂ may be described by reaction (1):



277

278 **Figure 10 – Nyquist diagram for variations of the HCl concentration – ASC700.**

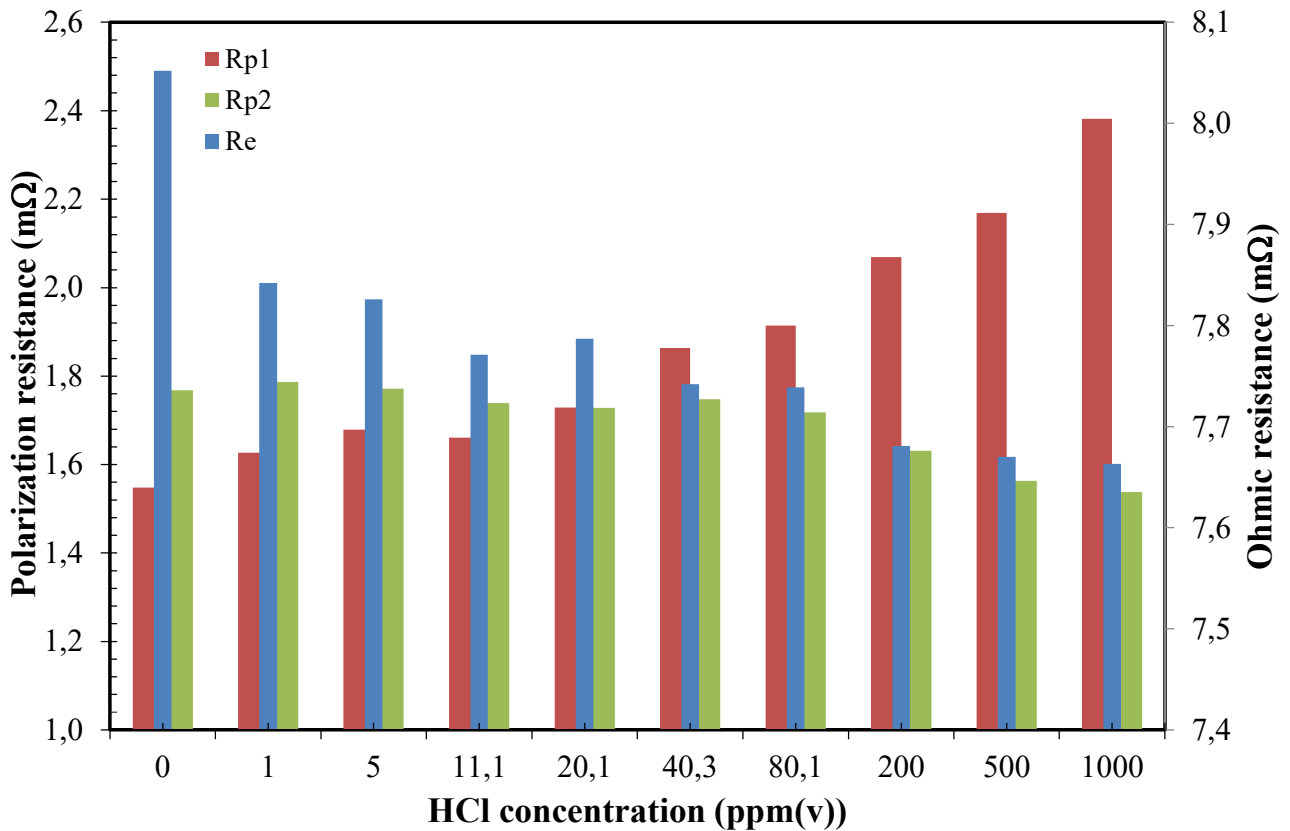


Figure 11 – Re and Rp values for variations of the HCl concentration – ASC700.

279

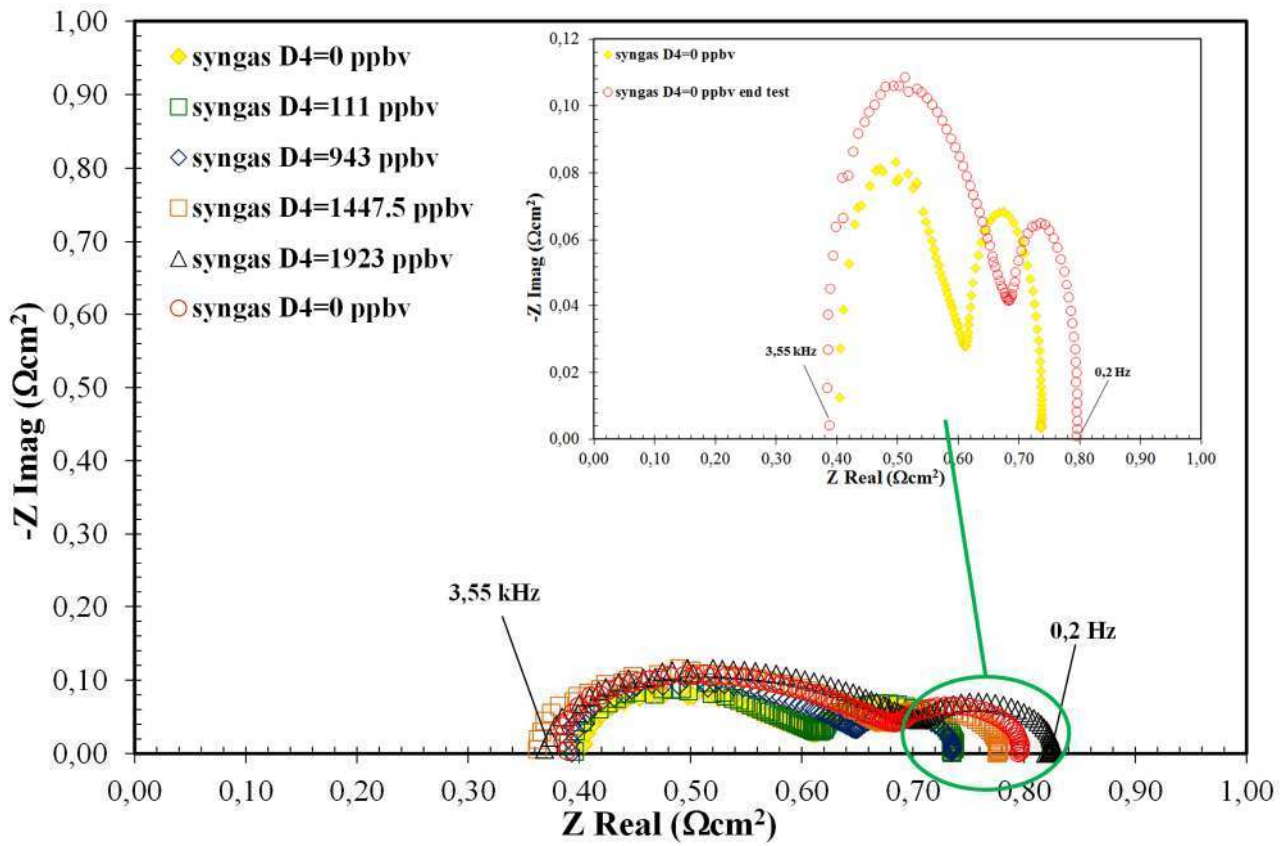
280

281 If HCl concentrations ranging from 1 to 1000 ppm(v) are considered, the related power losses
 282 remain quite stable, and range from 0.17 – 0.3% of the nominal power. This means that if the
 283 exposure time to the pollutants is increased, the electrical power loss will remain unchanged. This is
 284 due to compensation among the resistance terms, as can be seen in figure 11. The ohmic
 285 contribution increases for lower values of the polarization terms at lower HCl concentrations, while
 286 the ohmic value decreases and the polarization term increases for higher HCl concentrations.

287 The influence of Octamethylcyclotetrasiloxane on SOFC performance

288 Siloxanes, which are organosilicon compounds, are often contained in the biogas obtained from the
 289 anaerobic digestion of sewage sludge and, to a lesser extent, in the biogas of OFMSW. Siloxanes
 290 originate from many different industrial processes and consumer products, such as hygiene
 291 products, cosmetics and biopharmaceuticals, fuel additives, car waxes, detergents and antifoams
 292 [45,46]. The influence of siloxanes on SOFC performance has been studied by a few researchers.

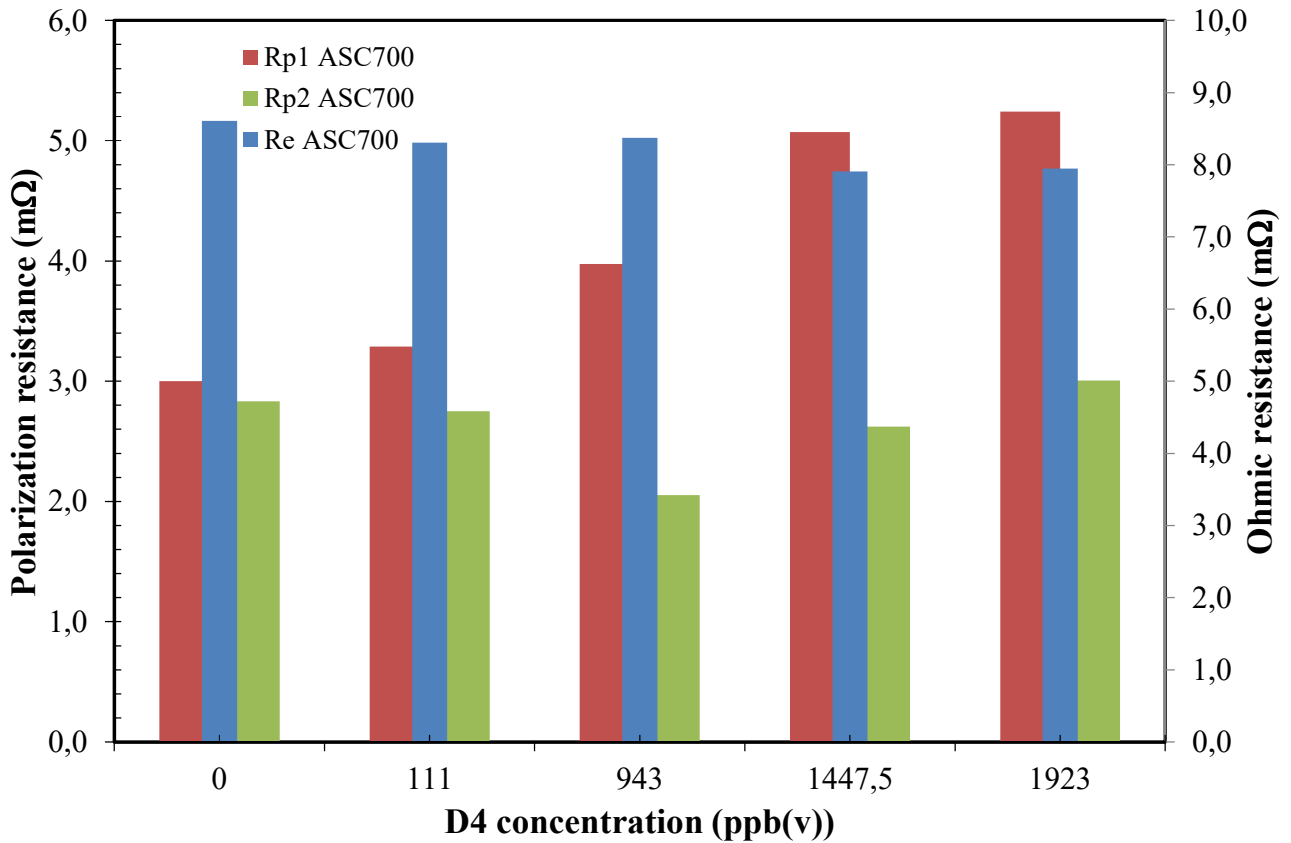
293 Haga et al., (2008) showed that changes in cell voltage occurred when adding 10 ppm(v) of D5 in
294 3%-humidified H₂ at 800 °C, 900 °C, and 1000 °C. The cell voltage decreased gradually in time
295 and, after 30–50 h, resulted in a fatal degradation of the cell performance. This degradation was
296 confirmed from an observation of the formation of SiO₂ (s) in the porous cermet anodes. Madi et al.,
297 (2015) studied the effect of D4 in a single anode based SOFC [20]. The results highlighted an
298 important influence of siloxanes on SOFC performance. In the present study,
299 octamethylcyclotetrasiloxane (D4) was tested with a biogas reformat mixture in a commercial
300 TOFC cell. The concentration ranged from 111 ppb(v) to 1.92 ppm(v). This concentration range
301 was selected to reproduce a possible biogas mixture from a real plant. In fact, data recorded from a
302 real WWTP (SMAT site) showed a D4 concentration that ranged from 0.1 to 0.25 ppm(v) and an
303 L4 concentration that ranged from 0.2 to 0.92 ppm(v). Figure 12 depicts the Nyquist diagram for
304 the TOFC cell fed with a variable D4 concentration. Figure 13 shows the three contributions to the
305 cell losses. As can be seen from the results, if the D4 concentration is increased, the R_{high} value
306 rises, while the other two terms remain constant. The upper right part of Figure 12 shows how the
307 cell performance is irreversibly affected by the D4 test. This is due to silica precipitation, which
308 may cause a decrease in the active triple phase boundary (TPB) areas.



309

310

Figure 12 – Nyquist diagram for variations of the D4 concentration – TOFC.



311

312 **Figure 13 – Re and Rp values for variations of the D4 concentration – TOFC.**

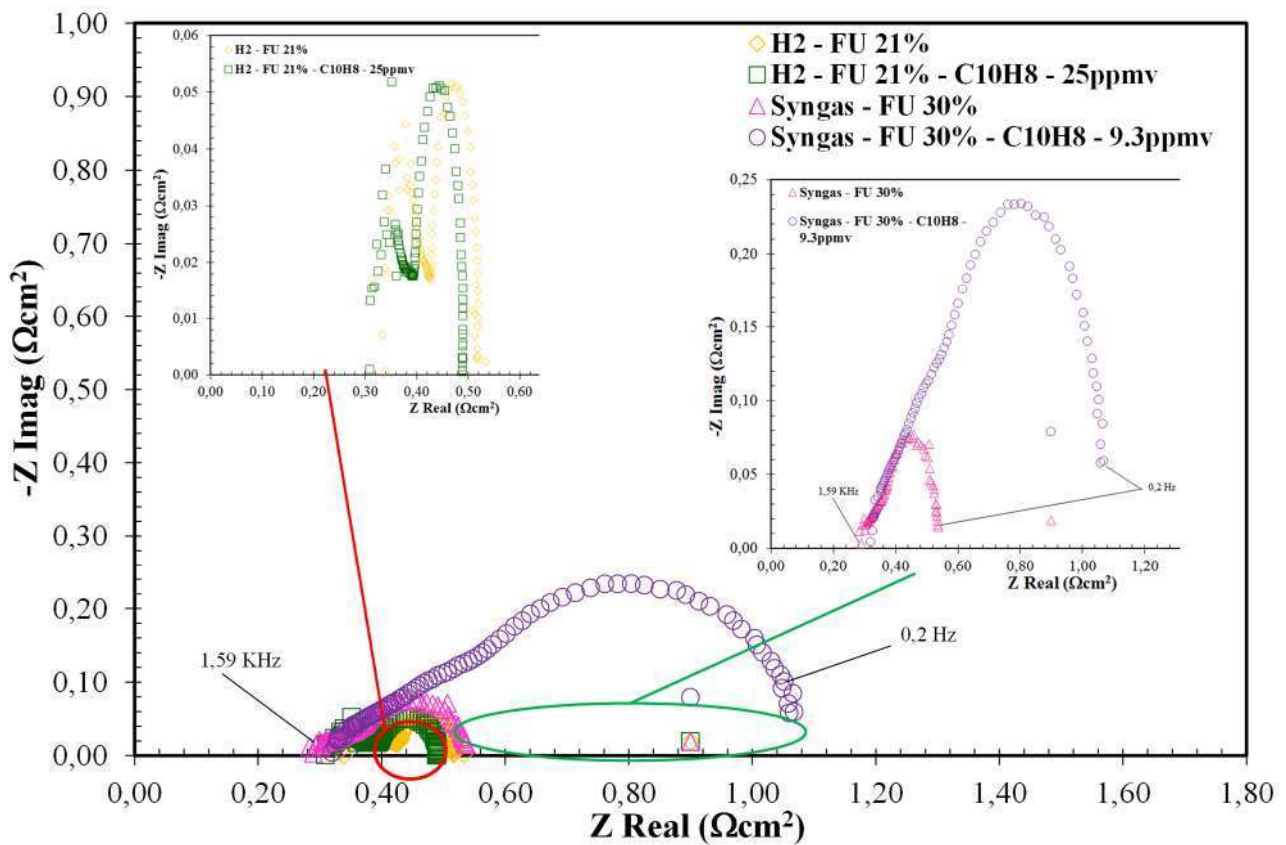
313 If D4 concentrations ranging from 111 to 1923 ppb(v) are considered, the power losses increase for
314 D4 values above 1 ppm(v). The power loss ranges from 0.17 – 2.32 % of the nominal power value.
315 This means that if the exposure time to the pollutants is increased, the electrical power loss will also
316 rise, thereby increasing the resistance value, especially as far as the Rp1 term is concerned.

317 The influence of tars, toluene and naphthalene on SOFC performance

318 Naphthalene

319 The direct use of biosyngas may degrade the performance of SOFCs as it contains a number of
320 minor species. Among these trace species, tars have been identified as one of the main concerns in
321 the development of gasifier + SOFC power systems, as they can potentially deactivate the anode
322 catalysts and degrade the performance of the fuel cells through carbon deposition. Aravind et al.,
323 (2008) studied the performance of an Ni-GDC anode operation with a naphthalene content of about
324 110 ppm(v) in an H₂+N₂ matrix. No performance loss was observed and no carbon or other product
325 gas trace constituent contamination of the anodes was found when the SOFC membranes were
326 examined by means of SEM/EDS after the tests [43].

327 The results reported in this section are in agreement with those of Aravind et al., (2008). An H₂+N₂
328 mixture with a naphthalene content of 25 ppm(v) does not in fact show any remarkable cell
329 performance decrease (see figure 14). If a syngas mixture is instead considered, the cell
330 performance is influenced to a great extent by the C₁₀H₈ content. Figure 14 depicts the Nyquist
331 curves with and without the pollutant concentration. A syngas mixture with 9.3 ppm(v) of C₁₀H₈
332 shows a notable resistance increase.



333

334

Figure 14 – Nyquist diagram for variations of the $C_{10}H_8$ concentration FU 30% – ASC700.

335

In figure 15 the three contributions of loss, are showed: at high, medium and low frequency value.

336

For the H_2 case, the ohmic term (Re) and the polarization terms (R_{p1} and R_{p2}) remain constant

337

throughout the test. This demonstrates that the $C_{10}H_8$ concentration is not a problem in this

338

condition, as also reported in literature studies [43]. On the contrary, if a syngas mixture and a

339

$C_{10}H_8$ concentration of 9.3 ppm(v) are considered, the polarization losses show a significant

340

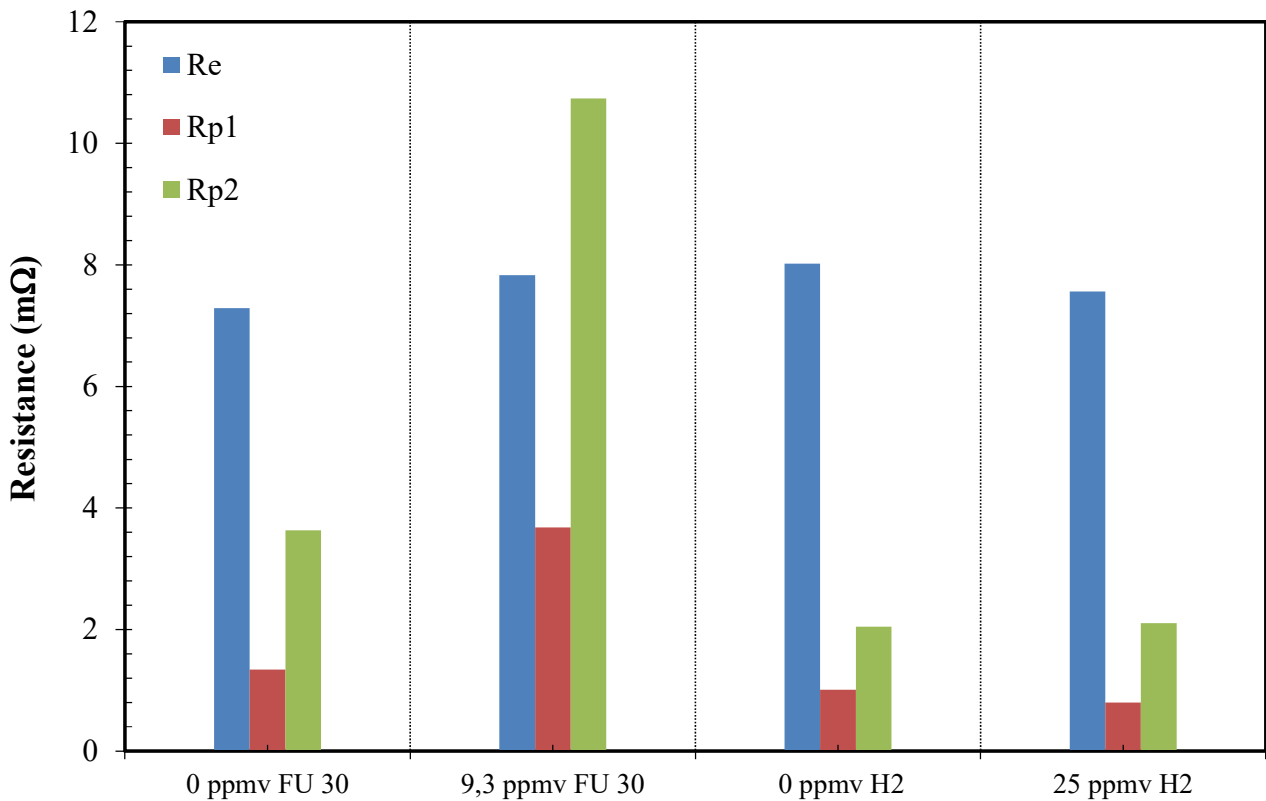
increase. The low frequency term (R_{p2}), related to the resistance of the mass transport phenomena,

341

shows the largest increase. The high frequency term (R_{p1}), related to the electrochemical processes,

342

also increases, but to a lesser extent.



343

344

Figure 15 – Re and Rp values for variations of the C₁₀H₈ concentration – ASC700.

345

These results show how a low C₁₀H₈ concentration could be dangerous, depending on which gas mixture is used to feed the fuel cell. The adsorption and desorption of naphthalene obviously interfere with the reforming of methane and WGS (i.e., CO conversion to H₂) by decreasing the reactive surface of the anodes.

349

If C₁₀H₈ concentrations ranging from 0 to 9.3 ppm(v) are considered, the power losses increase to achieve 15.5% of the nominal power value at zero time. This means that, if the exposure time to the pollutants is increased, the electrical power loss will also rise, thereby increasing the resistance value, especially as far as the Rp2 term is concerned.

353

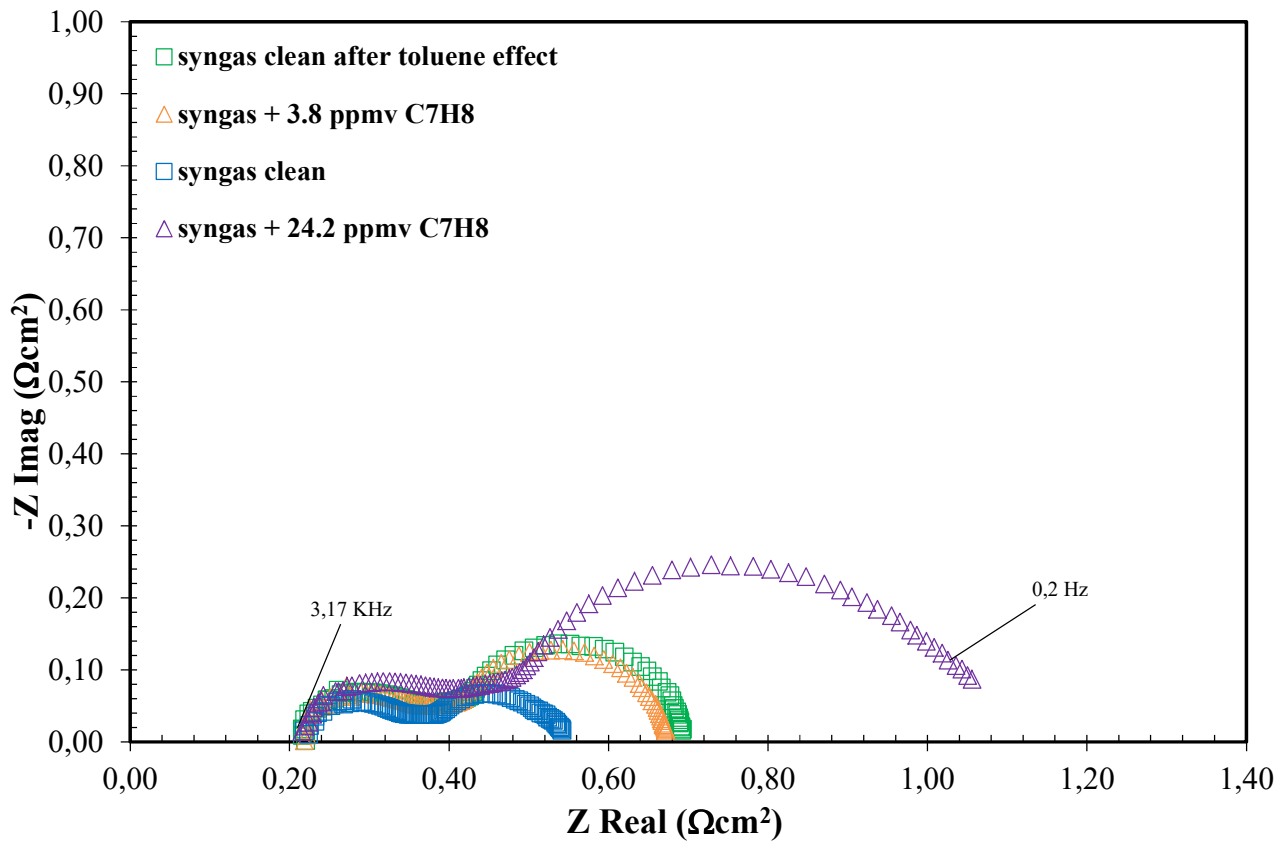
Toluene

354

Toluene is one of the lightest tar compounds and it can be easily detected in biogenous fuels, such as biogas from organic waste [9]. Several studies have investigated the impact of tars on the

355

356 performance of SOFCs [18,43,47–49]. Most of these studies have focused on the influence of the
357 tar compound without considering the carbon content in the gas mixture [18,47,48]. Lorente et al.,
358 (2012) studied Ni/CGO and Ni/YSZ cells under a tar load of 15 g/Nm³ (with toluene as the model
359 compound) [18]. In this study, it was found that Ni/CGO shows a better performance (less carbon
360 formation) than Ni/YSZ in the presence of toluene. This result is in agreement with the expected
361 behavior of ceria-based anodes, which have been recognized to be effective in suppressing carbon
362 deposition due to the redox nature of ceria [50]. The amount of carbon deposited on the catalyst was
363 seen to decrease for an increasing steam content in the gas [18]. Toluene, due to the high reactivity
364 of lower weight hydrocarbons, represents the worst case scenario for tar compounds and for this
365 reason it has been selected in the present study. No attempts have been made to study the effects of
366 low toluene concentrations on SOFC performance. The results of tests on low concentrations of
367 toluene, considering a slip over from a gas cleaning section, are presented in this section. The
368 experimental works have demonstrated that if the most dangerous compounds for SOFCs: sulfurs,
369 aromatic, terpenes and carbonyl compounds, are lowered to just a few ppm(v), the performances of
370 SOFCs remain stable [1].



371

372

Figure 16 – Nyquist diagram for variations of the C₇H₈ concentration – ASC700.

373

Figure 16 shows the Nyquist diagram of a SOFC cell being fed with a syngas mixture with

374

variations in the C₇H₈ concentration. As can be seen, already after 3.8 and 24.2 ppm(v) of toluene,

375

the SOFC performances are irreversibly influenced. In fact, if the toluene content is removed, the

376

impedance curve does not recover the starting value. The ohmic contribution remains unchanged,

377

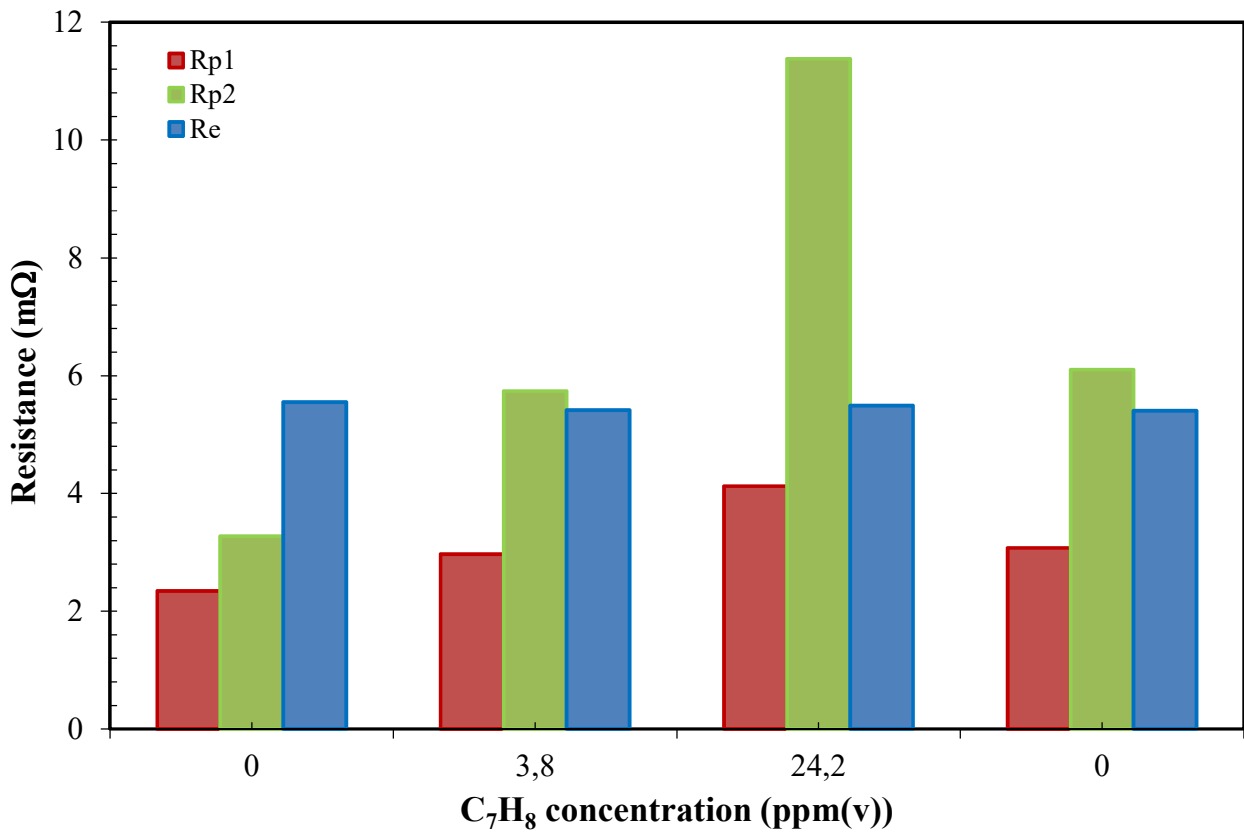
but the polarization losses increase, see figure 17. If the toluene concentration is increased, the

378

polarization losses increase significantly, especially at the low frequency value. This circle is

379

related to the mass transport phenomenon.



380

381

Figure 17 – Re and Rp values for variations of the C₇H₈ concentration – TOFC.

382

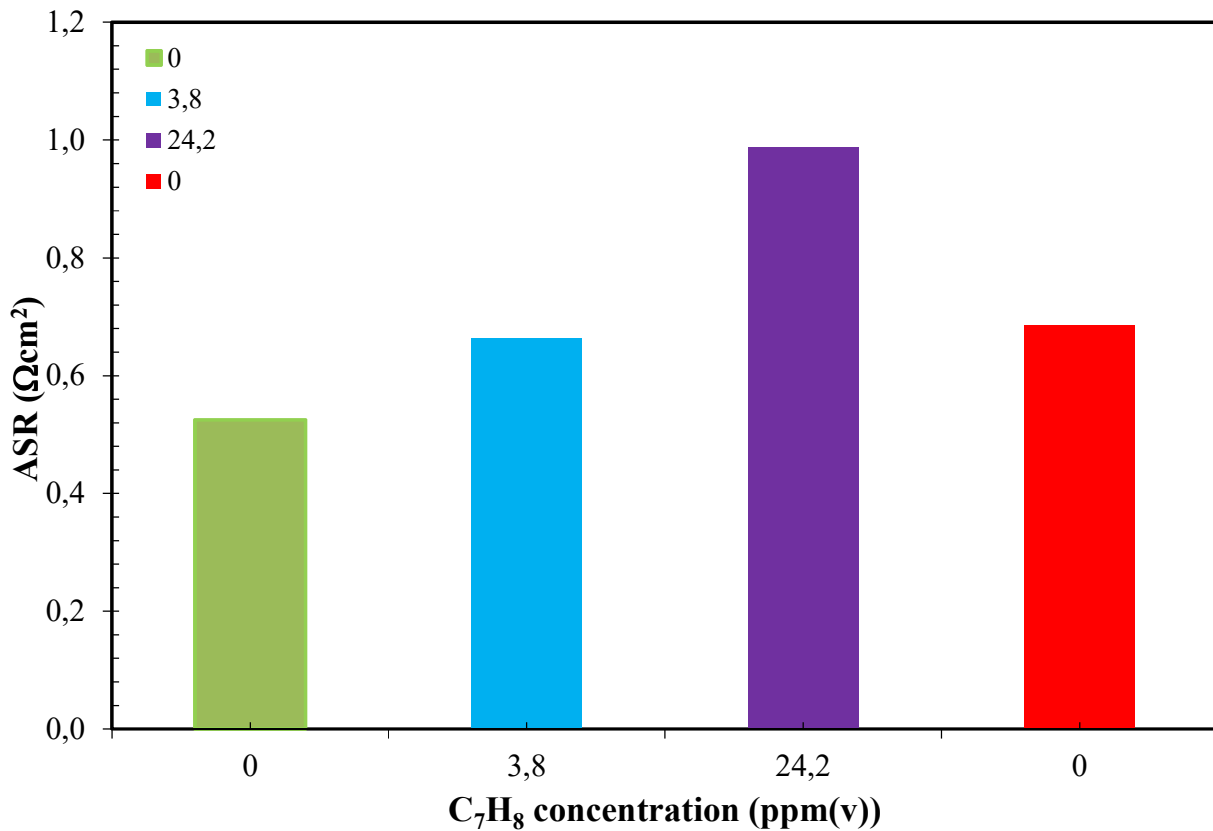
As reported for the naphthalene test, toluene adsorption and desorption obviously interferes with the

383

reforming of methane and WGS (i.e., CO conversion to H₂) by decreasing the reactive surface and

384

SOFC performance.



385

386

Figure 18 – Area specific resistance diagram for variations of the C₇H₈ concentration – ASC700.

387

Figure 18 shows the ASR values. A slight increase in the ASR can be observed at 3.8 ppm(v) –

388

which is an almost tolerable limit for SOFC performance – but if the toluene concentration

389

increases to 24.2 ppm(v), the performance decreases to a great extent (+40% losses).

390

If C₇H₈ concentrations ranging from 0 to 24.2 ppm(v) are considered, the power losses increase to

391

achieve 14.58% of the nominal power value at zero time. This means that if the exposure time to the

392

pollutants is increased, the electrical power loss will also rise, thereby increasing the resistance

393

value, especially as far as the Rp2 term is concerned.

394

The influence of ethylene Hydrocarbons on SOFC performance

395

Ethylene is a common hydrocarbon that can be detected in almost all biogenous fuels. Ethylene is a

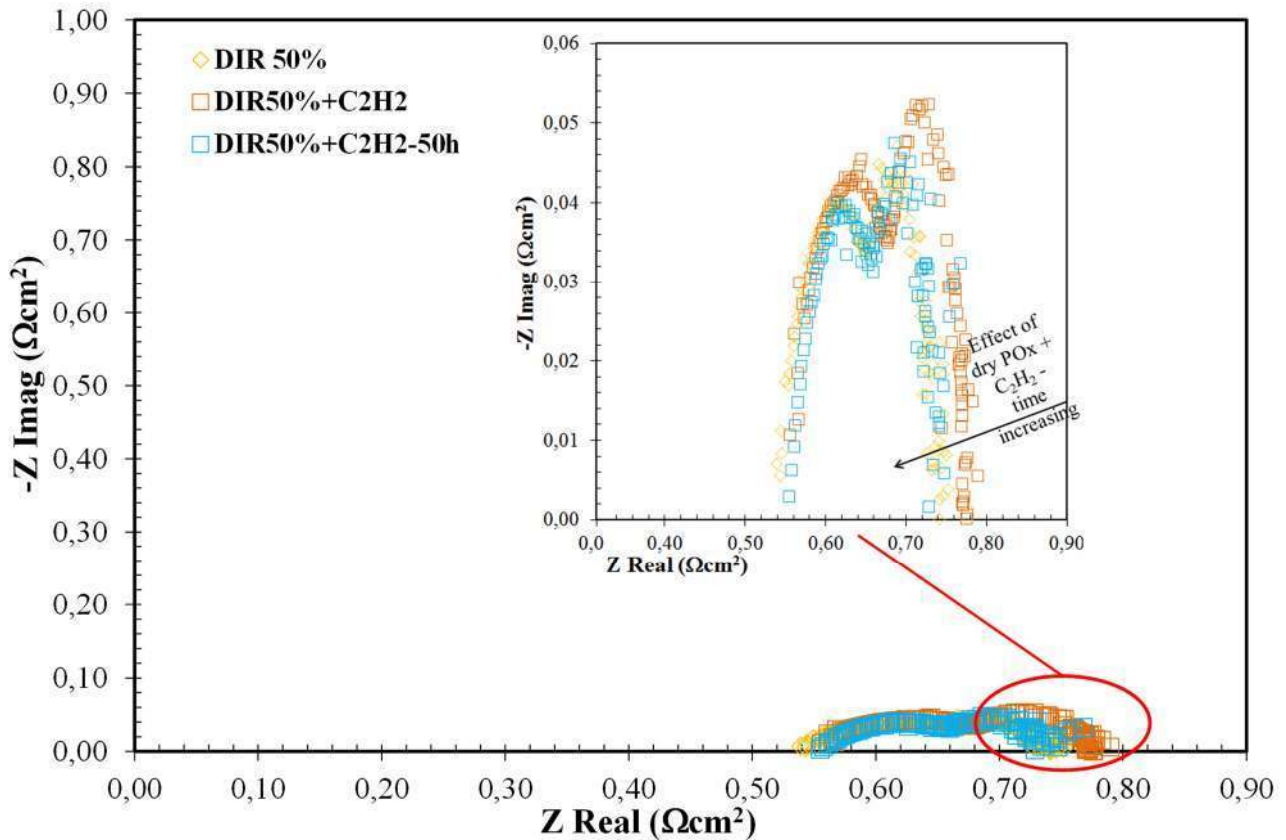
396

fuel like methane, and like the latter it has to be reformed into hydrogen and carbon monoxide.

397

Ethylene concentrations above a certain level, which mainly depends on the operating temperature,

398 are difficult to reform. The steam reforming of ethylene is dealt with in this section, considering a
399 concentration value that is representative of a biogas obtained from organic waste digestion. Figure
400 19 shows the impedance spectra of two gas mixtures containing 0 ppm(v) of ethylene and 371.2
401 ppm(v) of C₂H₂. By observing the zoom window, it can be seen that ethylene does not influence
402 SOFC performance negatively.

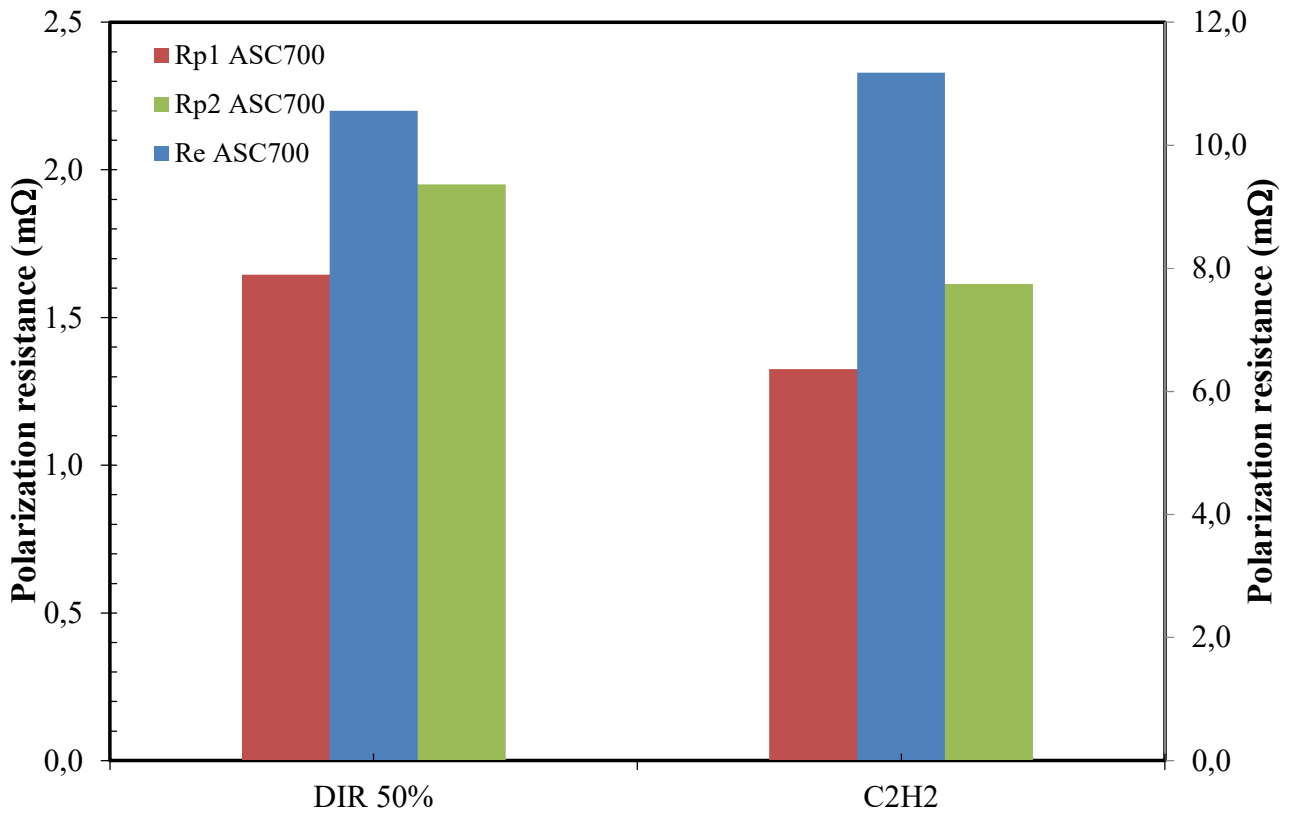


403

404

Figure 19 – Nyquist diagram for variations of the C₂H₂ concentration – ASC700.

405 Figure 20 depicts the contribution of the performance losses. Instead of increasing the polarization
406 losses, ethylene improves SOFC performance. This is due to the increase in the available
407 electrochemical fuel, which is caused by an improvement in the reforming reactions.



408

409

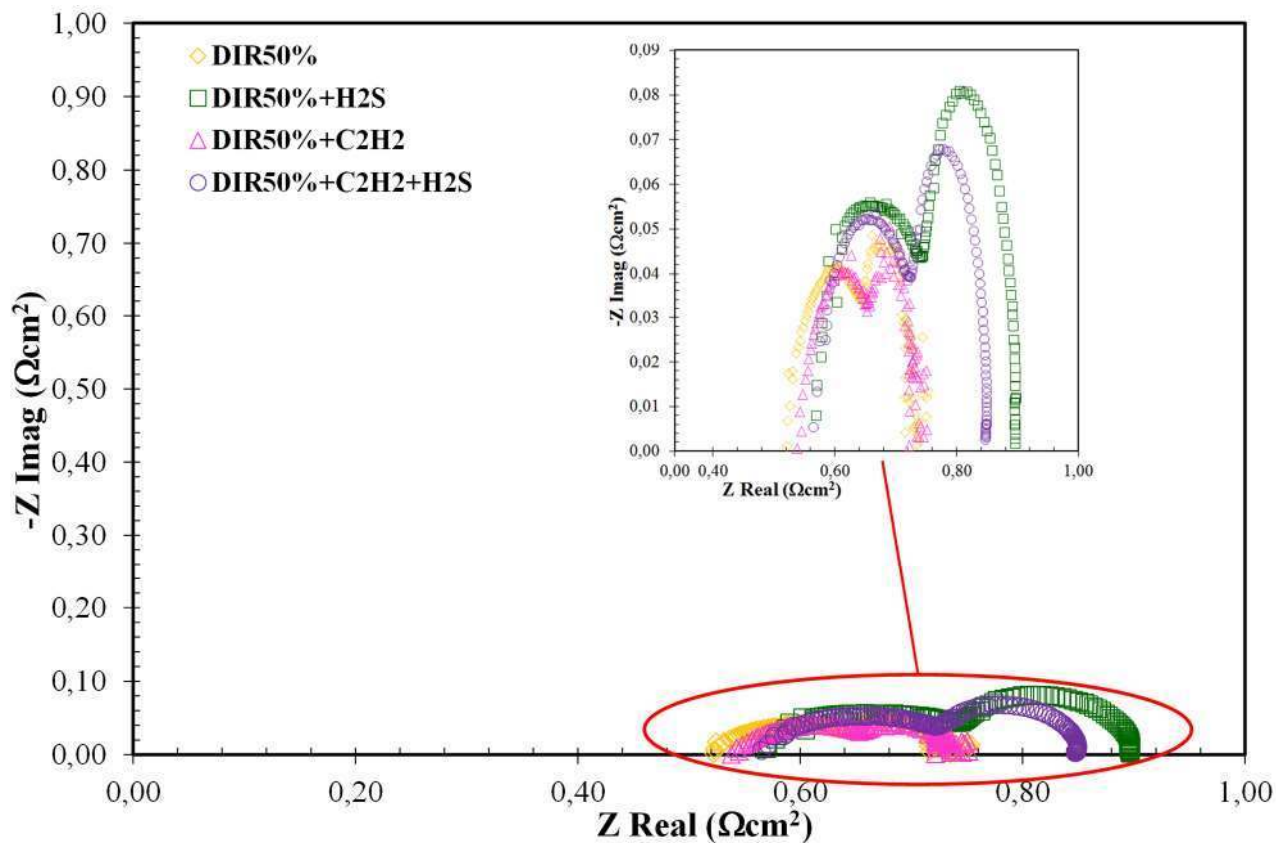
Figure 20 – Re and Rp values for variations of the the C₂H₂ concentration – ASC700.

410 The influence of Multi concentrations on SOFC performance

411 Since the H₂S concentration has been considered as the most dangerous compound for SOFCs, its
 412 contemporary presence with other trace compounds has been studied.

413 H₂S + C₂H₂

414 The addition of a hydrogen sulfide content of 1.34 ppm(v) to a gas mixture influences the SOFC
 415 performance. An increase in the total ASR value has been registered, see figure 21. The H₂S
 416 concentration mainly affects the mass transport phenomena and the electrochemical processes, thus
 417 reducing the TPB areas, as reported in figure 22.



418

419

Figure 21 – Nyquist diagram for variations of the C₂H₂ and C₂H₂+H₂S concentrations – ASC700.

420

If a C₂H₂ concentration of 371.2 ppm(v) is added to the H₂S concentration, the total losses decrease,

421

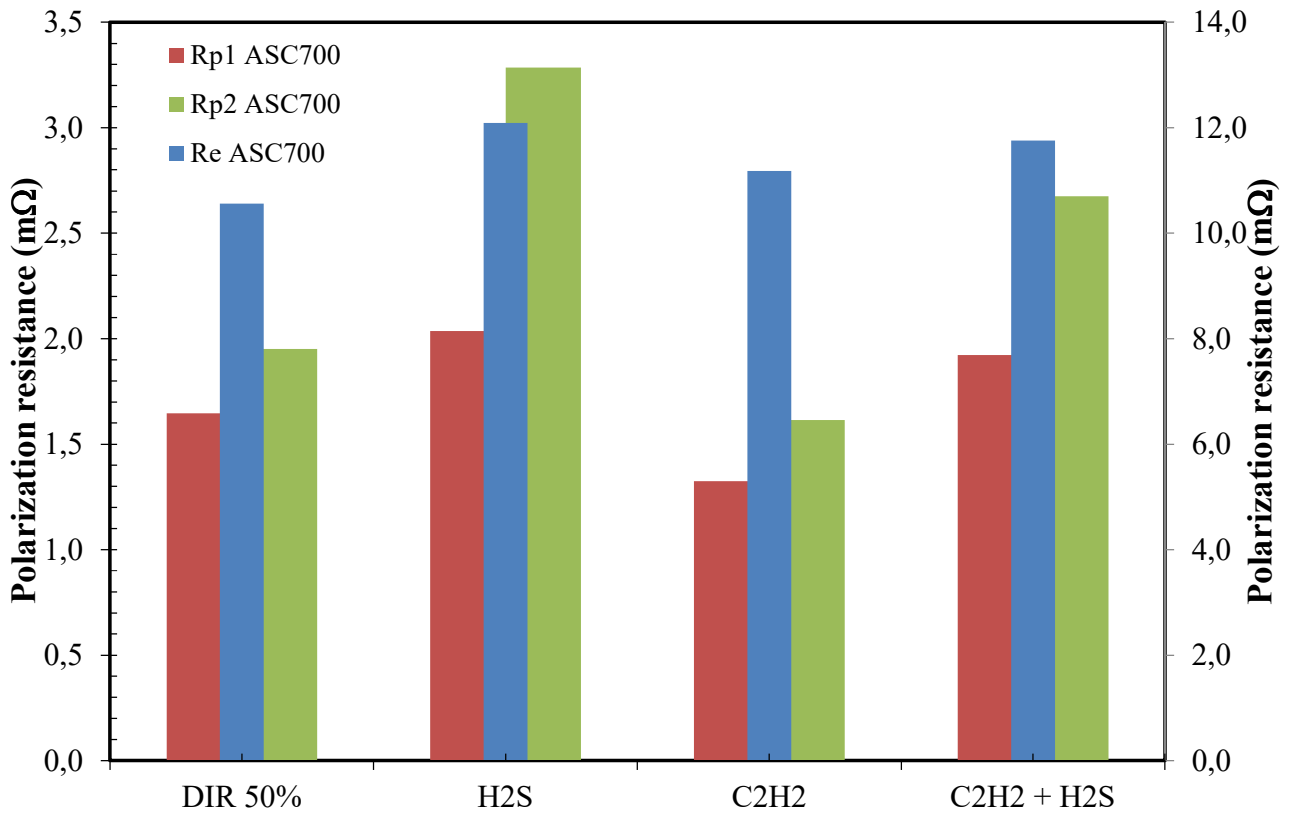
see figure 20. C₂H₂ affects the reduction of the polarization losses and in particular the mass

422

transport resistance, see figures 22 and 23.

423

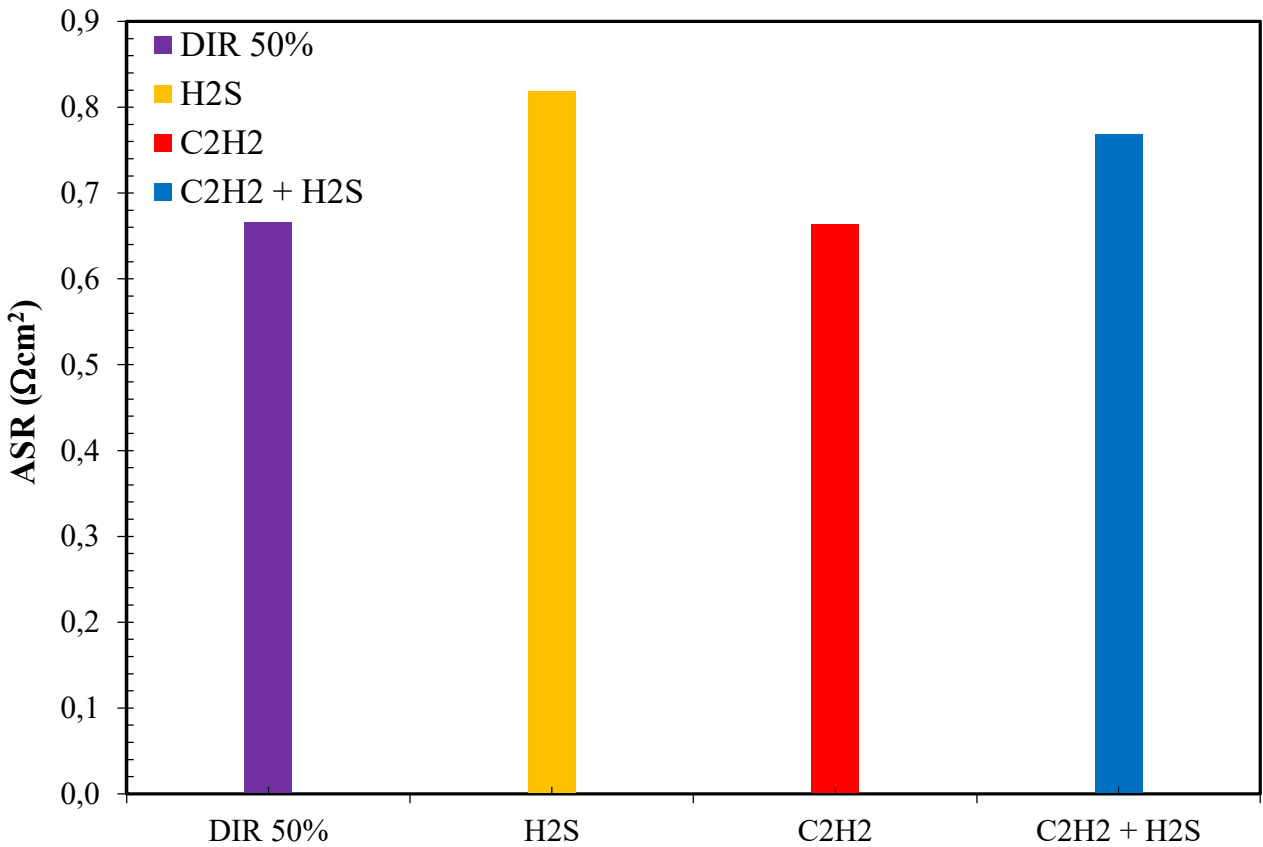
424



425

426

Figure 22 – Re and Rp values for variations of the C₂H₂ and C₂H₂+H₂S concentration – ASC700.

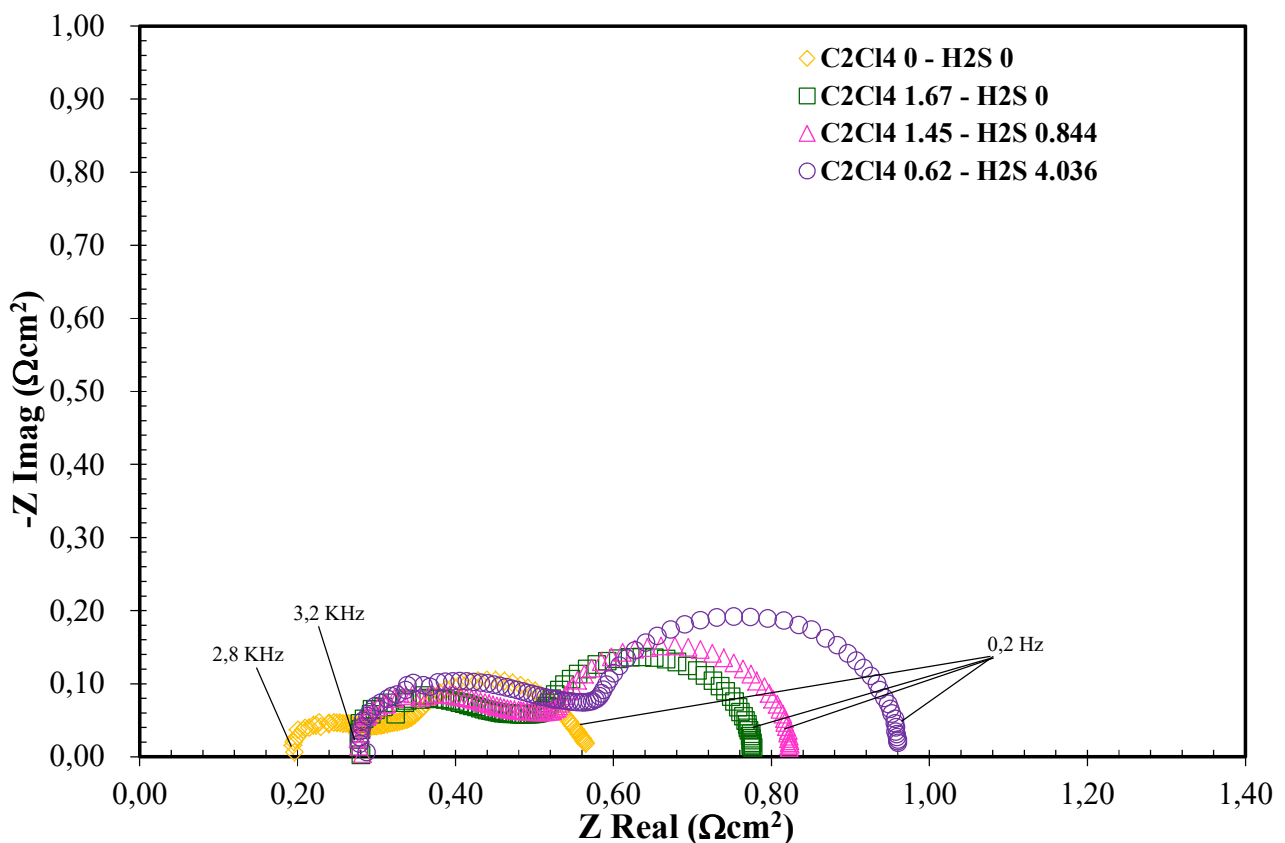


427

428 **Figure 23 – Area specific resistance diagram for variations of the C_2H_2 and $C_2H_2+H_2S$ concentrations – ASC700.**
429 The ASR values are influenced positively by the C_2H_2 concentration, and a reduction in the double
430 compound case is registered for H_2S .

431 $H_2S + C_2Cl_4$

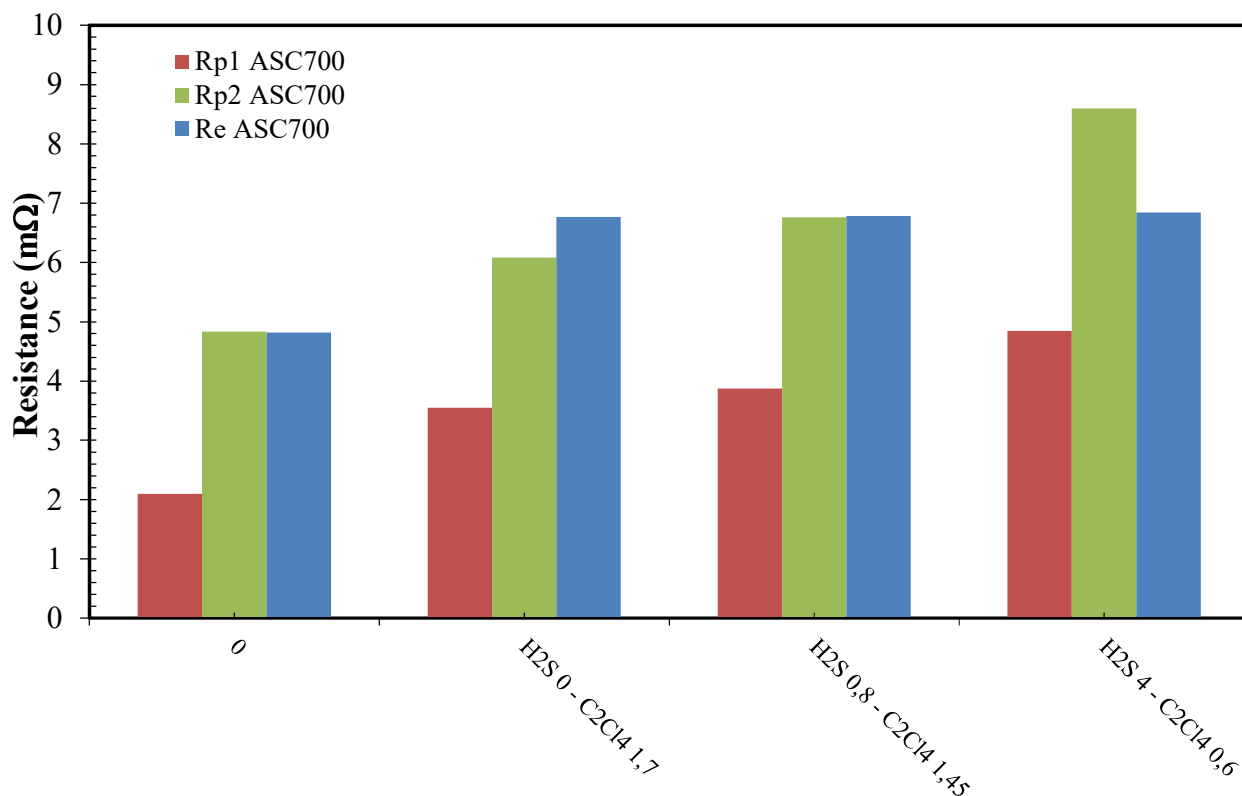
432 As previously mentioned, H_2S is the most detrimental compound, and the addition of chlorine has
433 therefore been studied. Tetrachloroethylene (TCE) is a chloro compound that can be detected in a
434 biogenous fuel, especially from waste water sludges. The possible implications of the inclusion of
435 this compound on SOFC performance have been studied and the results are presented in this
436 section. Concentrations ranging from 0.62 to 1.67 ppm(v) of TCE and 4 to 0 ppm(v) of H_2S have
437 been considered.



438

439 **Figure 24 – Nyquist diagram for variations of the $C_2Cl_4+H_2S$ concentration – ASC700.**

440 If the spectra obtained from the clean condition (C_2Cl_4 -0 ppm(v) + H_2S -0 ppm(v)) are compared
 441 with those of the other gas mixture, it can be seen that the ohmic part rises by the same quantity in
 442 all three mixtures. This result is related to the different electrochemical molar fuel contents. As
 443 reported in figure 25, the ohmic contribution remains constant in the double contaminant case. The
 444 polarization losses increase the most for the highest H_2S concentration case. This shows how the
 445 sulfur compound is a heavier contaminant than chlorine. C_2Cl_4 acts mainly on the high frequency
 446 polarization term, that is, on the electrochemical processes caused by the adsorption/desorption
 447 behavior of chlorine. The term related to the transport phenomena is instead influenced more by the
 448 sulfur compound.

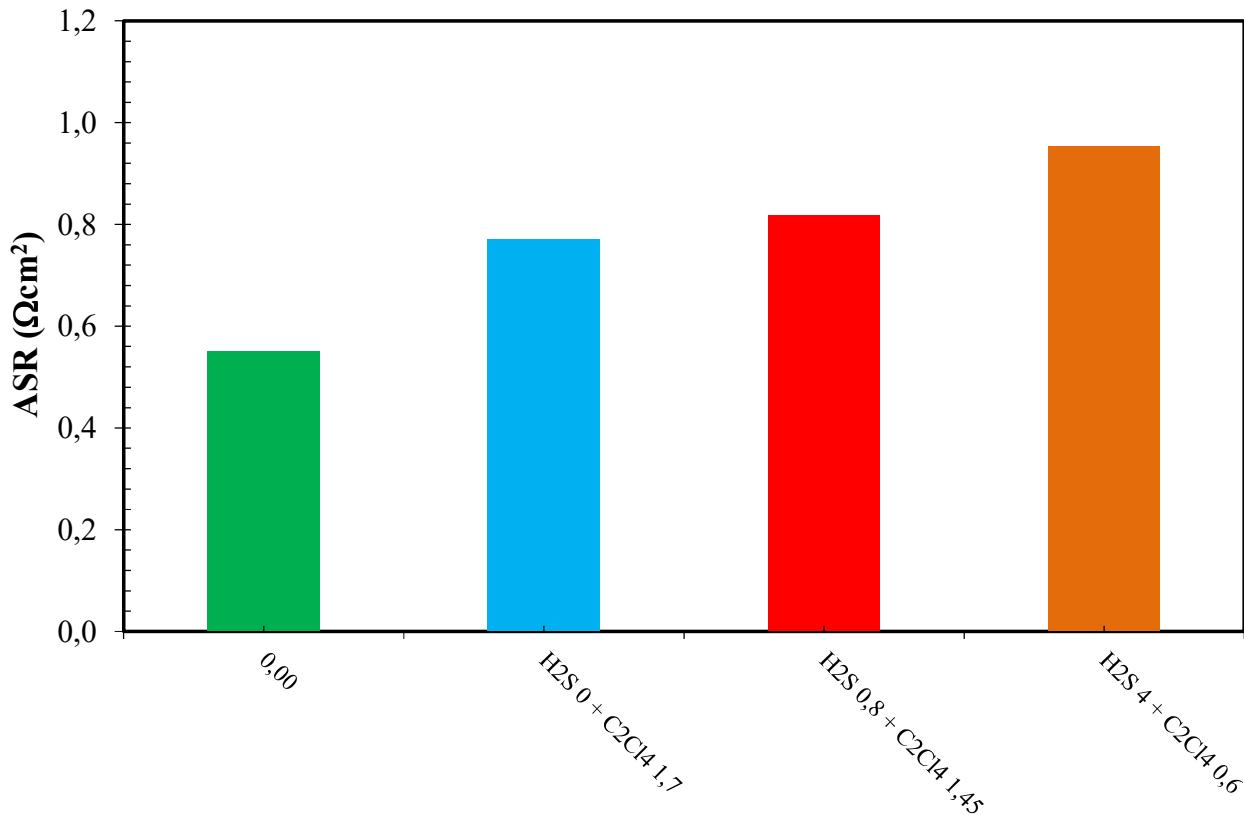


449

450 **Figure 25 – Re and Rp values for variations of the $C_2Cl_4+H_2S$ concentration – ASC700.**

451 The worst case scenario for the SOFC performance is related to the sulfur compound content, as
 452 reported in figure 25, where the highest ASR value is achieved. If the H_2S 4 ppm(v) + C_2Cl_4 0.6

453 ppm(v) case is compared with the H₂S 4 ppm(v) case, it can be seen that chlorine does not cause a
454 deterioration of the cell performance.



455

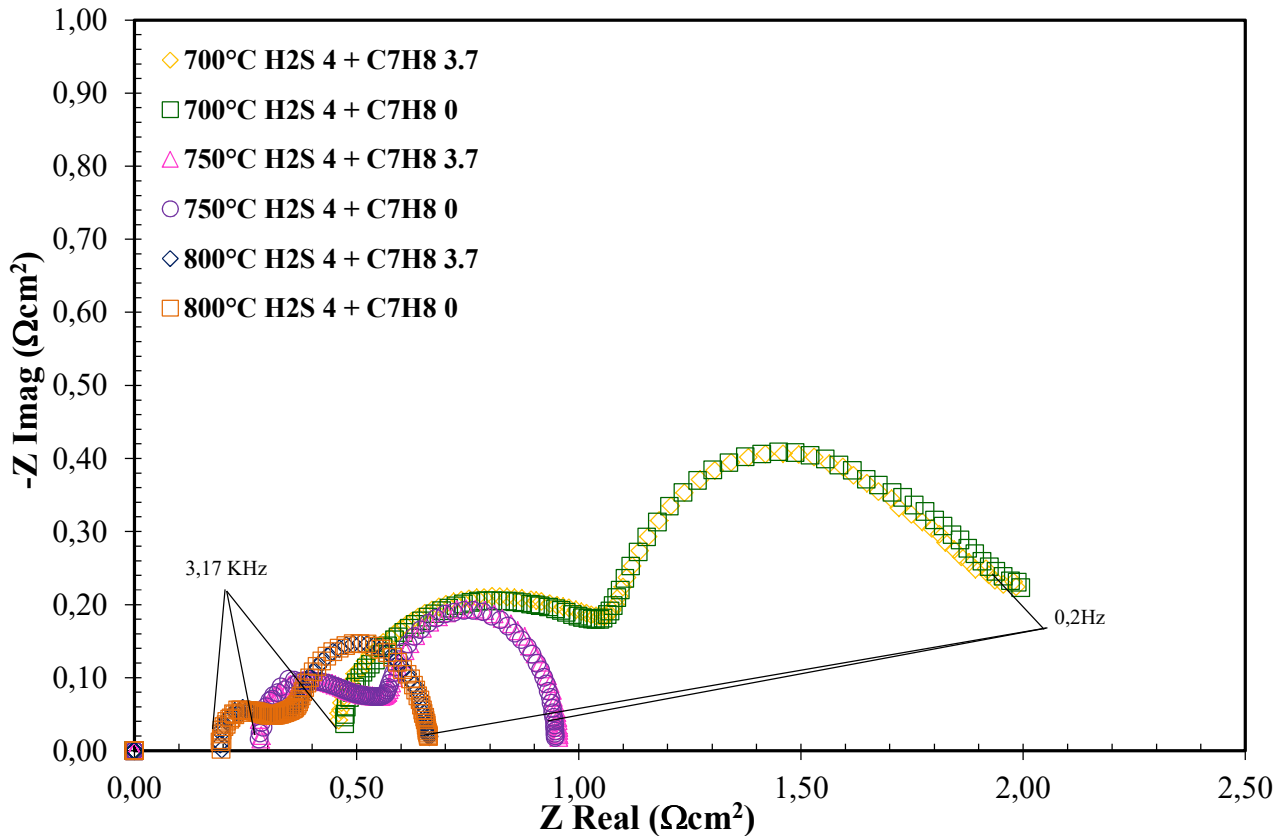
456 **Figure 26 – Area specific resistance diagram for variations of the C₂Cl₄+H₂S concentration – ASC700.**

457 The power loss increases directly as H₂S concentration increases until it reaches 12.86% of the
458 nominal power value at zero time. This means that if the exposure time to the pollutants is
459 increased, the electrical power loss will also rise, thereby increasing the resistance value, especially
460 as far as the Rp2 term is concerned. The contemporary presence of C₂Cl₄ and H₂S causes a two-fold
461 power loss compared to the single pollutant case.

462 H₂S + C₇H₈

463 Figure 27 depicts the Nyquist diagram for the case of the contemporary presence of H₂S and C₇H₈.
464 The concentration of H₂S was fixed at 4 ppm(v), while C₇H₈ was fixed at 3.7 ppm(v). The test was
465 conducted by adding or not adding the toluene concentration at three different temperatures. It has

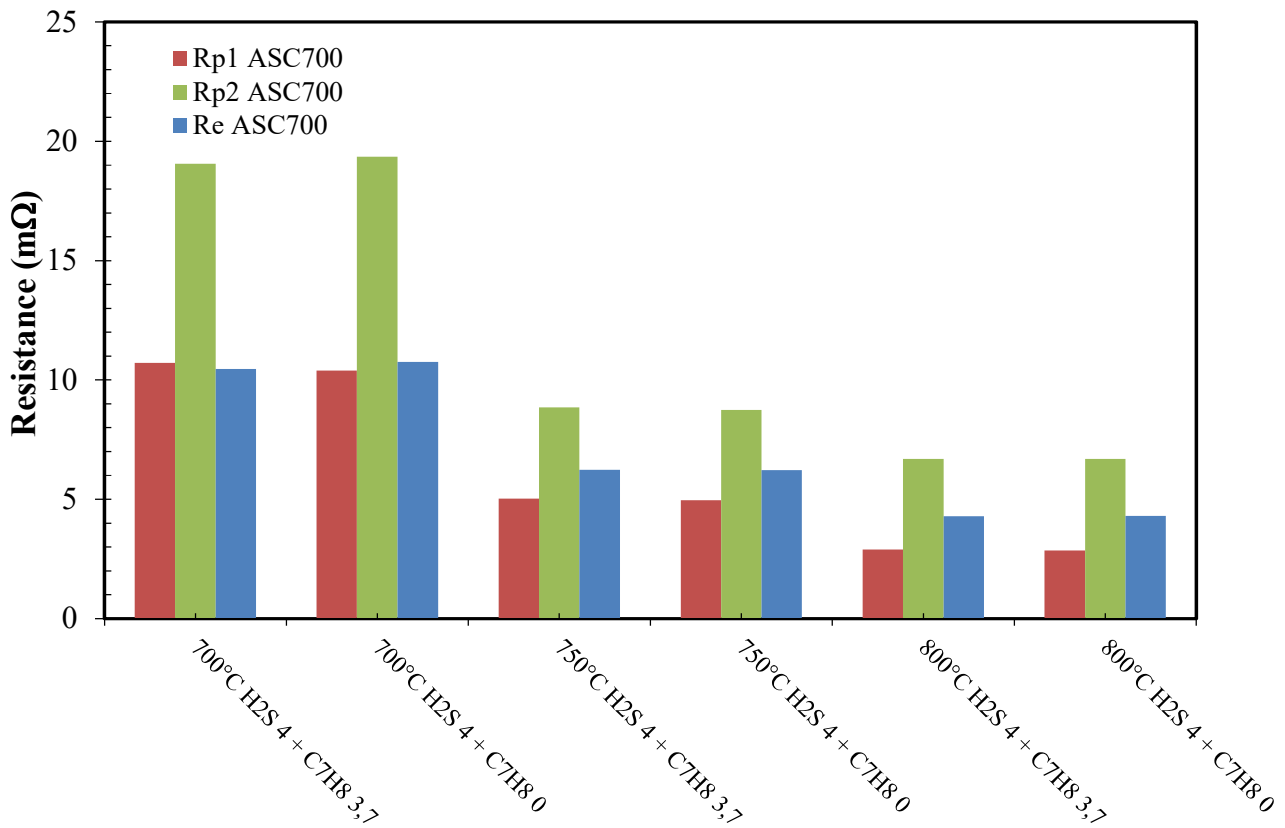
466 been observed that the toluene concentration affects the SOFC performance to a lesser extent than
 467 the temperature. Figures 27, 28 and 29 show that when the operating temperature is decreased, an
 468 increase in the cell resistance is registered. This is caused by a decrease in the electronic
 469 conductivity of the electrodes and in the ionic conductivity of the cell layer. This is especially true
 470 for the electrolyte layer, but also for the composite electrodes.



471

472 **Figure 27 – Nyquist diagram for variations of the H₂S + C₇H₈ concentration – ASC700.**

473 Figure 28 shows the three term losses considered singularly; R_{high} is the only contribution that
 474 seems to be affected by the addition of toluene to the gas mixture in which H₂S is already present.
 475 This percentage increases as the operating temperature decreases. Moreover, the electrochemical
 476 reaction kinetics is slowed down, and this leads to an increase in the activation polarization
 477 resistance. Finally, the diffusion capability of the chemical species is reduced both on the bulk flow
 478 in the channels and on the porous electrodes.



479

480

Figure 28 – Re and Rp values for variations of the H₂S + C₇H₈ concentration – ASC700.

481

The ASR value is affected more by the temperature variation than by the contemporary presence of

482

toluene and hydrogen sulfide. Even in this case, the sulfur concentration weighs more than the

483

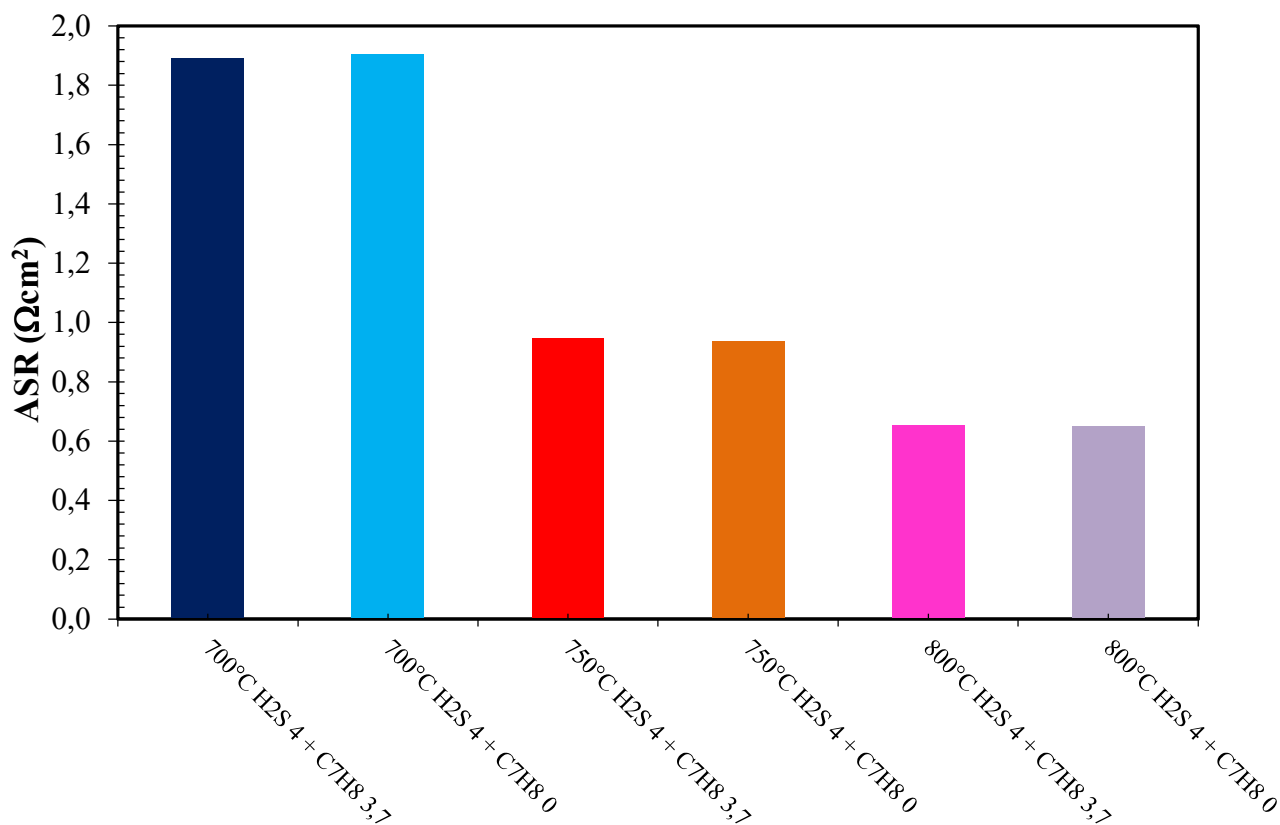
toluene concentration at the same operating temperature. The toluene concentration needs to be

484

increased before significant effects on the SOFC performance can be observed, but this condition is

485

not realistic of a real clean up gas condition used to feed a SOFC system.



486

487 **Figure 29 – Area specific resistance diagram for variations of the H₂S + C₇H₈ concentration – ASC700.**

488 **Conclusions**

489 This paper has investigated the performance of an anode supported solid oxide fuel cell considering
 490 a wide range of trace compounds. These compounds are found in biogenous fuels, such as biogas
 491 from OFMSW or from sewage sludge: H₂S, HCl, D4, C₁₀H₈, C₇H₈, C₂H₂, C₂Cl₄. Various
 492 concentrations of Hydrogen sulfide have been studied in three tests. The first two tests considered
 493 high and low concentration ranges, thus simulating an early breakthrough slip from the clean-up
 494 section under operation with digester biogas. The third test considered the literature threshold limit
 495 for SOFCs (≈1 ppm(v)). The effect of Chlorine has been tested for variable concentrations of HCl,
 496 ranging from 1 to 1000 ppm(v). The effect of Siloxanes on SOFC performance has been studied
 497 considering concentrations ranging from 111 ppb(v) to 1.9 ppm(v), in order to simulate a clean-up
 498 section slip. In the same way, C₁₀H₈ and C₇H₈ have been tested on SOFC performance and in a

499 double compound condition test ($C_2H_2+H_2S$, $C_2Cl_4+H_2S$ and $C_7H_8+H_2S$). All these tests have been
500 conducted to simulate possible biogas conditions that could arise from biological matter.

501 Electrochemical impedance spectroscopy has been used to study an SOFC cell in order to identify
502 the main contribution to the cell losses from trace compound contaminations. This was done with an
503 electrical equivalent circuit constituted by an ohmic resistance, R_e , and two parallel combinations
504 of a resistance and a constant phase element, CPE. The polarization resistance, R_p , related to the
505 concentration and activation polarizations, has been obtained from the sum of the low and high
506 frequency resistances. The different sources of performance limitation have been obtained from fuel
507 cell impedance considering the action of different trace compounds.

508 In particular it has been found that:

- 509 ▪ The ohmic contribution is almost independent of the fuel composition and it is only affected
510 minimally by the H_2S concentration. However, this contribution is influenced by the
511 modification of the nickel grain caused by cell operation with an H_2S concentration, as also
512 reported by Ivey et al., (2010) [51]. The electrochemical fuel content of hydrocarbons can
513 influence this term: lower values are achieved in an H_2 condition, compared to the same
514 electrochemical molar value in a $CH_4 + CO$ condition.
- 515 ▪ The H_2S concentration mainly affects the polarization losses, especially the mass transport
516 resistance through the electrodes caused by the sulfur blocking sites. The three-phase boundary
517 decreases as a consequence of the sulfur action on nickel active sites.
- 518 ▪ Ultra low concentrations of sulfur, around 100 – 200 ppb(v), do not cause any changes in the
519 loss terms.
- 520 ▪ The influence of HCl on SOFC performance is mainly due to the increase in R_{high} , related to the
521 electrochemical processes that occur at the electrodes. Below 40 ppm(v), HCl concentrations
522 only have a slight influence on the SOFC performance.

- 523 ▪ D4, a model compound for siloxanes, already acts on SOFC performance at ppb(v) levels. The
524 term that is influenced most is R_{high} , thus highlighting the action of siloxanes on SOFC
525 performance. In fact, these compounds, together with the formation of silica oxide in the anode
526 cermet, reduce the porosity and the flow of the fuel toward the active sites, and thus limit the
527 energy generation of a SOFC.
- 528 ▪ Naphthalene and toluene have been considered as model compounds for tars. No performance
529 losses have been observed in an H_2 mixture. When a syngas mixture was considered, it was
530 observed that even 9.3 ppm(v) of C_{10}H_8 can reduce SOFC performance. The polarization losses
531 are those that are influenced the most, and the largest increase has been recorded for the low
532 frequency term R_{p2} , related to mass transport resistance. The same behavior has been observed
533 for the toluene case.
- 534 ▪ The tested concentrations of ethylene have been shown to positively influence SOFC
535 performance and, at the same time, to limit the action of H_2S in a case in which two
536 contaminants were considered together.
- 537 ▪ H_2S , introduced with other contaminants (C_2Cl_4), has led to an increased instantaneous
538 deterioration, and the more types of contaminants included, the larger the initial deterioration.
- 539 ▪ H_2S , introduced with another contaminant (C_7H_8), has shown how the operating temperature has
540 more influence than 3.7 ppm(v) of toluene.

541 The worst case scenario is represented by the presence of higher H_2S concentrations than 1 ppm(v)
542 and by the presence of D4 already at the ppb(v) level. The contemporary presence of these
543 compounds has led to an increase in the detrimental effects on SOFC performance, and even to fatal
544 cell degradation.

545

546

547 **Acknowledgments**

548 This work has been partly funded by the European Union under the SOFCOM project
549 (www.sofcom.eu, contract number 278798). In addition, this research has been conducted as a part
550 of the BioWaste for SOFCs (BWS) project carried out together with Fondazione Edmund Mach and
551 SOLIDpower SpA. The project has been funded with the contribution of Fondazione Caritro (TN).

552

553

554

555

556

557

558

559

560

561

562

563

564

565

566

567 **References**

- 568 [1] D. Papurello, A. Lanzini, L. Tognana, S. Silvestri, M. Santarelli, Waste to energy:
569 Exploitation of biogas from organic waste in a 500 W solid oxide fuel cell (SOFC) stack,
570 Energy. 85 (2015) 145–158. doi:10.1016/j.energy.2015.03.093.
571
- 572 [2] A.J. Appleby, Fuel cell technology: Status and future prospects, Energy. 21 (1996) 521–653.
573 doi:10.1016/0360-5442(96)00030-8.
574
- 575 [3] D.D. Papadimas, S. Ahmed, R. Kumar, Fuel quality issues with biogas energy - An economic
576 analysis for a stationary fuel cell system, Energy. 44 (2012) 257–277.
577 doi:10.1016/j.energy.2012.06.031.
578
- 579 [4] S.W. (Volume E. Narottam P. Bansal (Editor), Mihails Kusnezoff (Editor), Soshu Kirihara
580 (Volume Editor), Advances in Solid Oxide Fuel Cells IV: Ceramic Engineering and Science
581 Proceedings, 2013.
582
- 583 [5] K. Sasaki, K. Haga, T. Yoshizumi, D. Minematsu, E. Yuki, R. Liu, et al., Chemical durability
584 of Solid Oxide Fuel Cells: Influence of impurities on long-term performance, J. Power
585 Sources. 196 (2011) 9130–9140. doi:10.1016/j.jpowsour.2010.09.122.
586
- 587 [6] D. Papurello, A. Lanzini, P. Leone, M. Santarelli, S. Silvestri, Biogas from the organic
588 fraction of municipal solid waste: Dealing with contaminants for a solid oxide fuel cell
589 energy generator, Waste Manag. (2014).
590
- 591 [7] E. Bocci, A. Di Carlo, S.J. McPhail, K. Gallucci, P.U. Foscolo, M. Moneti, et al., Biomass to
592 fuel cells state of the art: A review of the most innovative technology solutions, Int. J.
593 Hydrogen Energy. 39 (2014) 21876–21895. doi:10.1016/j.ijhydene.2014.09.022.
594
- 595 [8] D. Thimsen, Gas Fueled Power Generation, 3 (2006).
596
- 597 [9] D. Papurello, C. Soukoulis, E. Schuhfried, L. Cappellin, F. Gasperi, S. Silvestri, et al.,
598 Monitoring of volatile compound emissions during dry anaerobic digestion of the Organic
599 Fraction of Municipal Solid Waste by Proton Transfer Reaction Time-of-Flight Mass
600 Spectrometry, in: Bioresour. Technol., 2012: pp. 254–265.
601
- 602 [10] D. Papurello, E. Schuhfried, A. Lanzini, A. Romano, L. Cappellin, T.D. Märk, et al.,
603 Influence of co-vapors on biogas filtration for fuel cells monitored with PTR-MS (Proton
604 Transfer Reaction-Mass Spectrometry), Fuel Process. Technol. 118 (2014) 133–140.
605
- 606 [11] D. Papurello, L. Tognana, A. Lanzini, F. Smeacetto, M. Santarelli, I. Belcari, et al., Proton
607 transfer reaction mass spectrometry technique for the monitoring of volatile sulfur
608 compounds in a fuel cell quality clean-up system, Fuel Process. Technol. 130 (2015) 136–
609 146. doi:10.1016/j.fuproc.2014.09.041.

610

- 611 [12] L. Sigot, G. Ducom, B. Benadda, C. Labouré, Comparison of adsorbents for H₂S and D4
612 removal for biogas conversion in a solid oxide fuel cell, *Environ. Technol.* 3330 (2015) 1–10.
613 doi:10.1080/09593330.2015.1063707.
614
- 615 [13] A. Weber, S. Dierickx, A. Kromp, E. Ivers-Tiffée, Sulfur poisoning of anode-supported
616 SOFCs under reformat operation, *Fuel Cells*. 13 (2013) 487–493.
617 doi:10.1002/fuce.201200180.
618
- 619 [14] A. Hauch, A. Hagen, J. Hjelm, T. Ramos, Sulfur Poisoning of SOFC Anodes: Effect of
620 Overpotential on Long-Term Degradation, *J. Electrochem. Soc.* 161 (2014) F734–F743.
621 doi:10.1149/2.080406jes.
622
- 623 [15] D. Papurello, A. Lanzini, S. Fiorilli, F. Smeacetto, R. Singh, M. Santarelli, Sulfur poisoning
624 in Ni-anode solid oxide fuel cells (SOFCs): Deactivation in single cells and a stack, *Chem.*
625 *Eng. J.* 283 (2016) 1224–1233. doi:10.1016/j.cej.2015.08.091.
626
- 627 [16] A.L. da Silva, N.C. Heck, Thermodynamics of sulfur poisoning in solid oxide fuel cells
628 revisited: The effect of H₂S concentration, temperature, current density and fuel utilization,
629 *J. Power Sources*. 296 (2015) 92–101. doi:10.1016/j.jpowsour.2015.07.046.
630
- 631 [17] M. Błesznowski, J. Jewulski, A. Zieleniak, Determination of H₂S and HCl concentration
632 limits in the fuel for anode supported SOFC operation, *Cent. Eur. J. Chem.* 11 (2013) 960–
633 967. doi:10.2478/s11532-013-0228-1.
634
- 635 [18] E. Lorente, M. Millan, N.P. Brandon, Use of gasification syngas in SOFC: Impact of real tar
636 on anode materials, *Int. J. Hydrogen Energy*. 37 (2012) 7271–7278.
637 doi:10.1016/j.ijhydene.2011.11.047.
638
- 639 [19] K. Haga, S. Adachi, Y. Shiratori, K. Itoh, K. Sasaki, Poisoning of SOFC anodes by various
640 fuel impurities, *Solid State Ionics*. 179 (2008) 1427–1431. doi:10.1016/j.ssi.2008.02.062.
641
- 642 [20] H. Madi, A. Lanzini, S. Diethelm, D. Papurello, J. Van herle, M. Lualdi, et al., Solid oxide
643 fuel cell anode degradation by the effect of siloxanes, *J. Power Sources*. 279 (2015) 460–471.
644 doi:10.1016/j.jpowsour.2015.01.053.
645
- 646 [21] M.J. Jørgensen, S. Primdahl, M. Mogensen, Characterisation of composite SOFC cathodes
647 using electrochemical impedance spectroscopy, *Electrochim. Acta*. 44 (1999) 4195–4201.
648 doi:10.1016/S0013-4686(99)00134-6.
649
- 650 [22] N. Wagner, K. a. Friedrich, Application of electrochemical impedance spectroscopy for fuel
651 cell characterization: PEFC and oxygen reduction reaction in alkaline solution, *Fuel Cells*. 9
652 (2009) 237–246. doi:10.1002/fuce.200800071.

653

- 654 [23] H. Schichlein, H. Schichlein, E. Ivers-tiffe, E. Ivers-tiffe, Deconvolution of electrochemical
655 impedance spectra for the identification of electrode reaction mechanisms in solid oxide fuel
656 cells, *J. Appl. Electrochem.* 32 (2002) 875–882. doi:10.1023/A:1020599525160.
657
- 658 [24] P. V. Aravind, J.P. Ouweltjes, J. Schoonman, Diffusion Impedance on Nickel/Gadolinia-
659 Doped Ceria Anodes for Solid Oxide Fuel Cells, *J. Electrochem. Soc.* 156 (2009) B1417.
660 doi:10.1149/1.3231490.
661
- 662 [25] Q.A. Huang, R. Hui, B. Wang, J. Zhang, A review of AC impedance modeling and
663 validation in SOFC diagnosis, *Electrochim. Acta.* 52 (2007) 8144–8164.
664 doi:10.1016/j.electacta.2007.05.071.
665
- 666 [26] E. Brightman, D.G. Ivey, D.J.L. Brett, N.P. Brandon, The effect of current density on H₂S-
667 poisoning of nickel-based solid oxide fuel cell anodes, *J. Power Sources.* 196 (2011) 7182–
668 7187. doi:10.1016/j.jpowsour.2010.09.089.
669
- 670 [27] P. Leone, T. Matencio, M.E. Garcia, Z.R. Domigues, A. Lanzini, M. Santarelli, Limiting
671 Factors for a Planar Solid Oxide Fuel Cell Under Different Flow and Temperature
672 Conditions, *Fuel Cells.* (2013) n/a–n/a. doi:10.1002/fuce.201200154.
673
- 674 [28] S.H. Jensen, A. Hauch, P.V. Hendriksen, M. Mogensen, N. Bonanos, T. Jacobsen, A Method
675 to Separate Process Contributions in Impedance Spectra by Variation of Test Conditions, *J.*
676 *Electrochem. Soc.* 154 (2007) B1325. doi:10.1149/1.2790791.
677
- 678 [29] A. Leonide, V. Sonn, A. Weber, E. Ivers-Tiffée, Evaluation and Modeling of the Cell
679 Resistance in Anode-Supported Solid Oxide Fuel Cells, *J. Electrochem. Soc.* 155 (2008)
680 B36. doi:10.1149/1.2801372.
681
- 682 [30] W.G. Bessler, S. Gewies, Gas Concentration Impedance of Solid Oxide Fuel Cell Anodes, *J.*
683 *Electrochem. Soc.* 154 (2007) B548. doi:10.1149/1.2720639.
684
- 685 [31] M. Lang, C. Auer, A. Eismann, P. Szabo, N. Wagner, Investigation of solid oxide fuel cell
686 short stacks for mobile applications by electrochemical impedance spectroscopy,
687 *Electrochim. Acta.* 53 (2008) 7509–7513. doi:10.1016/j.electacta.2008.04.047.
688
- 689 [32] L.R.F. Allen J. Bard, *Electrochemical methods: Fundamentals and Applications*, New York,
690 2000. doi:10.1146/annurev.matsci.30.1.117.
691
- 692 [33] S. S, *High-Temperature Solid Oxide Fuel Cells: Fundamentals, Design and Applications*,
693 Elsevier science, Amsterdam The Netherlands, 2003.
694

- 695 [34] F.T. and E.I.-T. Cornelia Endler, André Leonide, André Weber, Cells, Long-Term Study of
696 MIEC Cathodes for Intermediate Temperature Solid Oxide Fuel Cells, *ECS Trans.* 25 (2009)
697 2381–2390. doi:doi: 10.1149/1.3205791.
698
- 699 [35] L.P. Hendriksen PV, Koch S, Mogensen M, Liu YL, Solid Oxide Fuel Cells VIII, (Eds. S. C.
700 Singhal, M. Dokiya), in: *Electrochem. Soc. Proc. Ser.*, Pennington, NJ, USA, 2003.
701
- 702 [36] Z. Cheng, S. Zha, M. Liu, Influence of cell voltage and current on sulfur poisoning behavior
703 of solid oxide fuel cells, *J. Power Sources.* 172 (2007) 688–693.
704 doi:10.1016/j.jpowsour.2007.07.052.
705
- 706 [37] Y. Zhang, Z. Lu, Z. Yang, T. Woo, Short communication the mechanism of sulfur poisoning
707 on the nickel/yttrium-stabilized zirconia anode of solid oxide fuel cells: The role of the
708 oxygen vacancy, *J. Power Sources.* 237 (2013) 128–131.
709 doi:10.1016/j.jpowsour.2013.03.030.
710
- 711 [38] Z. Cheng, J.-H. Wang, Y. Choi, L. Yang, M.C. Lin, M. Liu, From Ni-YSZ to sulfur-tolerant
712 anode materials for SOFCs: electrochemical behavior, in situ characterization, modeling, and
713 future perspectives, *Energy Environ. Sci.* 4 (2011) 4380. doi:10.1039/c1ee01758f.
714
- 715 [39] A. Hagen, J.F.B. Rasmussen, K. Thydén, Durability of solid oxide fuel cells using sulfur
716 containing fuels, *J. Power Sources.* 196 (2011) 7271–7276.
717 doi:10.1016/j.jpowsour.2011.02.053.
718
- 719 [40] J.F.B. Rasmussen, A. Hagen, The Effect of H₂S on the Performance of SOFCs using
720 Methane Containing Fuel, (2010) 1135–1142. doi:10.1002/fuce.201000012.
721
- 722 [41] D. Papurello, R. Borchiellini, P. Bareschino, V. Chiodo, S. Freni, A. Lanzini, et al.,
723 Performance of a Solid Oxide Fuel Cell short-stack with biogas feeding, *Appl. Energy.* 125
724 (2014) 254–263.
725
- 726 [42] F.N. Cayan, M. Zhi, S.R. Pakalapati, I. Celik, N. Wu, R. Gemmen, Effects of coal syngas
727 impurities on anodes of solid oxide fuel cells, *J. Power Sources.* 185 (2008) 595–602.
728 doi:10.1016/j.jpowsour.2008.06.058.
729
- 730 [43] P. V. Aravind, J.P. Ouweltjes, N. Woudstra, G. Rietveld, Impact of Biomass-Derived
731 Contaminants on SOFCs with Ni/Gadolinia-Doped Ceria Anodes, *Electrochem. Solid-State*
732 *Lett.* 11 (2008) B24. doi:10.1149/1.2820452.
733
- 734 [44] Veyo, EVALUATION OF FUEL IMPURITY EFFECTS ON SOLID OXIDE FUEL CELL
735 PERFORMANCE Final Technical Report, 1998.
736
- 737 [45] M. Arnold, T. Kajolinna, Development of on-line measurement techniques for siloxanes and

- 738 other trace compounds in biogas, *Waste Manag.* 30 (2010) 1011–1017.
739 doi:10.1016/j.wasman.2009.11.030.
740
- 741 [46] M. Arnold, Reduction and monitoring of biogas trace compounds, 2009.
742
- 743 [47] T. Namioka, T. Naruse, R. Yamane, Behavior and mechanisms of Ni/ScSZ cermet anode
744 deterioration by trace tar in wood gas in a solid oxide fuel cell, *Int. J. Hydrogen Energy.* 36
745 (2011) 5581–5588. doi:10.1016/j.ijhydene.2011.01.165.
746
- 747 [48] T. Namioka, Y. Nagai, K. Yoshikawa, T. Min, A tolerance criterion for tar concentration in a
748 model wood gas for a nickel/scandia-stabilized zirconia cermet anode in a solid oxide fuel
749 cell, *Int. J. Hydrogen Energy.* 37 (2012) 17245–17252. doi:10.1016/j.ijhydene.2012.09.005.
750
- 751 [49] R. Coll, J. Salvadó, X. Farriol, D. Montané, Steam reforming model compounds of biomass
752 gasification tars: Conversion at different operating conditions and tendency towards coke
753 formation, *Fuel Process. Technol.* 74 (2001) 19–31. doi:10.1016/S0378-3820(01)00214-4.
754
- 755 [50] W.Z. Zhu, S.C. Deevi, A review on the status of anode materials for solid oxide fuel cells,
756 *Mater. Sci. Eng. A.* 362 (2003) 228–239. doi:10.1016/S0921-5093(03)00620-8.
757
- 758 [51] D.G. Ivey, E. Brightman, N. Brandon, Structural modifications to nickel cermet anodes in
759 fuel cell environments, *J. Power Sources.* 195 (2010) 6301–6311.
760 doi:10.1016/j.jpowsour.2010.04.059.
761

1 **Table captions**

2 Table 1 – Test conditions.

3

4

5

6

7

8

9

10

11

12

13

14

15

16

17

18

19

20 **Table 1**

Pollutant test	Conc. Range (ppm(v))	Cell adopted	H ₂ (ml min ⁻¹)	CO (ml min ⁻¹)	CO ₂ (ml min ⁻¹)	CH ₄ (ml min ⁻¹)	N ₂ (ml min ⁻¹)	H ₂ O (ml min ⁻¹)	H ₂ O (g h ⁻¹)	T (°C)	FU	Fuel condition
H ₂ S high conc.	0,84-6,4	ASC700	151,5	136,4	68,2	15,2	386,4	60,2	2,9	750	30,0	syngas
H ₂ S high conc.	0,8-6,7	ASC4	250	0	41,7	62,5	0	124,5	6	750	20,9	DIR 50% biogas
H ₂ S low conc.	0,078-0,174	ASC4	250	0	41,7	62,5	0	124,5	6	750	20,9	DIR 50% biogas
HCl	1-1000	ASC700	348	133,7	62,1	5		136,5	6,58	750	29,9	biogas reformate
D4	0,11-1,92	TOFC	348	133,7	62,1	5		136,5	6,58	750	20,8	biogas reformate
C ₇ H ₈	3,8-24,2	ASC700	151,5	136,4	68,2	15,2	386,4	269,8	13	750	30,0	syngas
C ₁₀ H ₈	0-9,3	ASC700	151,5	136,4	68,2	15,2	386,4	269,8	13	750	30,0	syngas
C ₂ H ₂	371,2	ASC700	250	0	42	63	0	0,0	0	750	20,8	POx 50% biogas
H ₂ S	1,34	ASC700	250	0	42	63	0	0,0	0	750	20,8	POx 50% biogas
H ₂ S + C ₂ Cl ₄	0-4/1,7-0	ASC700	151,5	136,4	68,2	15,2	386,4	269,8	13	750	30,0	syngas
H ₂ S + C ₂ H ₂	1,34/371,2	ASC700	250	0	42	63	0	0,0	0	750	20,8	POx 50% biogas
H ₂ S + C ₇ H ₈	4/3,7	ASC700	151,5	136,4	68,2	15,2	386,4	269,8	13	750	30,0	syngas

21

1 **Figure captions**

- 2 Figure 1 – Equivalent fuel cell circuit: R_e , R_{high} and CPE_{high} are associated with the high frequency
3 semi-circle, R_{low} and CPE_{low} with the low frequency semi-circle.
- 4 Figure 2 – Nyquist diagram for variations of the H_2S concentration – ASC700.
- 5 Figure 3 – Nyquist diagram for variations of the H_2S concentration – ASC4.
- 6 Figure 4 – R_e and R_p values for variations of the H_2S concentration – ASC700.
- 7 Figure 5 – R_e and R_p values for variations of the H_2S concentration – ASC4.
- 8 Figure 6 – Nyquist diagram for the H_2S threshold concentration value – ASC700.
- 9 Figure 7 – Nyquist diagram for the H_2S threshold concentration value – time variation – ASC700.
- 10 Figure 8 – Nyquist diagram for variations of the H_2S “low concentration level” – ASC4.
- 11 Figure 9 – R_e and R_p values for variations of the H_2S “low concentration level” – ASC4.
- 12 Figure 10 – Nyquist diagram for variations of the HCl concentration – ASC700.
- 13 Figure 11 – R_e and R_p values for variations of the HCl concentration – ASC700.
- 14 Figure 12 – Nyquist diagram for variations of the $D4$ concentration – TOFC.
- 15 Figure 13 – R_e and R_p values for variations of the $D4$ concentration – TOFC.
- 16 Figure 14 – Nyquist diagram for variations of the $C_{10}H_8$ concentration FU 30% – ASC700.
- 17 Figure 15 – R_e and R_p values for variations of the $C_{10}H_8$ concentration – ASC700.
- 18 Figure 16 – Nyquist diagram for variations of the C_7H_8 concentration – ASC700.
- 19 Figure 17 – R_e and R_p values for variations of the C_7H_8 concentration – TOFC.
- 20 Figure 18 – Area specific resistance diagram for variations of the C_7H_8 concentration – ASC700.
- 21 Figure 19 – Nyquist diagram for variations of the C_2H_2 concentration – ASC700.
- 22 Figure 20 – R_e and R_p values for variations of the the C_2H_2 concentration – ASC700.
- 23 Figure 21 – Nyquist diagram for variations of the C_2H_2 and $C_2H_2+H_2S$ concentrations – ASC700.

24 Figure 22 – Re and Rp values for variations of the C_2H_2 and $C_2H_2+H_2S$ concentration – ASC700.

25 Figure 23 – Area specific resistance diagram for variations of the C_2H_2 and $C_2H_2+H_2S$
26 concentrations – ASC700.

27 Figure 24 – Nyquist diagram for variations of the $C_2Cl_4+H_2S$ concentration – ASC700.

28 Figure 25 – Re and Rp values for variations of the $C_2Cl_4+H_2S$ concentration – ASC700.

29 Figure 26 – Area specific resistance diagram for variations of the $C_2Cl_4+H_2S$ concentration –
30 ASC700.

31 Figure 27 – Nyquist diagram for variations of the $H_2S + C_7H_8$ concentration – ASC700.

32 Figure 28 – Re and Rp values for variations of the $H_2S + C_7H_8$ concentration – ASC700.

33 Figure 29 – Area specific resistance diagram for variations of the $H_2S + C_7H_8$ concentration –
34 ASC700.

35

36

37

38

39

40

41

42

43

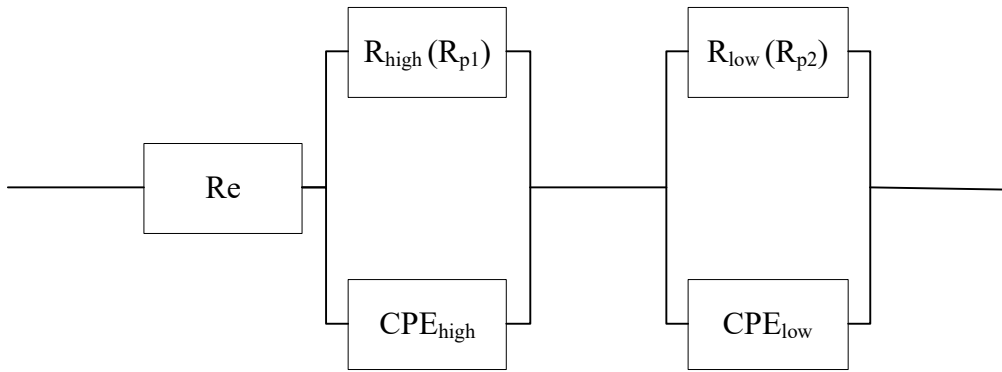
44

45

46

47

48 **Figure 1**



49

50

51

52

53

54

55

56

57

58

59

60

61

62

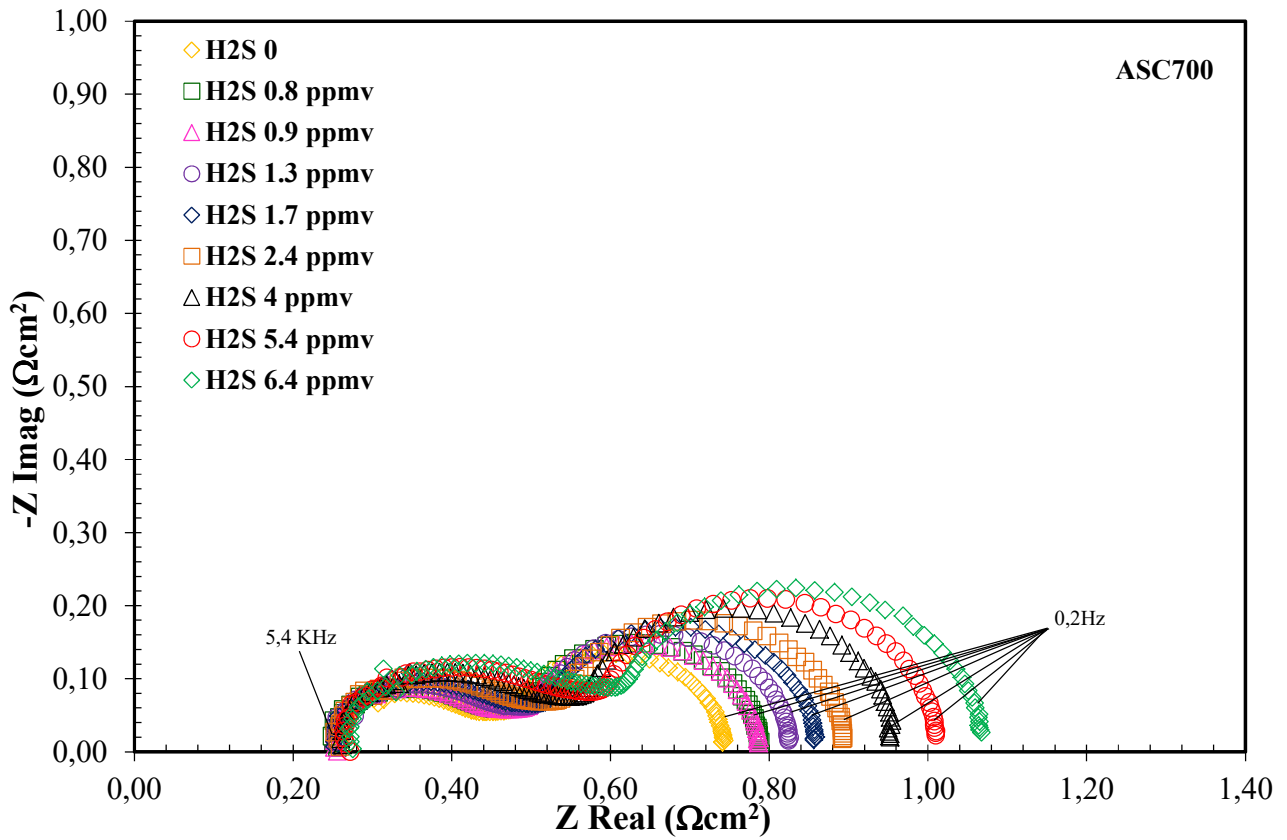
63

64

65

66

67 **Figure 2**



68

69

70

71

72

73

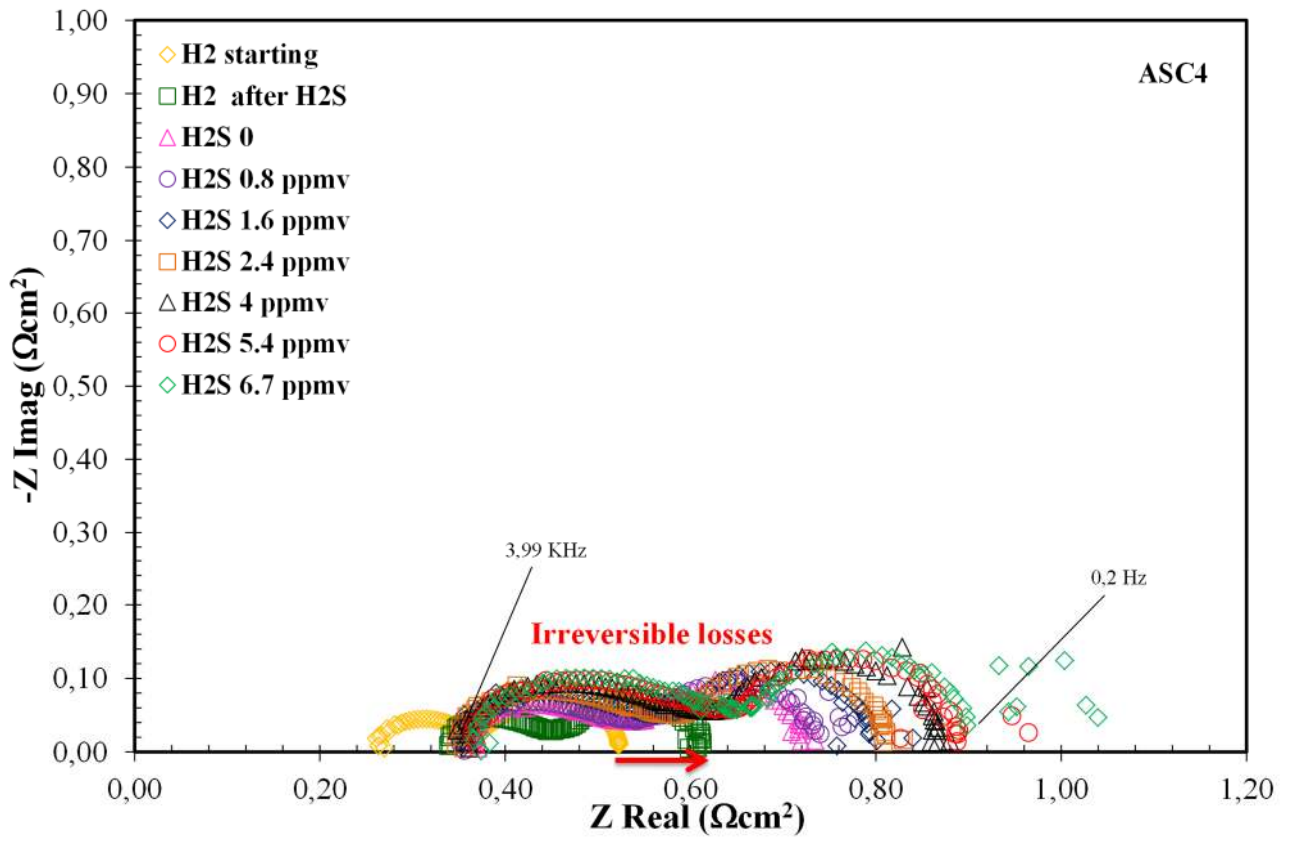
74

75

76

77

78 **Figure 3**



79

80

81

82

83

84

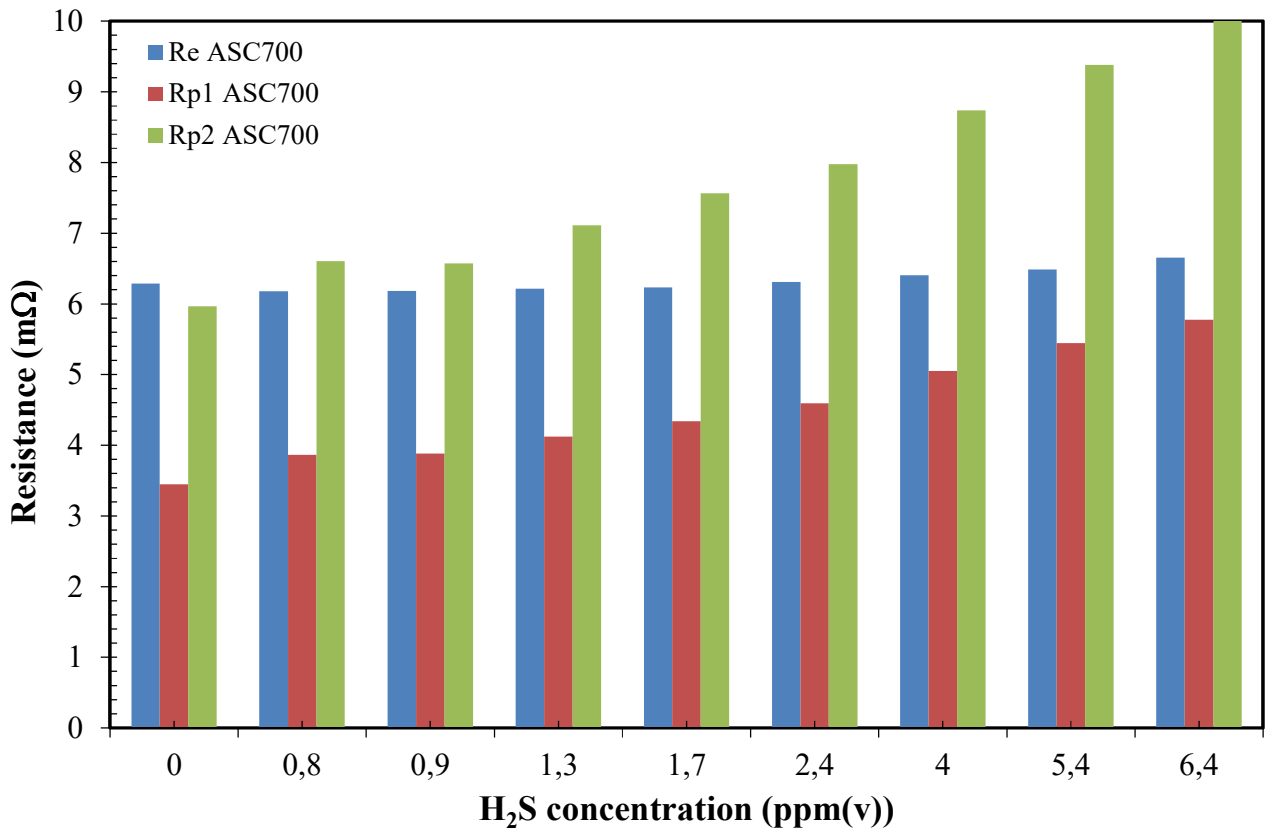
85

86

87

88

89 **Figure 4**



90

91

92

93

94

95

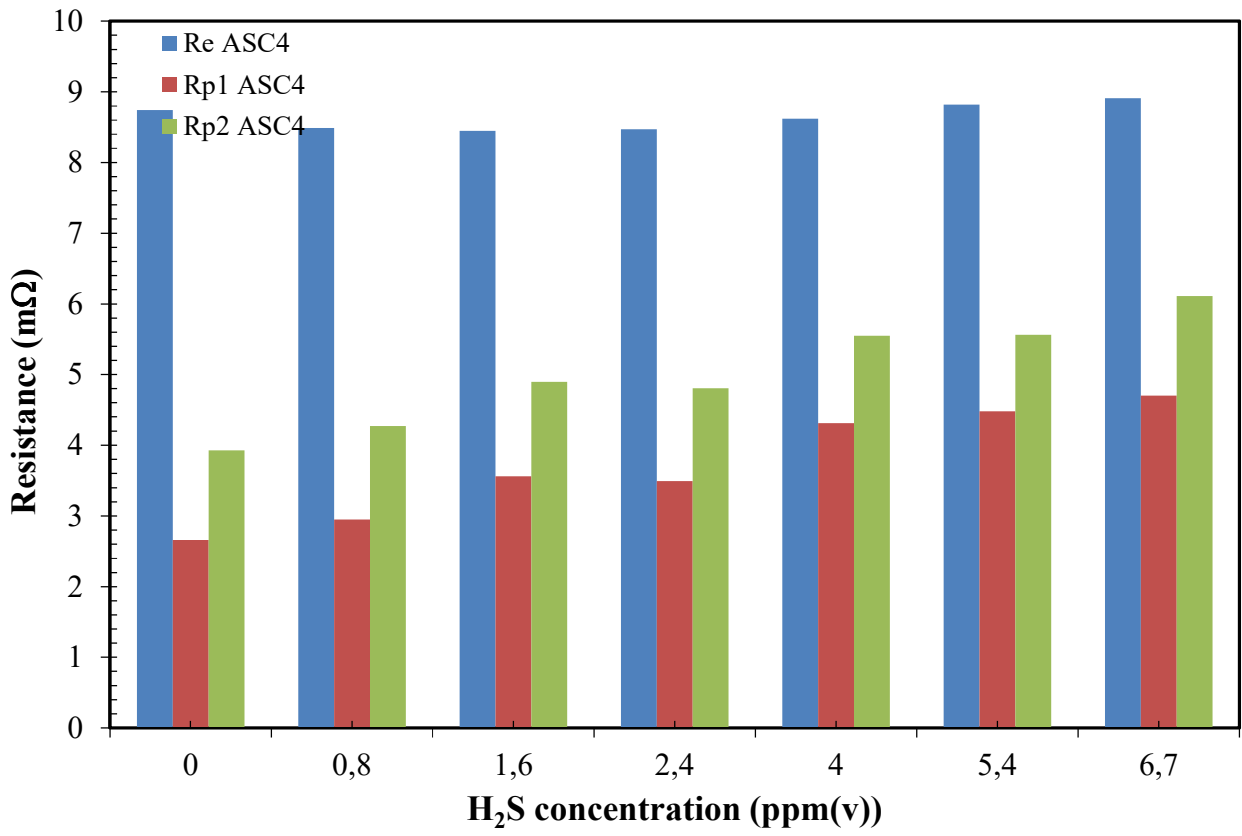
96

97

98

99

100 **Figure 5**



101

102

103

104

105

106

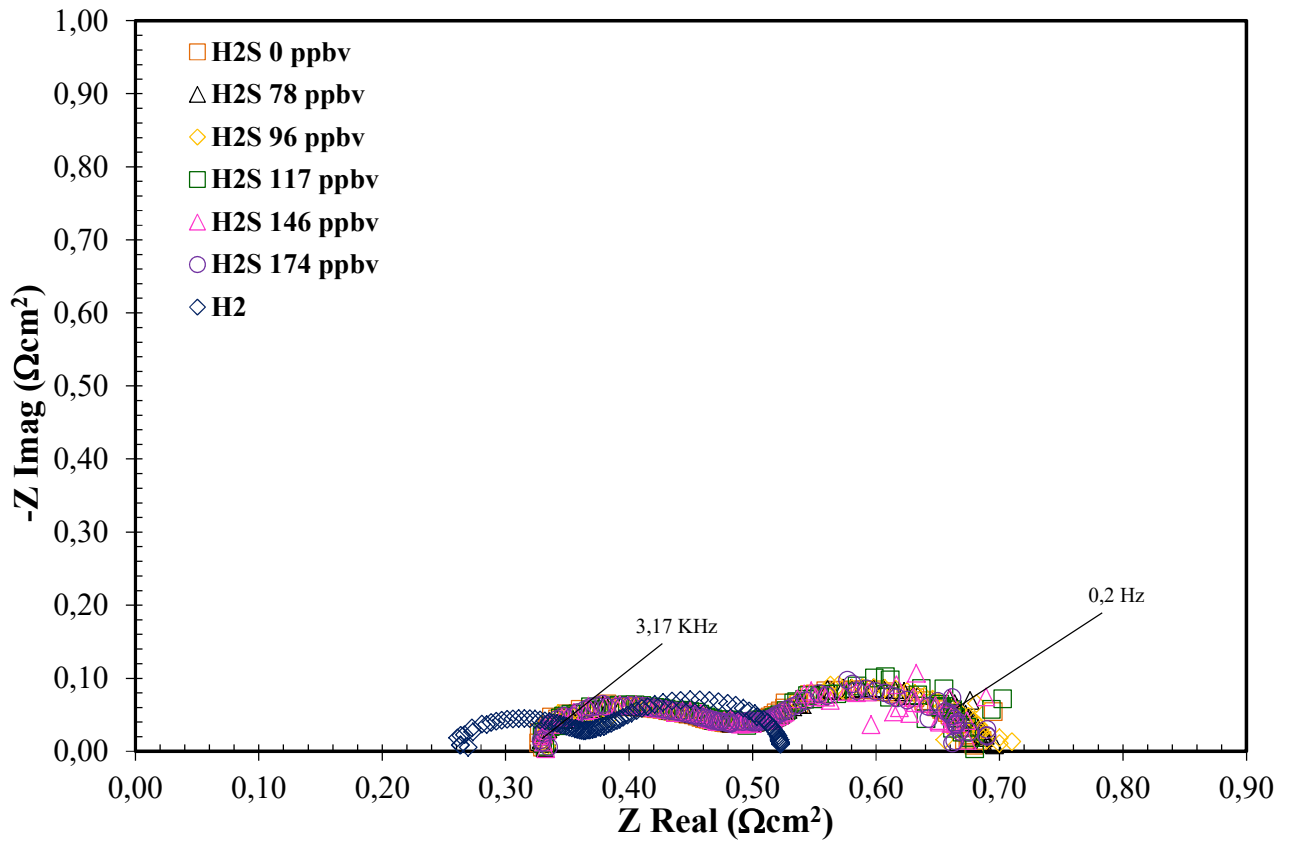
107

108

109

110

111 **Figure 6**



112

113

114

115

116

117

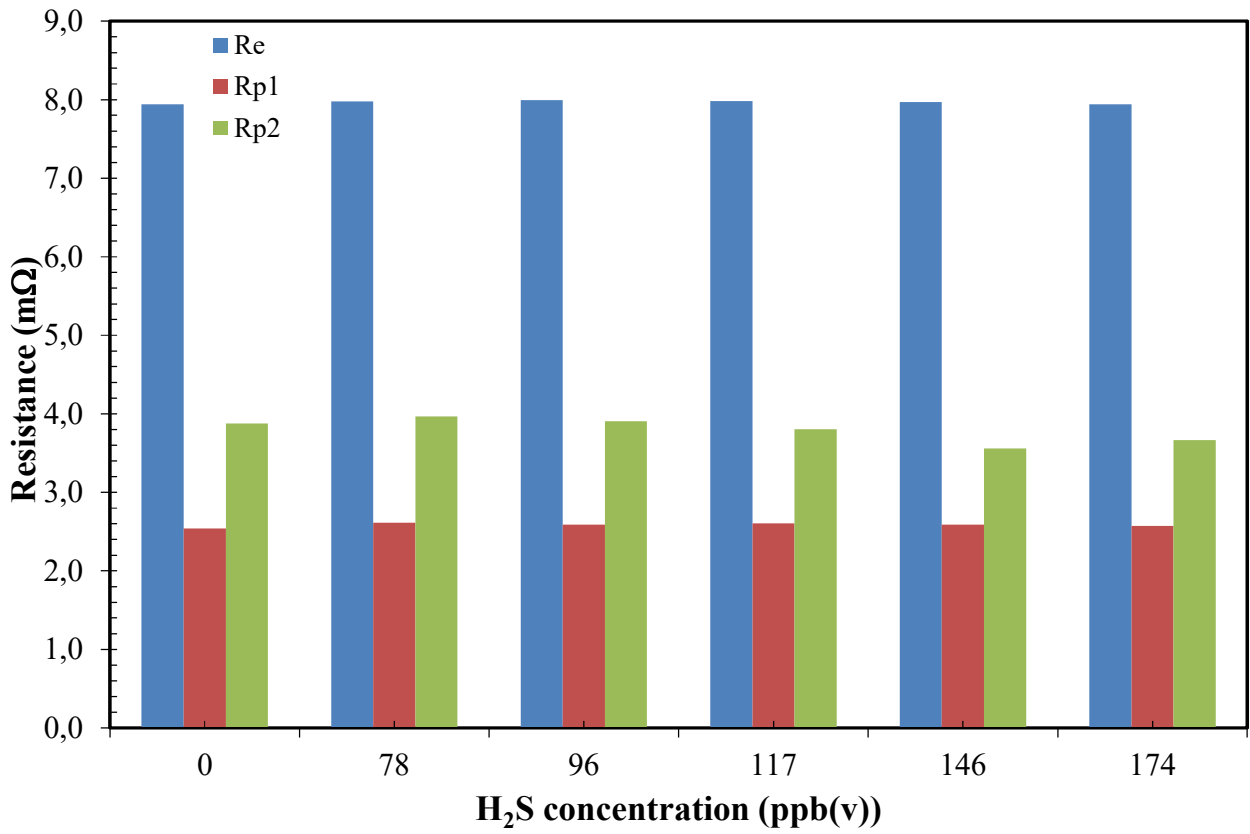
118

119

120

121

122 **Figure 7**



123

124

125

126

127

128

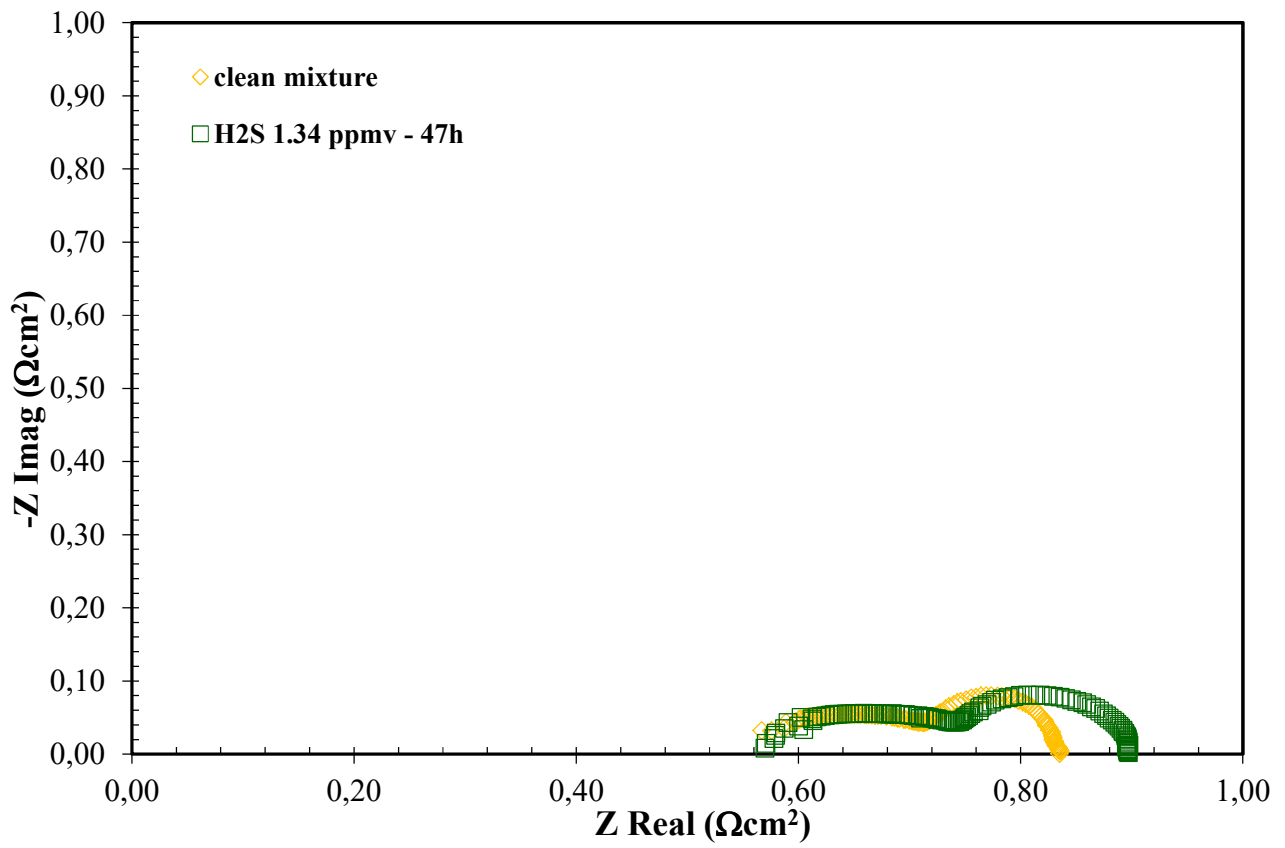
129

130

131

132

133 **Figure 8**



134

135

136

137

138

139

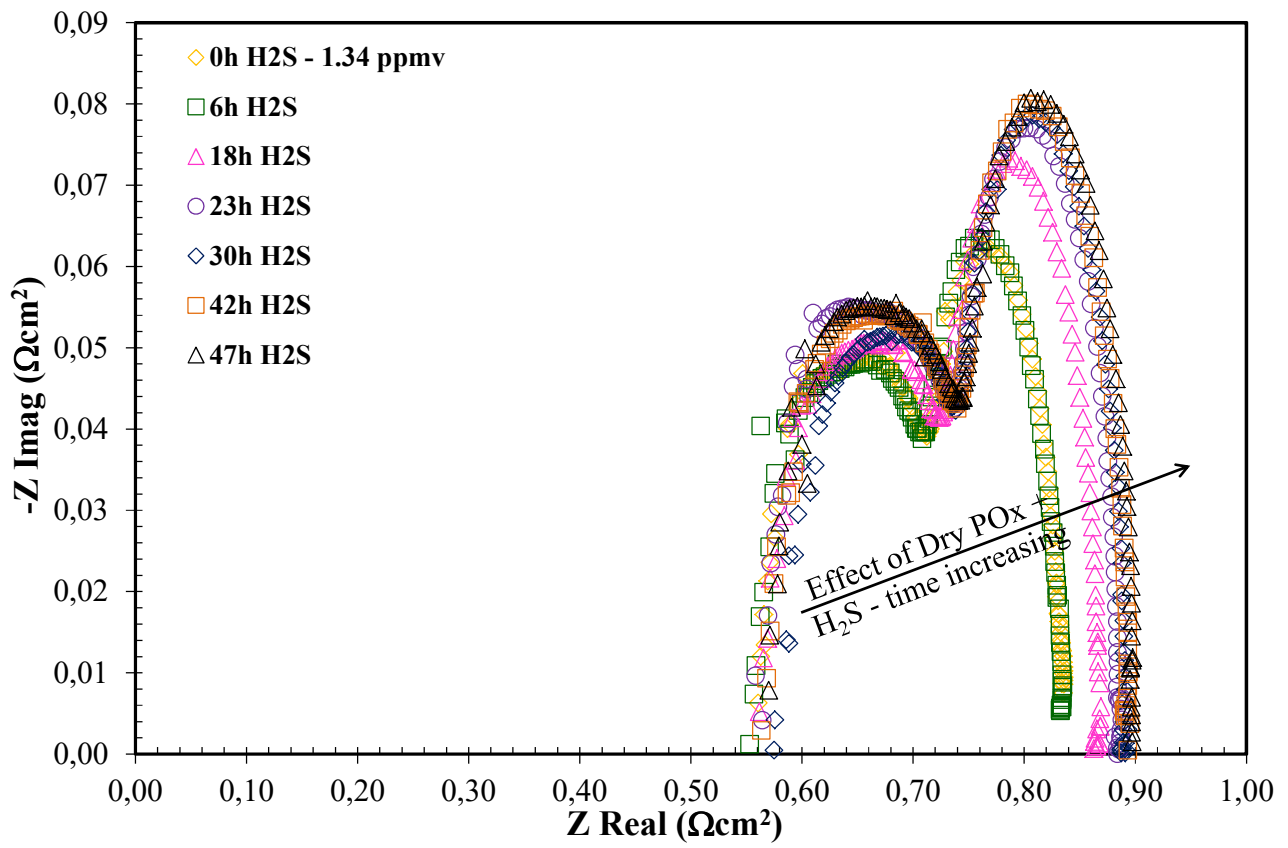
140

141

142

143

144 **Figure 9**



145

146

147

148

149

150

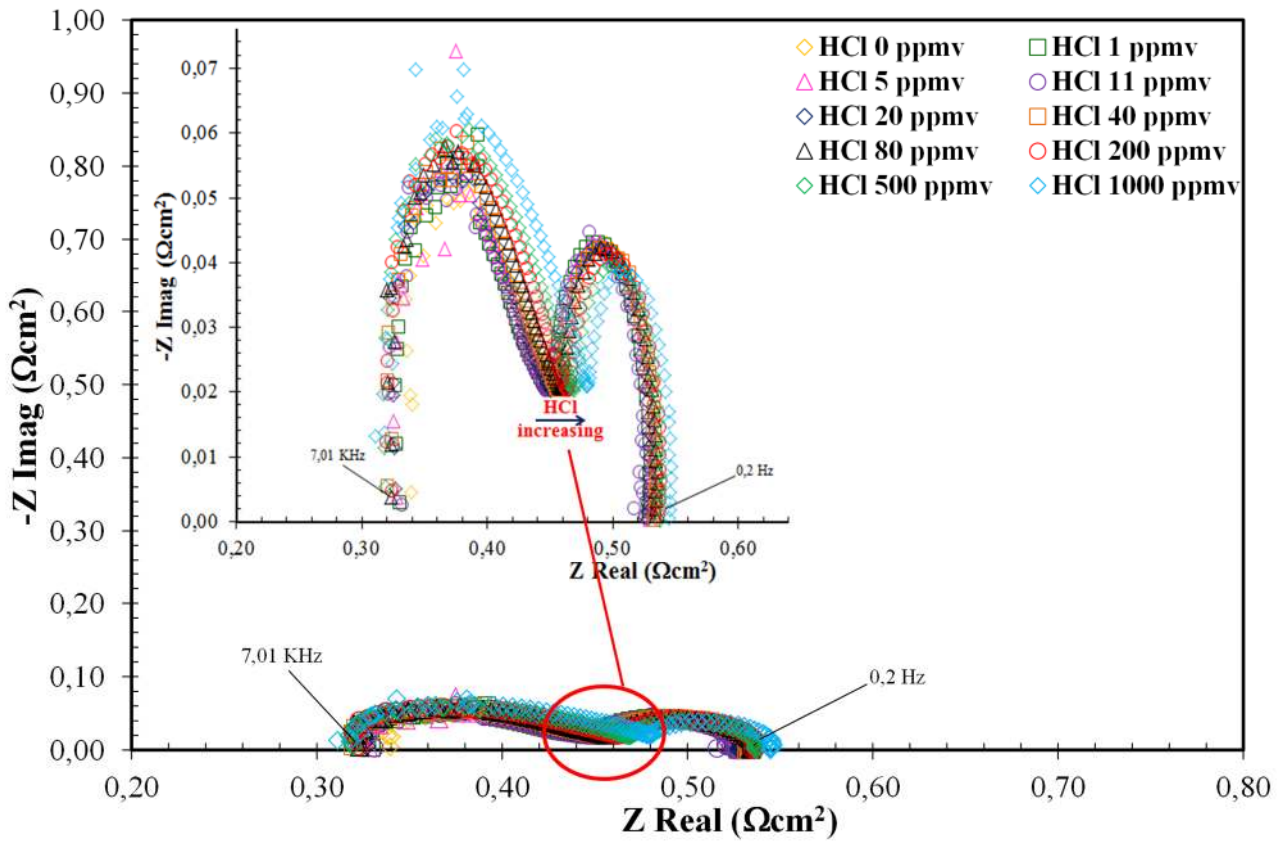
151

152

153

154

155 **Figure 10**



156

157

158

159

160

161

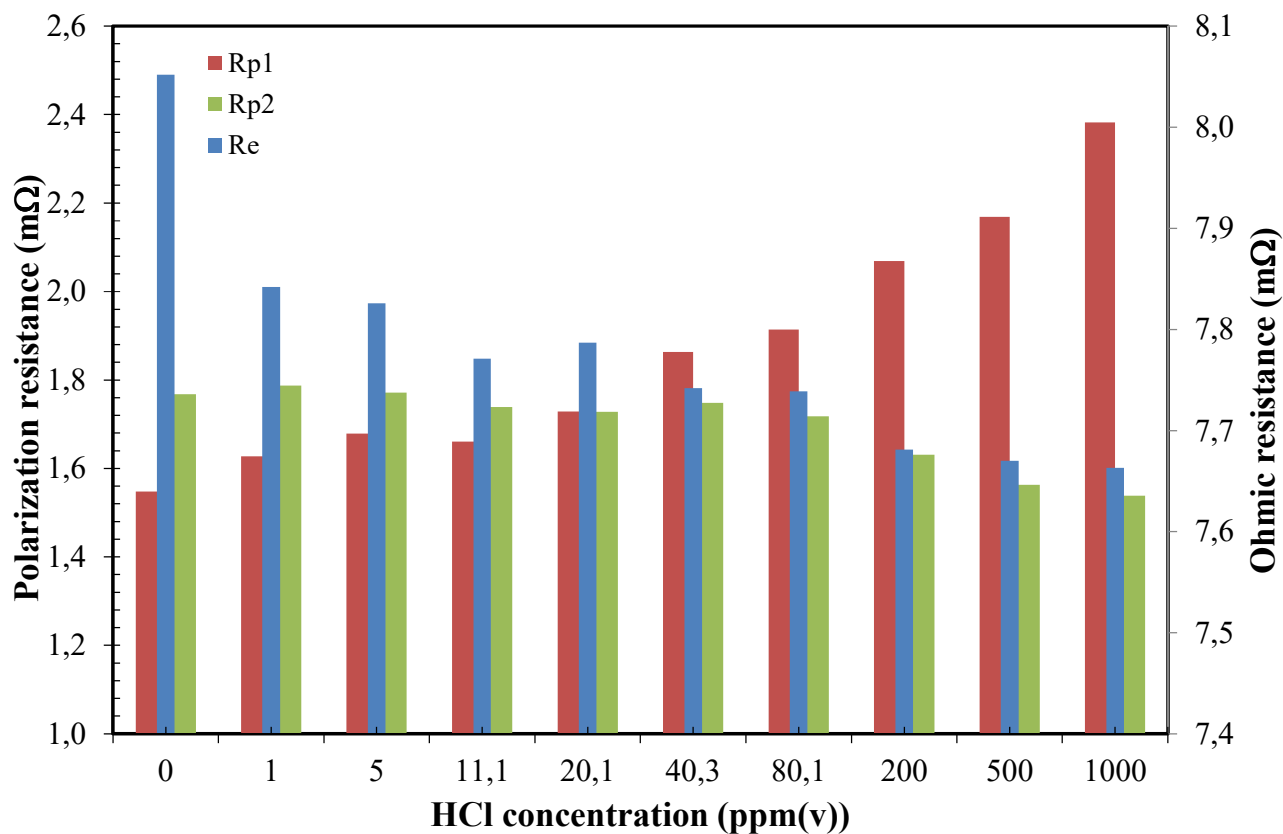
162

163

164

165

166 **Figure 11**



167

168

169

170

171

172

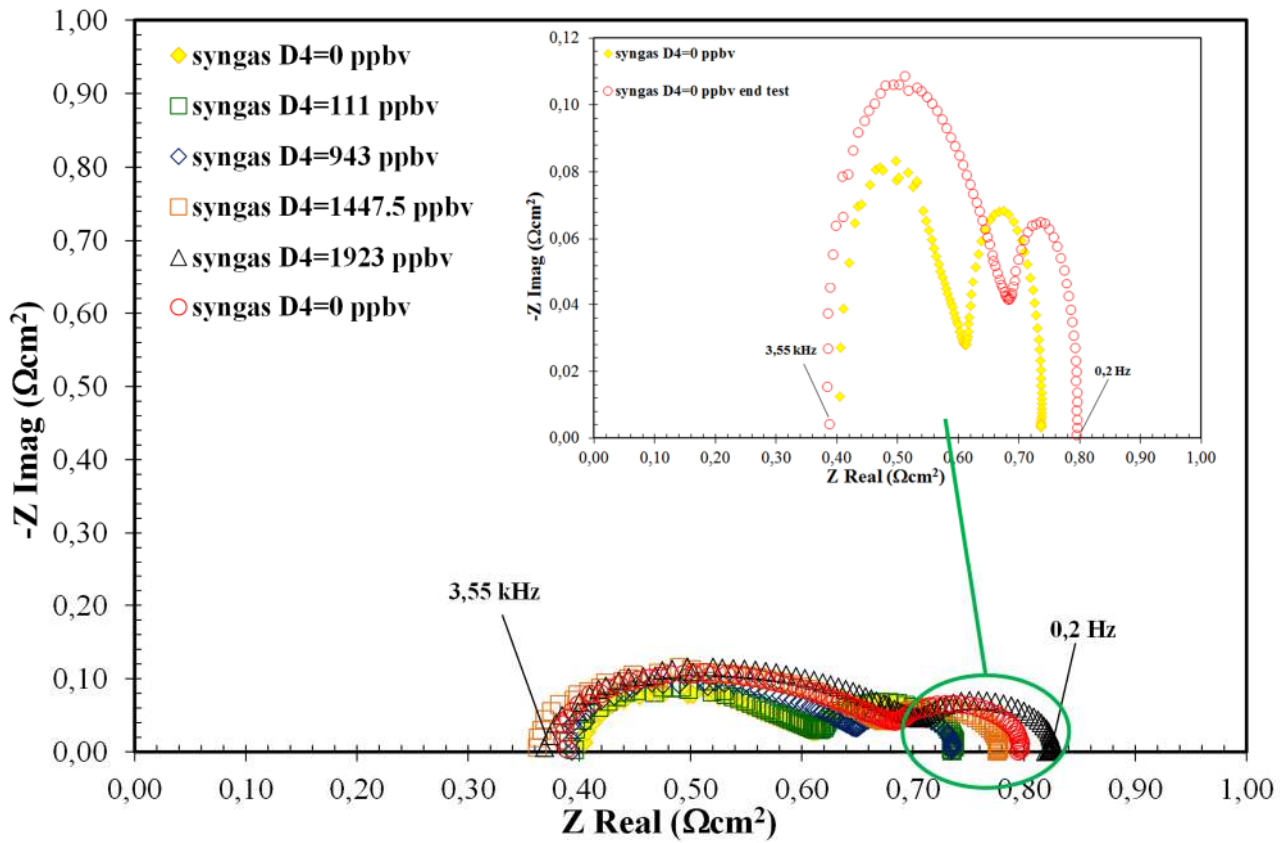
173

174

175

176

177 **Figure 12**



178

179

180

181

182

183

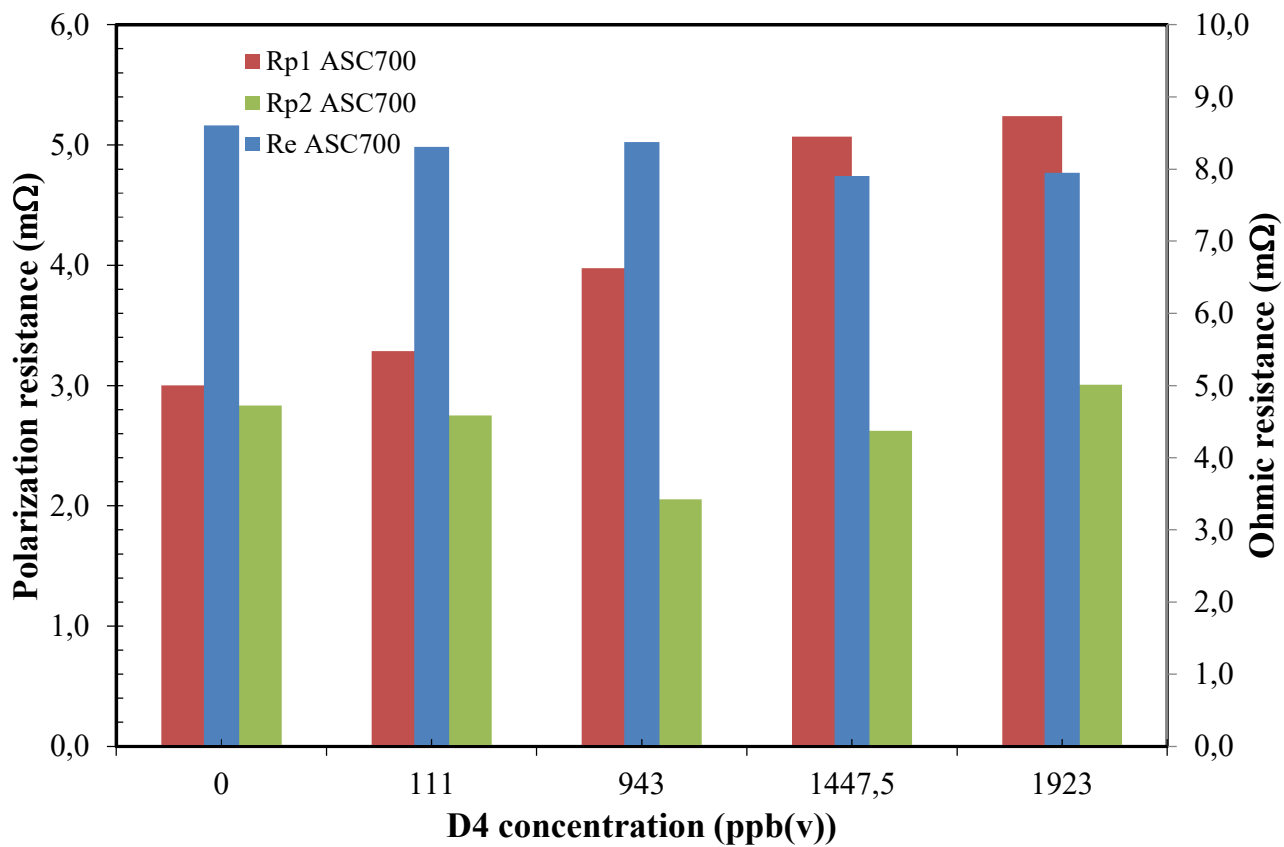
184

185

186

187

188 **Figure 13**



189

190

191

192

193

194

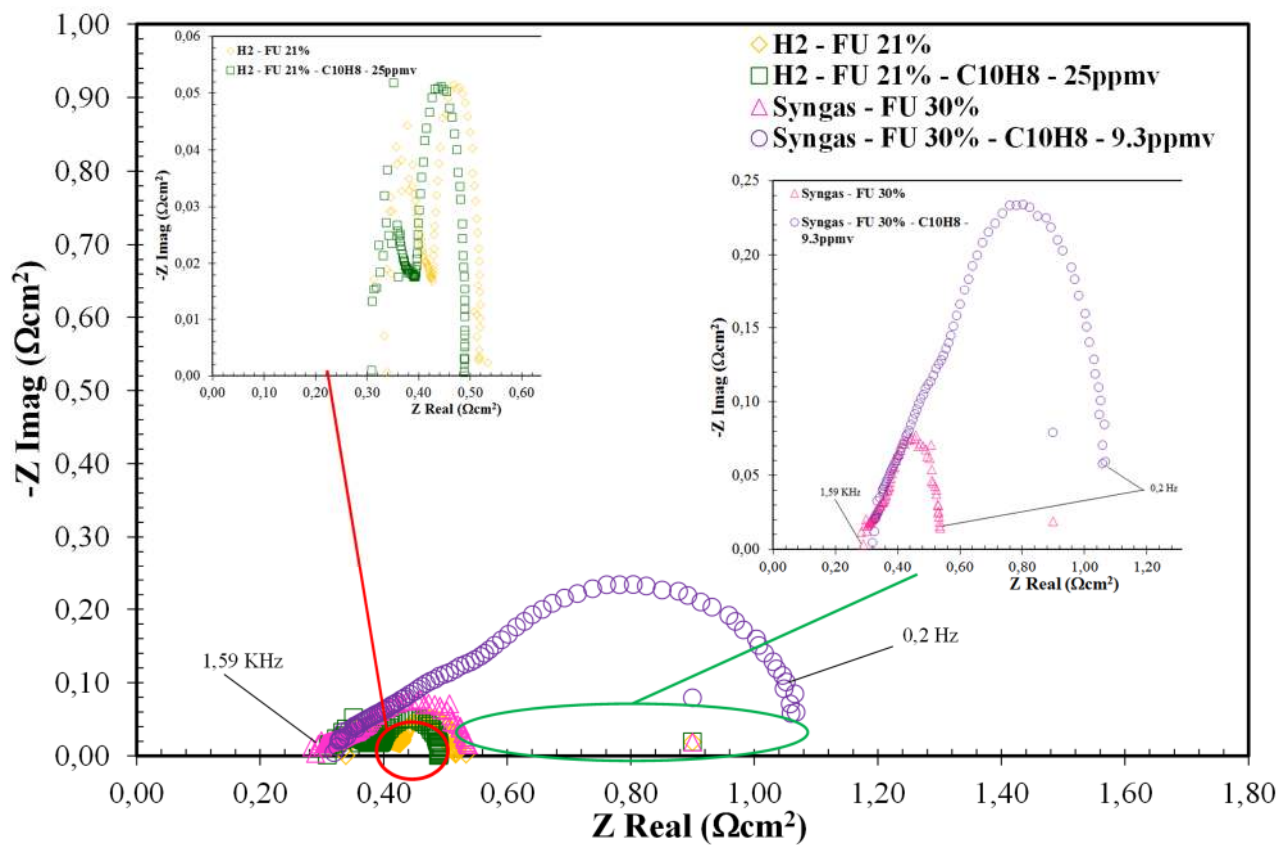
195

196

197

198

199 **Figure 14**



200

201

202

203

204

205

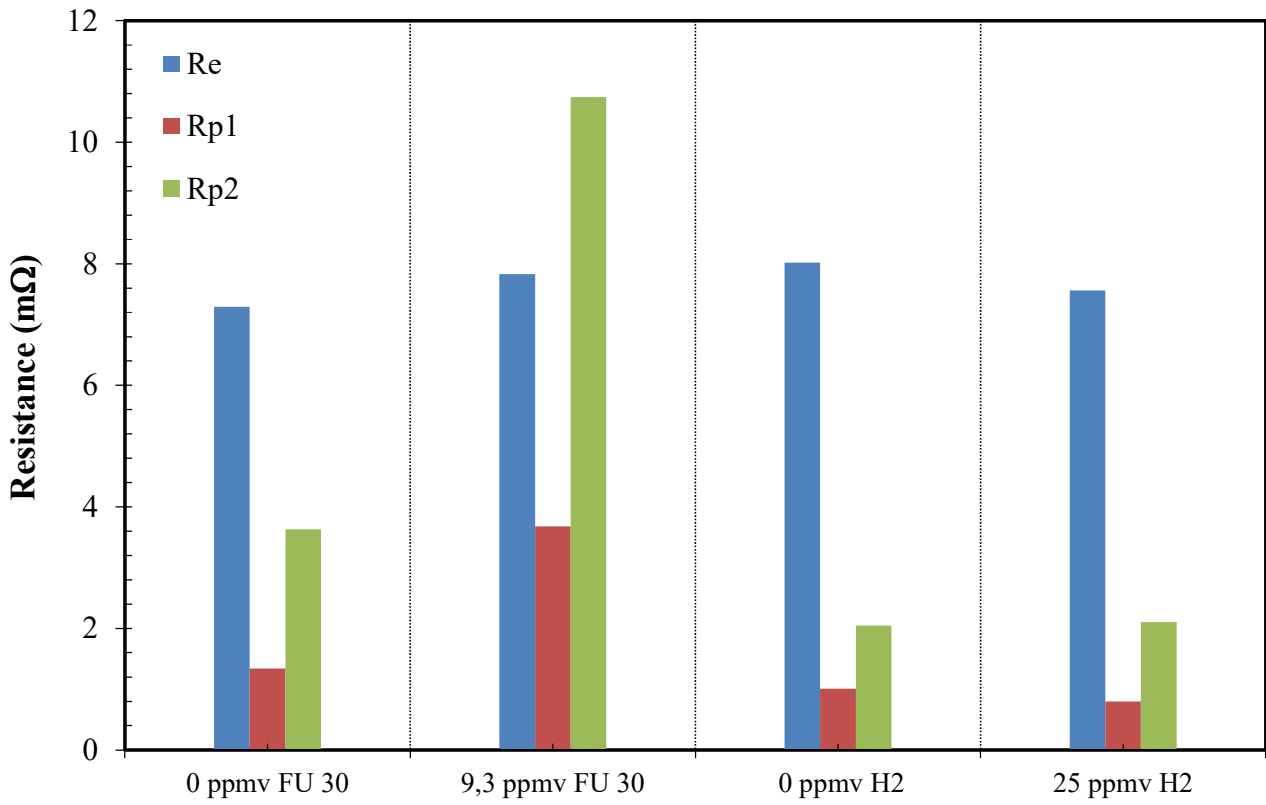
206

207

208

209

210 **Figure 15**



211

212

213

214

215

216

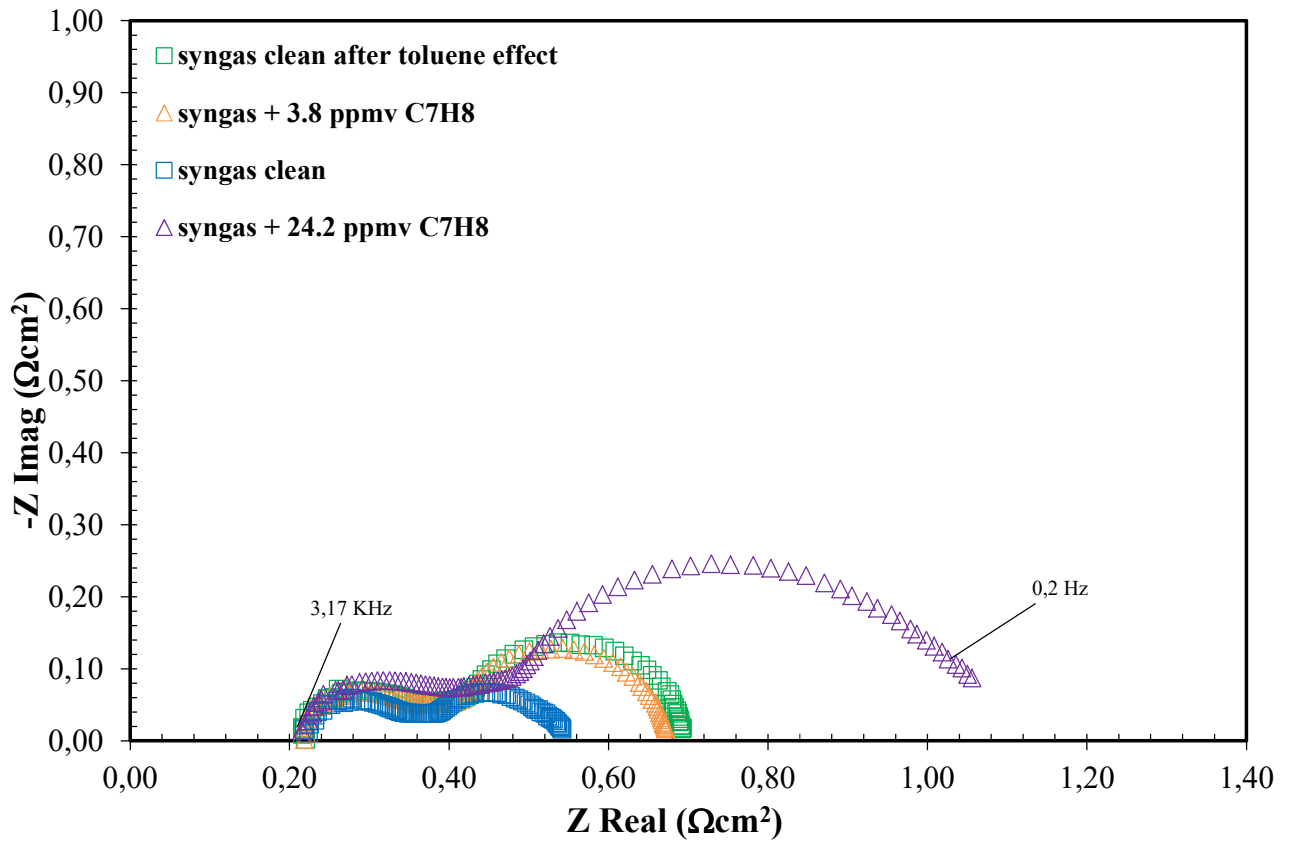
217

218

219

220

221 **Figure 16**



222

223

224

225

226

227

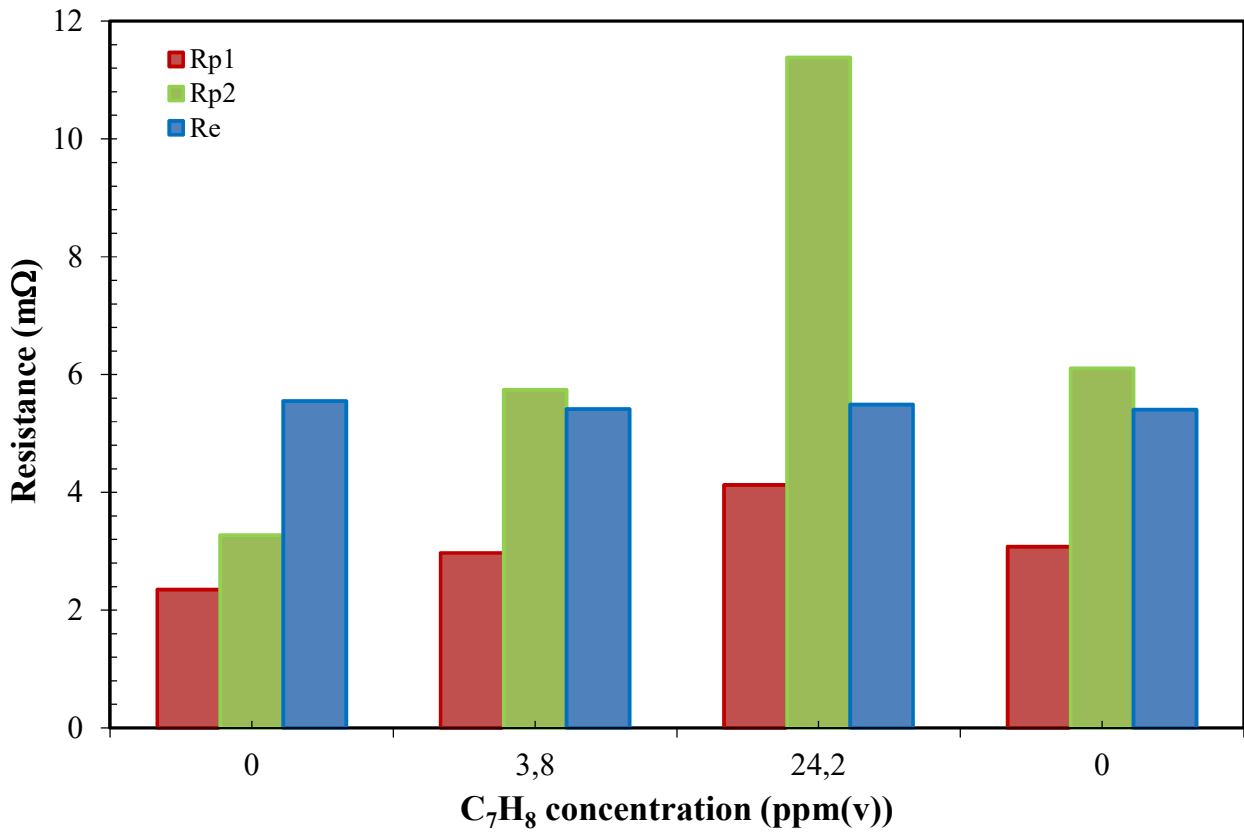
228

229

230

231

232 **Figure 17**



233

234

235

236

237

238

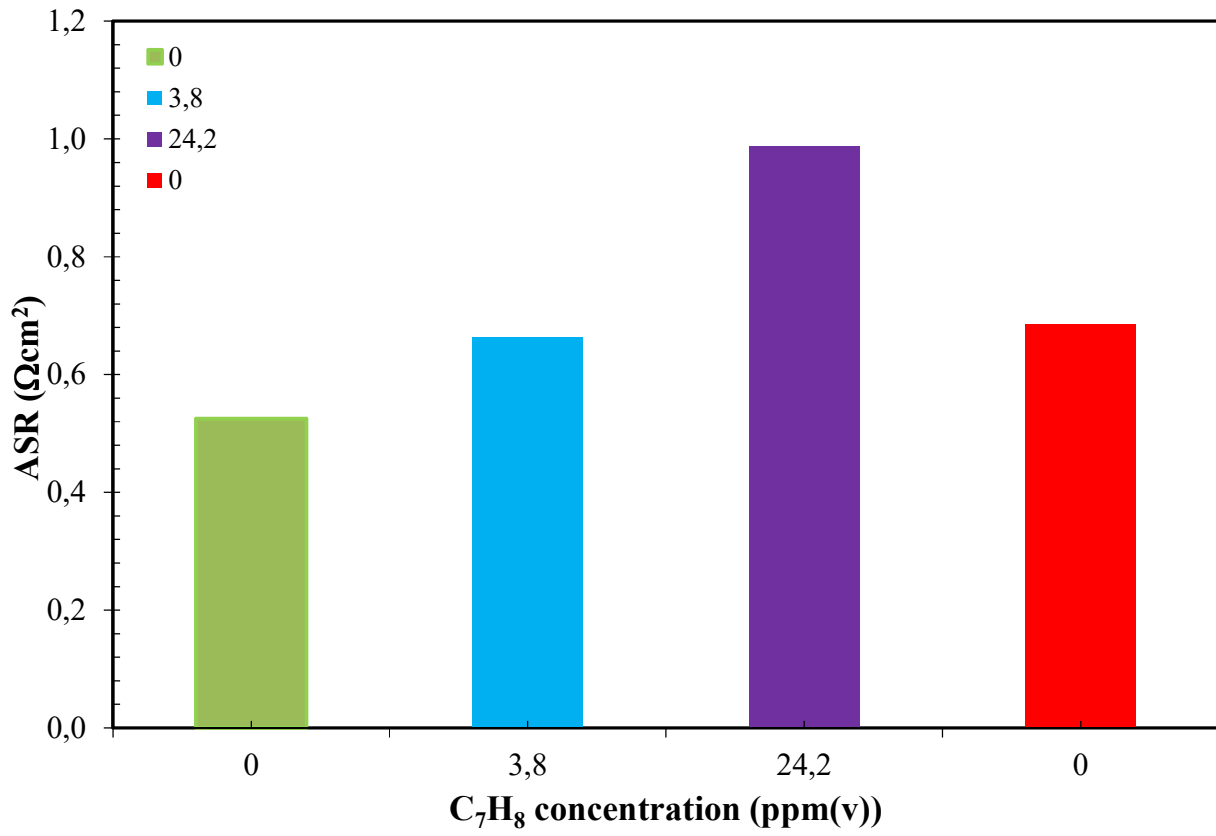
239

240

241

242

243 **Figure 18**



244

245

246

247

248

249

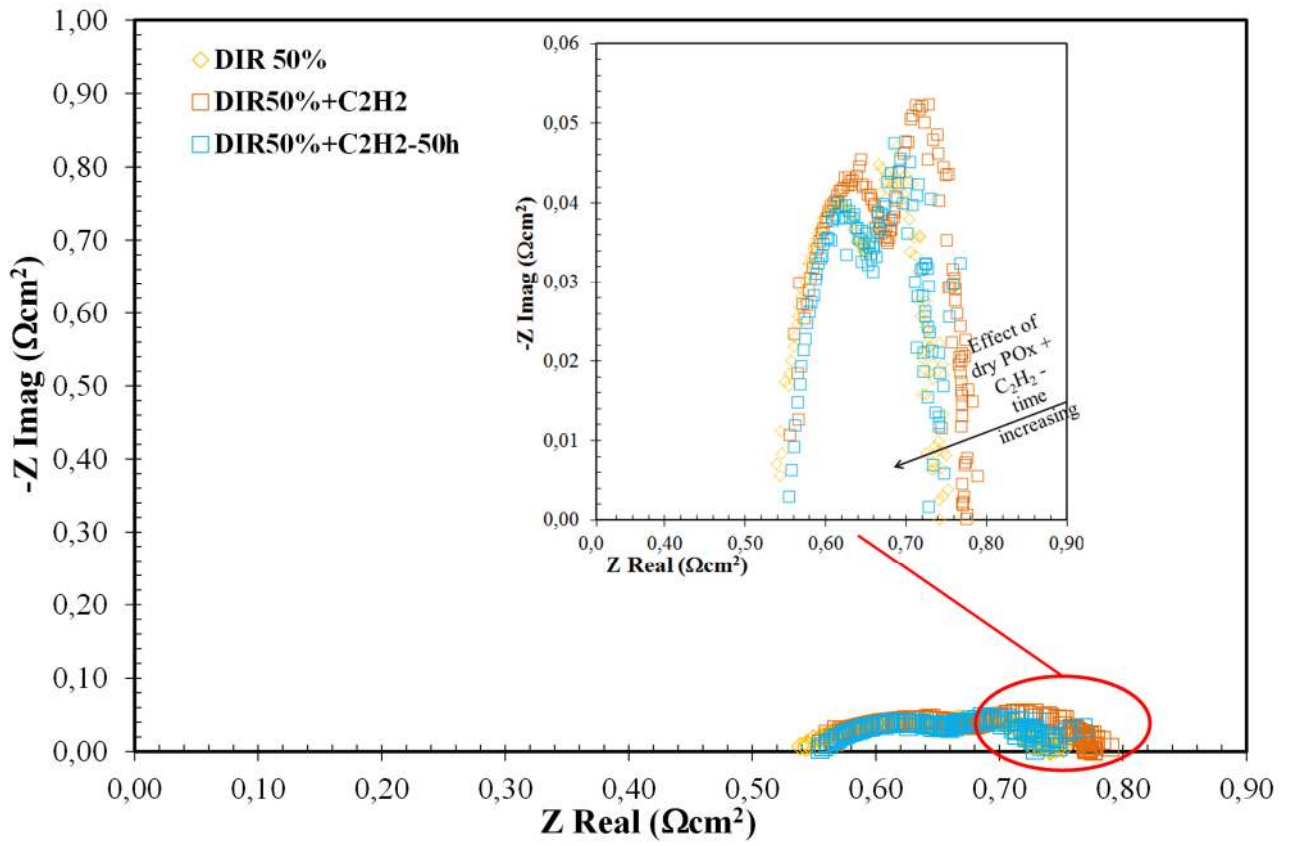
250

251

252

253

254 **Figure 19**



255

256

257

258

259

260

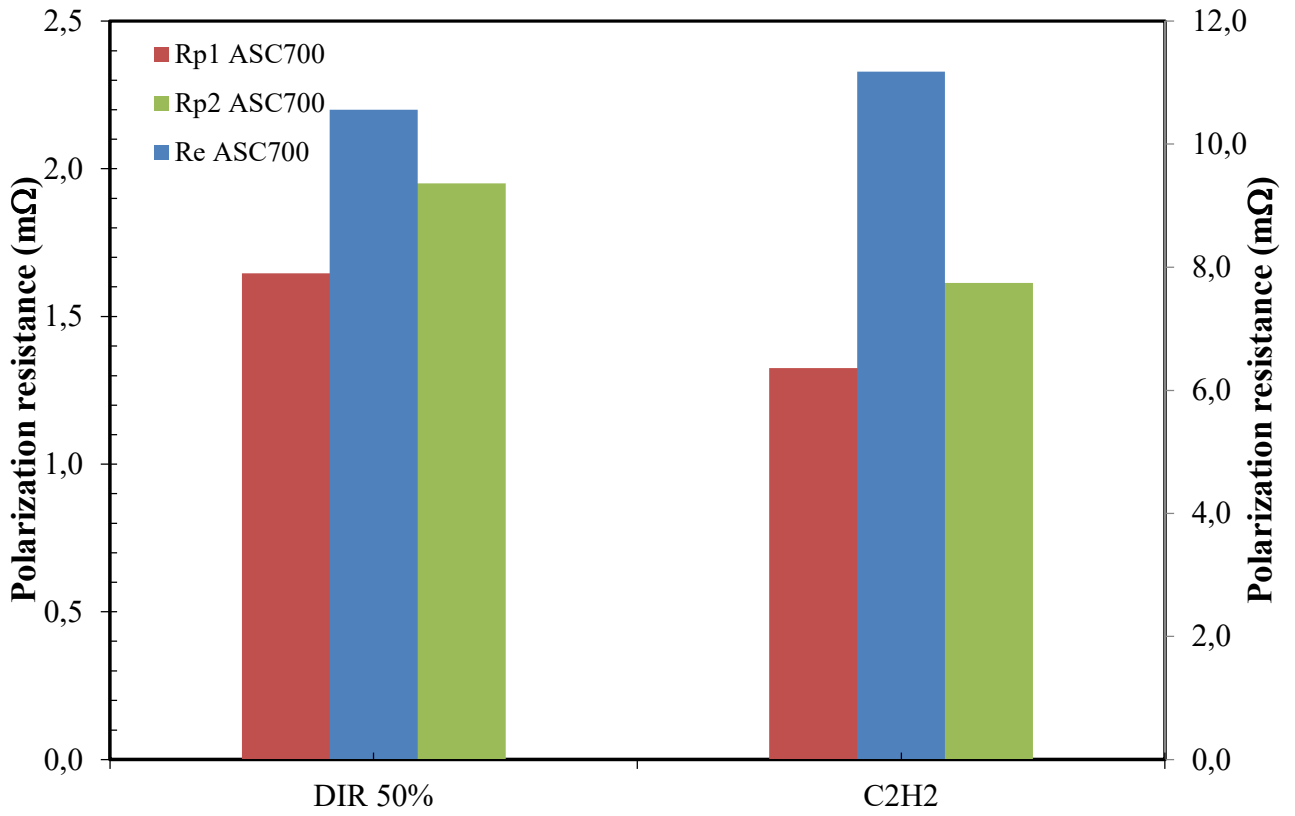
261

262

263

264

265 **Figure 20**



266

267

268

269

270

271

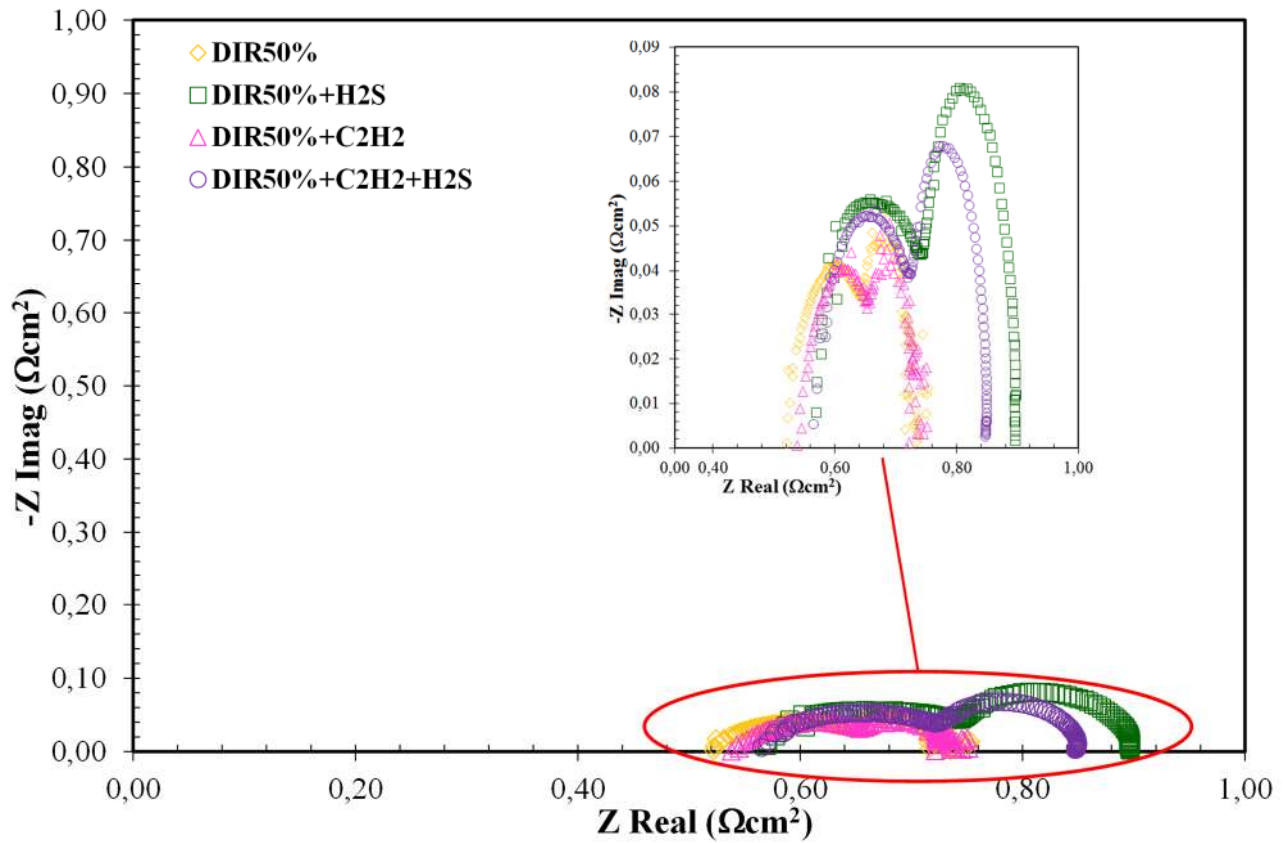
272

273

274

275

276 **Figure 21**



277

278

279

280

281

282

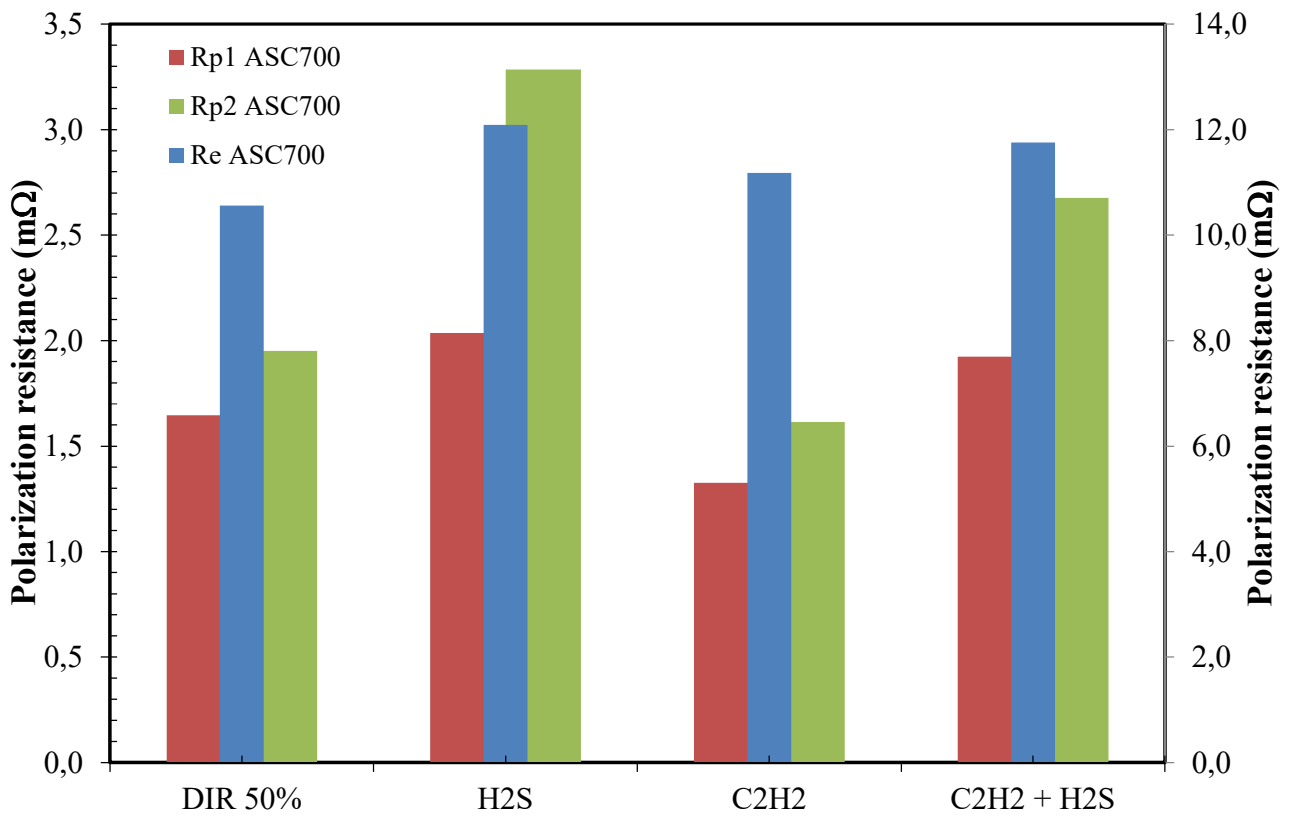
283

284

285

286

287 **Figure 22**



288

289

290

291

292

293

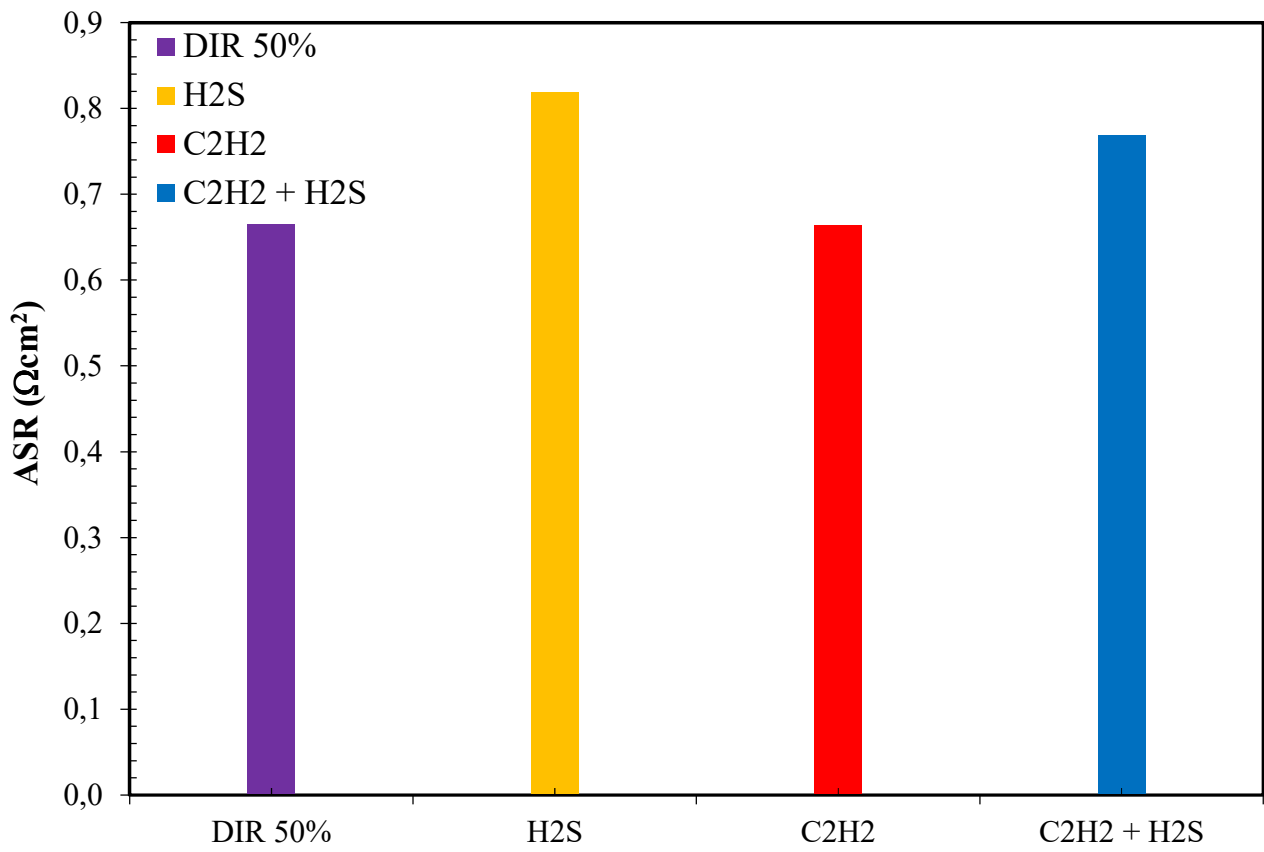
294

295

296

297

298 **Figure 23**



299

300

301

302

303

304

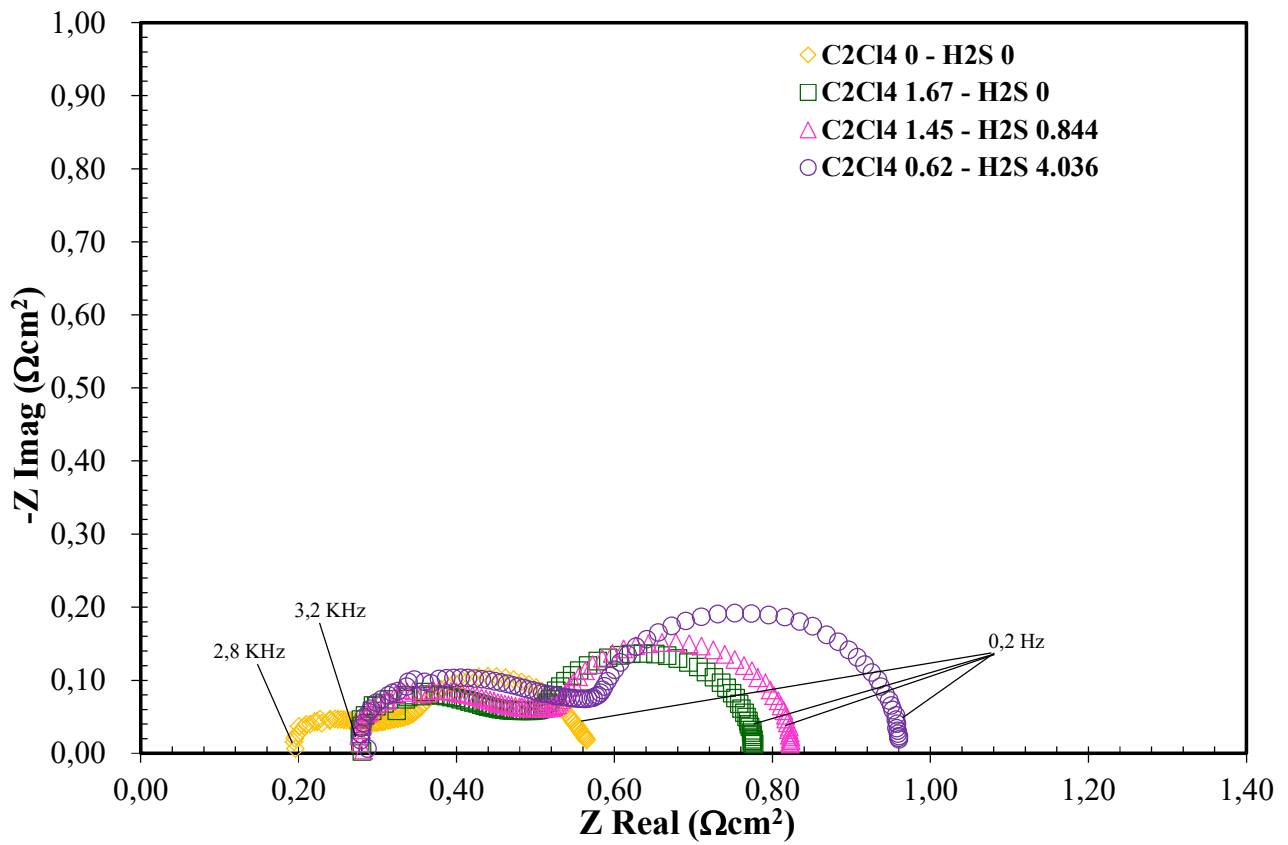
305

306

307

308

309 **Figure 24**



310

311

312

313

314

315

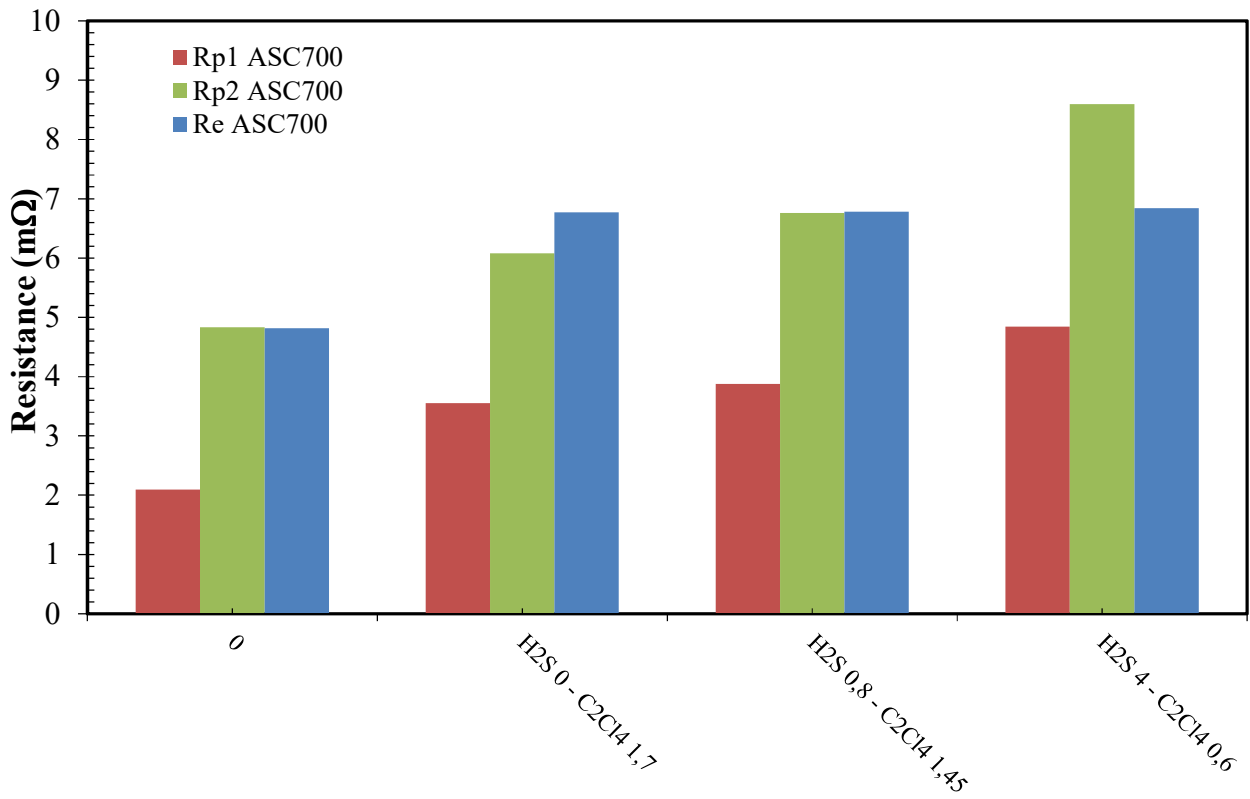
316

317

318

319

320 **Figure 25**



321

322

323

324

325

326

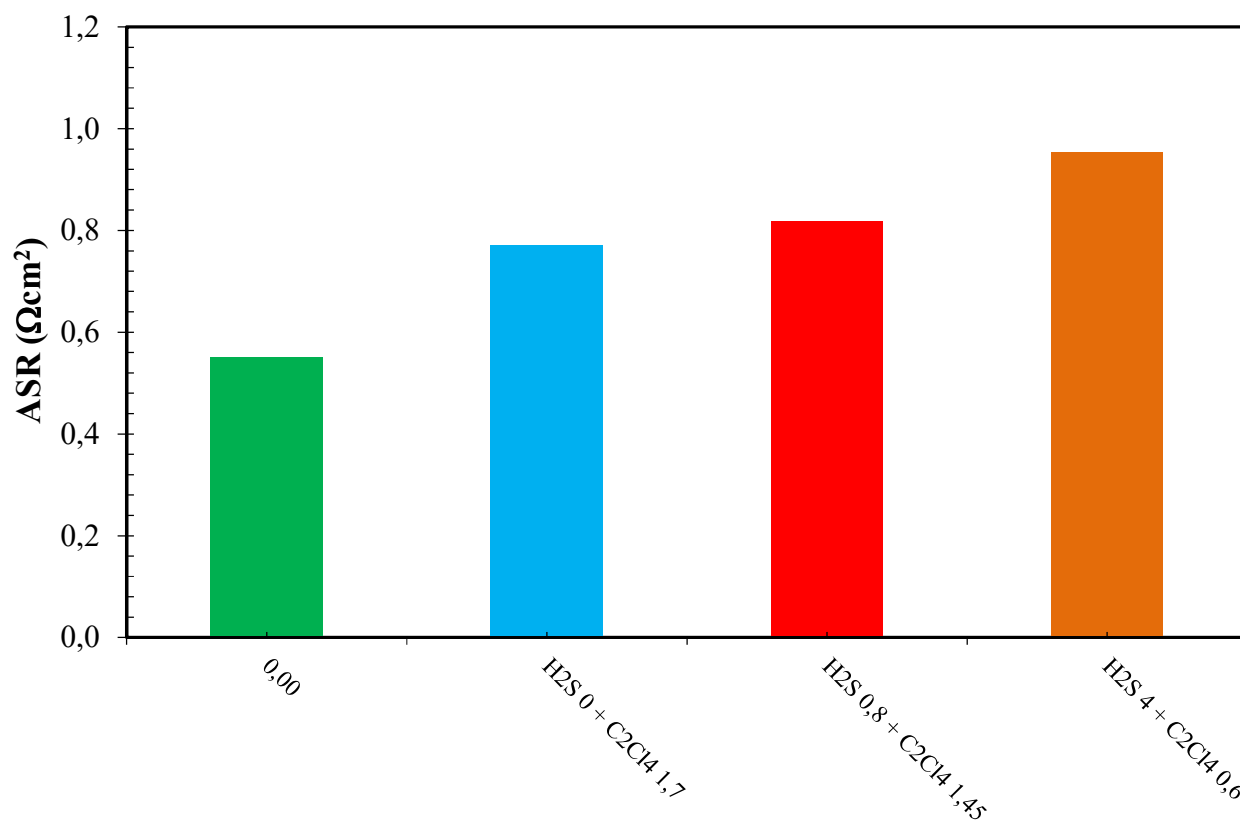
327

328

329

330

331 **Figure 26**



332

333

334

335

336

337

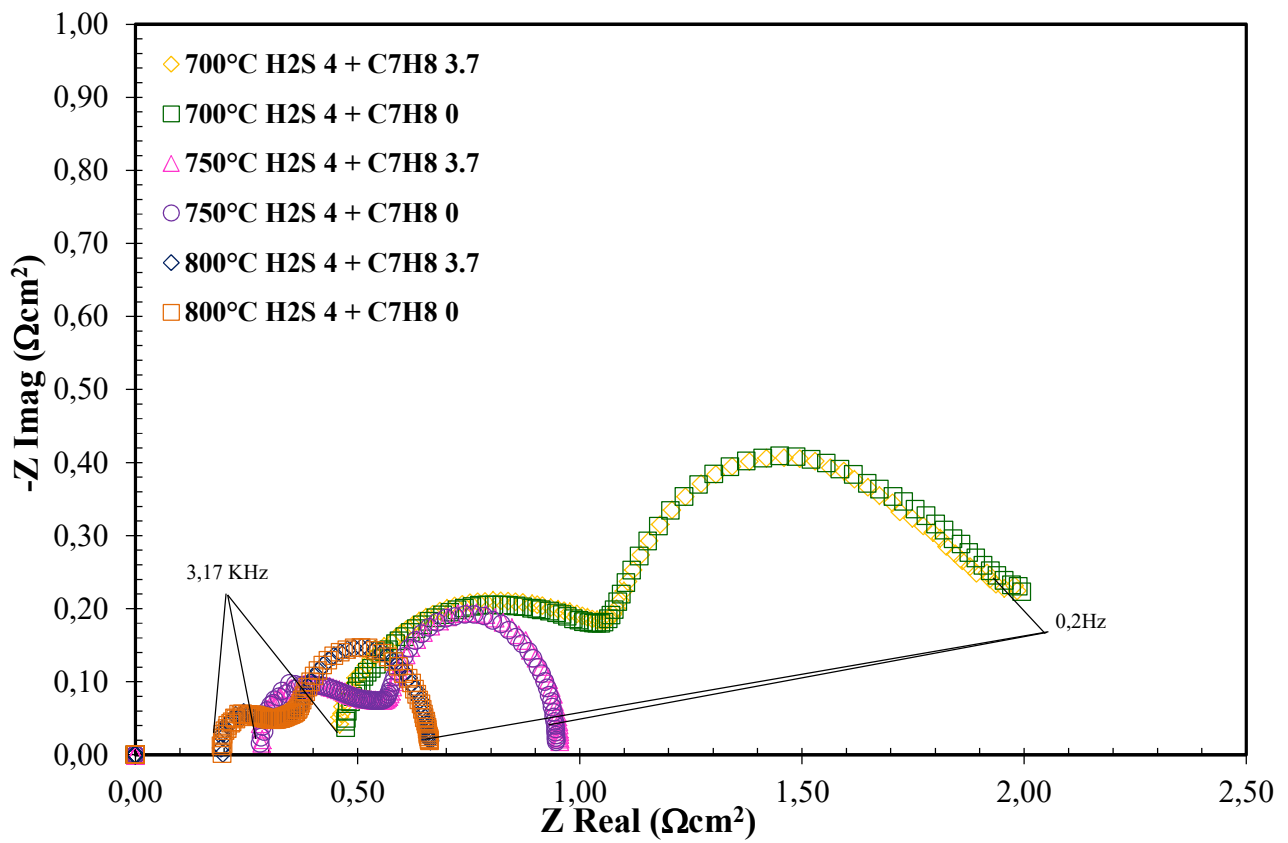
338

339

340

341

342 **Figure 27**



343

344

345

346

347

348

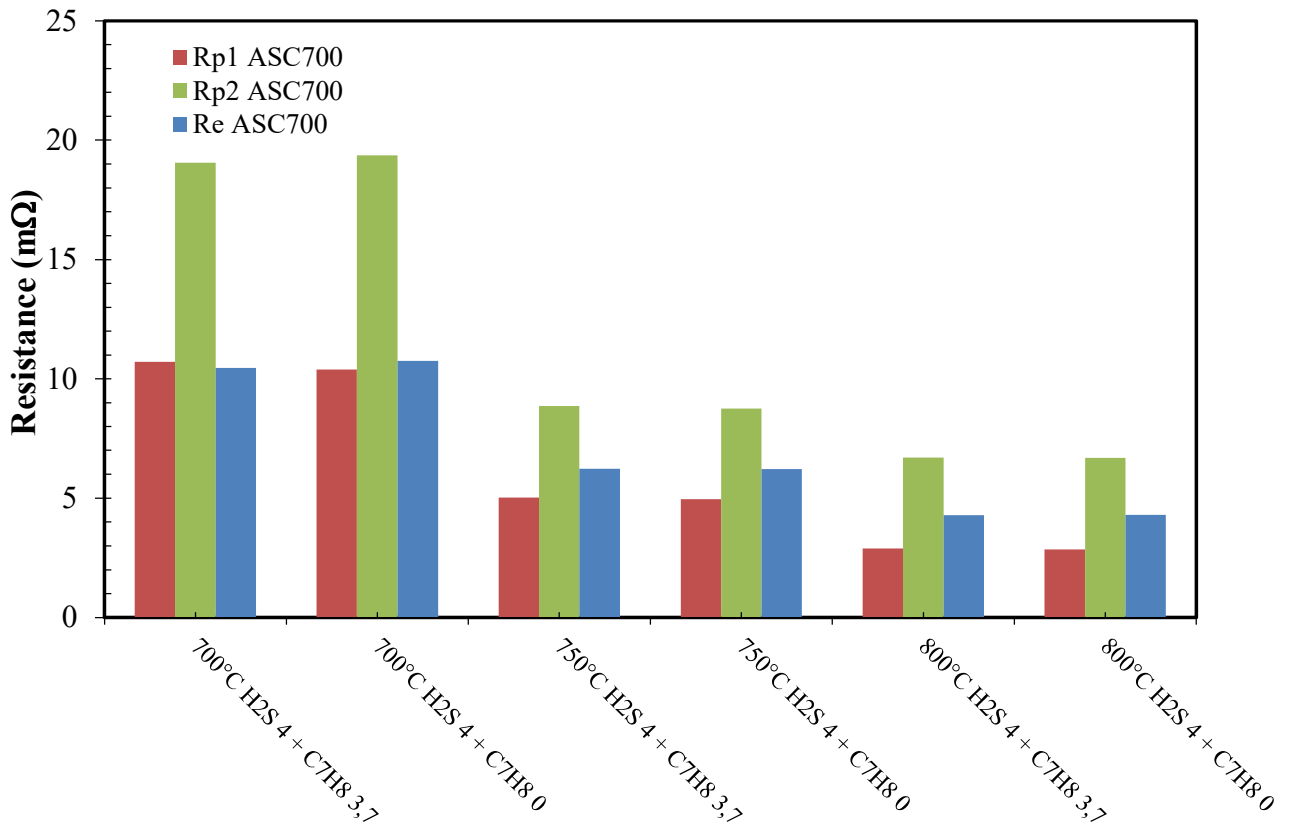
349

350

351

352

353 **Figure 28**



354

355

356

357

358

359

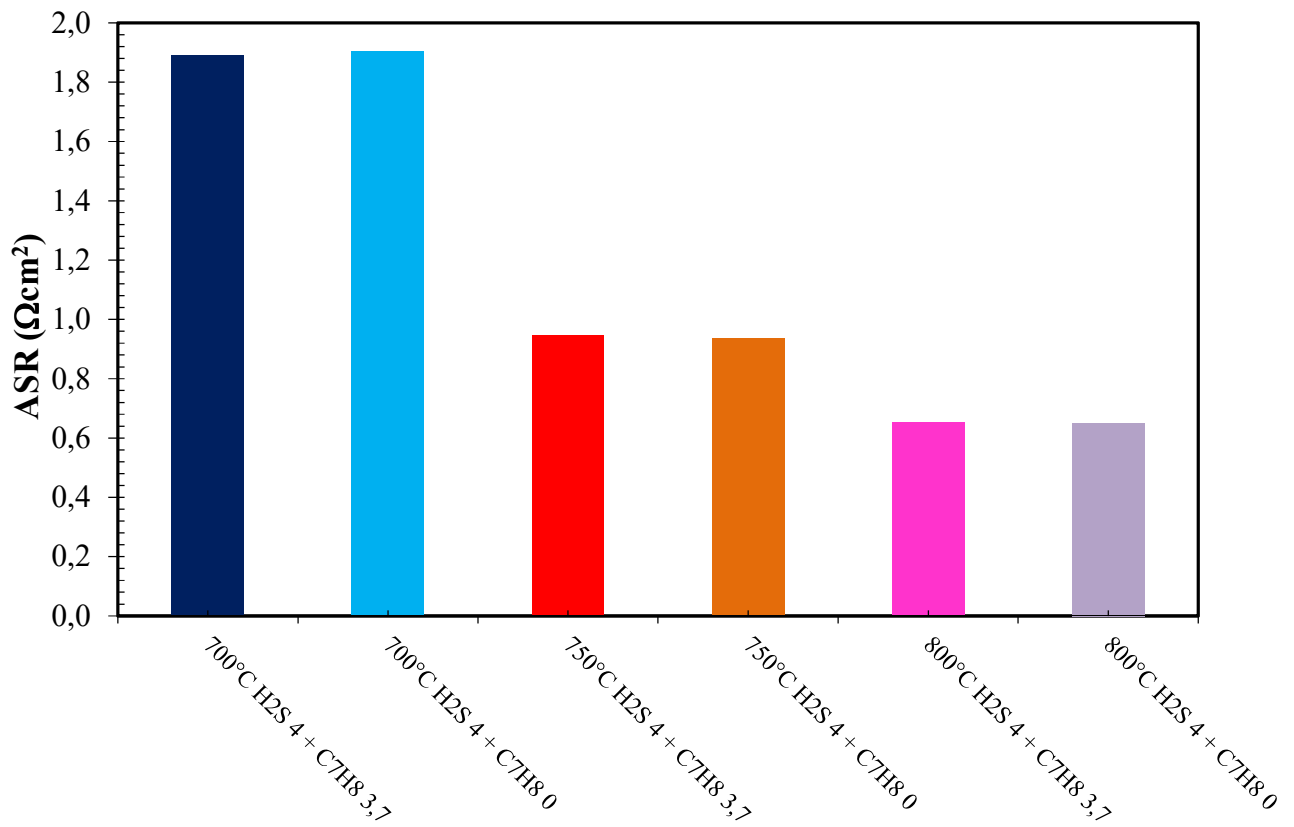
360

361

362

363

364 **Figure 29**



365

366

367

368

369

370

371

372

373

374

375

376

377

378